MARITIME TRANSPORTATION RESEARCH AND EDUCATION CENTER
TIER 1 UNIVERSITY TRANSPORTATION CENTER
U.S. DEPARTMENT OF TRANSPORTATION

Rapid and Non-Destructive Assessment of Levees for Strength and Liquefaction Resistance

Project January 1, 2015 – July 31, 2017

Clinton Wood, Ph.D., P.E. (PI, University of Arkansas, cmwood@uark.edu)
Michelle Bernhardt, Ph.D. (Co-PI, University of Arkansas, mlbernha@uark.edu)
Tim Moody (M.S. Student)
Behdad Kouchaki (M.S. Student)
Salman Rahimi (Ph.D. Student)

August 15, 2017

FINAL RESEARCH REPORT
Prepared for:
Maritime Transportation Research and Education Center

University of Arkansas
4190 Bell Engineering Center
Fayetteville, AR 72701
479-575-6021

ACKNOWLEDGEMENT
This material is based upon work supported by the U.S. Department of Transportation under Grant Award Number DTRT13-G-UTC50. The work was conducted through the Maritime Transportation Research and Education Center at the University of Arkansas.

Table of Contents

1 Project Description 1
2 Literature Review 2
2.1 Levee Defects and Failure Mechanisms 2
2.1.1 Overtopping Erosion 3
2.1.2 Internal erosion/ Piping 5
2.1.3 Surface erosion (Wet side) 7
2.1.4 Sliding 8
2.1.5 Wave/Structural impacts 8
2.1.6 Liquefaction 9
2.1.7 Tree damage 9
2.1.8 Slope failure 9
2.2 Detection and Evaluation Methods 10
2.2.1 Non-destructive Assessment Methods 10
3 Methodological Approach 24
3.1 Laboratory Resistivity Testing 25
3.2 Assessment of Kinion Lake Dam 27
3.2.1 Site Background 27
3.2.2 Geophysical Investigation 29
3.2.3 Electrical Resistivity Imaging (ERI) 31
3.2.4 Capacitively Coupled Resistivity (CCR) 32
3.2.5 Multichannel Analysis of Surface Waves (MASW) 33
3.3 Assessment of Mel-Price reach of Wood River Levee 35
3.3.1 Site Background 35
3.3.2 Geophysical Investigation 37
3.3.3 Capacitively-Coupled Resistivity (CCR) 38
3.3.4 Multichannel Analysis of Surface Waves (MASW) 39
4 Results/ Findings 42
4.1 Laboratory Resistivity Testing 42

4.1.1 Water composition 43
4.1.2 Temperature 43
4.1.3 Degree of saturation, dry density, bulk density, and volumetric water content 44
4.1.4 Verification studies 49
4.1.5 Additional Considerations 52
4.1.6 Application 53
4.1.7 Conclusions 54
4.2 Kinion Lake Dam 55
4.2.1 Crest of Dam 55
4.2.2 Toe 61
4.2.3 Conclusions 65
4.3 Mel-Price reach of Wood River Levee 65
4.3.1 General observation 65
4.3.2 Landside of the Levee 66
4.3.3 Top of the levee 68
4.3.4 Riverside 72
4.3.5 Combination of the MASW surveys for the top and landside 74
4.3.6 Empirical correlation between the raw N-SPT and Vs for the landside of levee ... 75
4.3.7 Conclusion 76
5 Impacts/ Benefits of Implementation 76
6 Recommendation and Conclusions 78
7 References 80

1 Project Description

Beginning with the first recorded levee construction in 1717 for the small village of New Orleans (Mitchell 1990), the United States levee system has been continuously adapted to respond to changing flood conditions and urban development. Although numerous flood related failures have occurred throughout history, prior to 2005, most of these failures were in low-risk rural areas where damages were mostly agricultural related. The first real failure to occur in an urban environment came in August of 2005 during Hurricane Katrina. The levees and floodwalls in and around New Orleans, Louisiana failed in over 50 locations, flooding more than 80% of the city, killing over 1,118 people, and resulting in an estimated $16.5 billion in damages (ASCE 2007). Considered the most costly US natural disaster on record, these events exposed the vulnerability and increased risk associated with levee systems surrounding growing urban developments. In 2007, Congress directed agencies to create a national levee database and in 2009 the American Society of Civil Engineers (ASCE) created a new category for levees in its report card for America's infrastructure. Levees received a grade of D-, which was a less than poor rating, but it increased awareness of the issue, the limited funds available, and provided a general plan to address the deteriorating system. Before the next report card was released, two additional major flood related disasters occurred in the Midwest in 2008 ($538 million in estimated damages) and in 2011 where record water levels resulted in over $2 billion in damages and repairs (ASCE 2013). In the 2013 report card for America's infrastructure, the American Society of Civil Engineers gave the levee system in the United States the same overall rating of D-, showing no change from the previous report. Although levee failures in the United States account for more economic impact than any other geo-related disasters, little improvement has been made to the overall levee system. This could prove to be a major problem in the coming decades, where continued deterioration, urban development, and an increase in extreme weather events will test these structures to and beyond their capacity and significantly increase the risk associated with their failure.

The problem is twofold with the common link being a lack of monetary funds. Firstly, there is no single database documenting the existing levee systems and their conditions. The report card rating is based in part on information from the National Levee Database (NLD) which is comprised of approximately 14,700 miles of levees operated by the U.S. Army Corps of Engineers (USACE). The NLD only contains levees which are designed, maintained, and inspected by USACE and it currently neglects over an estimated 85% of the nation's levees, which are locally owned and operated. It is estimated that approximately 100,000 miles of levees exist within the United States, affecting all 50 states and more than 43% of the population; however, the true extent is still unknown and gathering data from various owner entities is difficult. In fact, the Federal Emergency Management Agency (FEMA) manages the Midterm Levee Inventory (MLI) which contains roughly 35,600 miles of levees; however, the condition of many of these levees is unknown. Although the two agencies are working to combine the databases, limited funding is available to assess the condition of the levees. Without the condition and performance evaluation of a particular levee, there is no way to determine the risk associated with it. Typically, levees are evaluated based on a simple visual inspection program to identify critical or weak spots in the levee system (USACE 2014). This method can detect surface distress or erosion failures (post failure), but it cannot identify defects that exist within the inner core or foundation soil that could lead to a failure during an extreme event. This leads to a passive detection system that requires failures to occur before they are investigated and repaired. The methods currently used to proactively obtain this internal soil data are extremely time intensive, they require soil borings or

sampling which damages the levees, and they only provide a small discrete amount of data. With the limited funds available, it would be impossible to obtain the data needed to properly evaluate the condition of the nation's levees using these invasive methods. Therefore, there is a need for a rapid, proactive, non-destructive assessment procedure that can quickly and cost effectively gather continuous data, so that the most accurate performance evaluation can be made before defects in the levee lead to catastrophic failures.

The second issue is related to a lack of funding to rehabilitate or update the currently deficient levees. The levees in the NLD are more than 55 years old on average and were originally designed to protect farmland from flooding; however, due to urban sprawl and changes in land use, over 14 million people now live or work behind these structures. Unfortunately, only 8% of these levees are found to be in acceptable condition, while about 69% are minimally acceptable, and 22% are rated as unacceptable. ASCE estimates more than $100 billion is needed to repair and rehabilitate the US levee system; however, only a small portion of that money ($415 million per year) is currently allocated by the federal government for flood control. Therefore, the available money must be used to repair the most critical levees first. Unfortunately, there is no procedure in place currently which can quantitatively determine which repairs or which levees are critical. Therefore, there is a need for a framework which can quantitatively assess the extent and severity of detected defects and their influence on performance.

The goal of this research is to address both of these issues in a cost effective manner through the development of a rapid, non-destructive geophysical testing program. A series of geophysical field trials were completed to determine the most efficient methods and the best parameters for detecting various features or defects. A laboratory testing program were completed to determine the correlation between different soil types and resistivity values. The ability to quickly identify critical areas within a levee system so that they may be monitored or repaired is crucial if the levee system is to be improved with such limited funds.

2 Literature Review

2.1 Levee Defects and Failure Mechanisms

Many mechanisms could lead to a levee's failure. Some of the most common failure mechanisms are shown in Figure 2-1. These failure mechanisms are often divided into two categories: structural failures and failures due to hydraulic forces. Structural failures include damage to the embankment from debris or tree uprooting, slope failures, and sliding, while failures from hydraulic forces include underseepage, overtopping or wave erosion, piping, and liquefaction.

The following sections summarize the most common levee failure modes and the defects that lead to these failures (Ellis et al., 2008; Vrjiling, 2003). It should be noted that although these are termed failure modes, their occurrence does not guarantee catastrophic failure of the levee. Breaching is often caused by a combination of these failure modes.

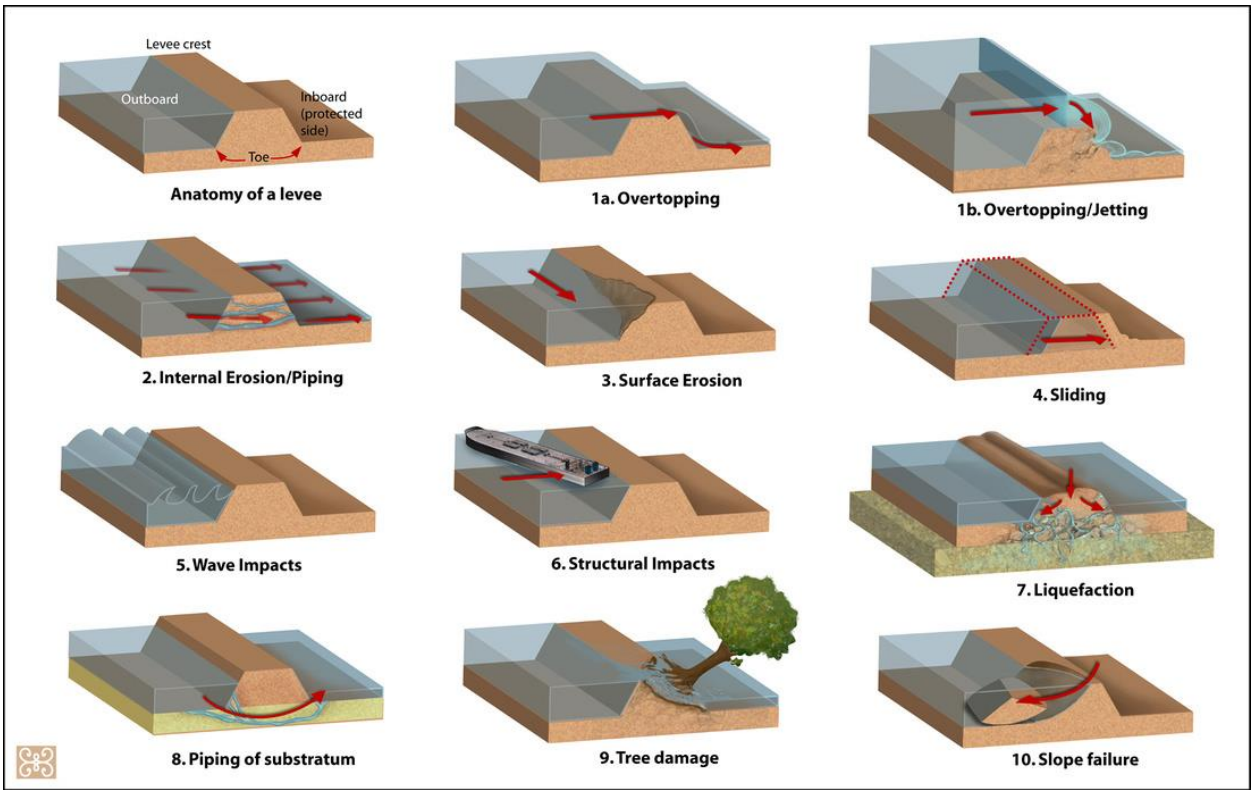

Figure 2-1 – Deretsky, Z. (2010) Ten ways a levee can fail. [Online image], retrieved on July 18, 2017 from http://www.zina-studio.com/p489212137/h1834C228#h1834c228

2.1.1 Overtopping Erosion

One of the most common phenomenon causing levee failures is surface erosion due to overtopping (Figure 2-2). In this process, the dry side of the levee will start being eroded by the forces of the overtopping water which may result in steepening of the downstream slope, lowering of crest, head cut development, and eventual collapse of the structure. There are many factors which affect the rate of erosion including grain size distribution, compaction energy, salinity of water, levee geometry and vegetative cover. As indicated by Briaud et al. (2008), larger grained soils such as sands are more susceptible to erosion compared to fine grained soils such as clays. The slope of the levee, determines the velocity of the water jet on the dry side where higher velocity corresponds with a higher rate of erosion. Generally, plants with extensive root networks help protect the soil from eroding by keeping the soil particles in place and decreasing the speed of water flow (Figure 2-3). There are number of ways to mitigate this erosion process including adequate design to prevent overtopping, providing vegetation cover, avoiding erodible soils and steep slopes. Visual inspection of the levee is sufficient in assessing the susceptibility to overtopping erosion and there is no need for additional assessment tools. The two items which should be checked are a comparison of the current height of the levee with the design height, and the vegetative coverage. As shown in Figure 2-3, good vegetative cover can help armor the levee from surface erosion.

Figure 2-2 - overtopping erosion in a levee west of Oakford, IL (Rutherford et al., 2016)

Figure 2-3 - vegetative cover laid down and acting as an armor on the landside slope of the levee near Olive Branch, IL (Rutherford et al., 2016)

2.1.2 Internal erosion/ Piping

Another common failure mechanism associated with levees is failure due to internal erosion or piping. In this phenomenon, a series of pipes or water paths will develop in the body of the levee, due to the existing hydraulic gradient, enabling the transportation of water from the wet side to the dry side of the levee. In this process water goes through the path which satisfies the criteria for relatively higher hydraulic conductivity and higher hydraulic gradient. Through time, water carries smaller soil particles with itself causing cavities to form in the levee. These cavities start forming on the dry side of the levee and propagate towards the wet side through time. Therefore, as time passes, these cavities expand and weaken the levee's core, making it more susceptible to collapse.

There are several visual signs which may indicate the occurrence of this phenomenon including the appearance of sand boils on the dry side of the levee (Figure 2-4), levee toe erosion, cracks on levee surface, absence of fine grain overburden materials on the dry side. The piping can also be initiated by the presence of voids from tree roots or animal burrows (Figure 2-5). While all levees are susceptible to piping, relatively thin levees, presence of high hydraulic gradients, and levees built with erodible soils are more susceptible to piping.

This internal erosion may occur in the foundation as well. In this case, the foundation material is much more permeable than the body material which provides a higher hydraulic gradient for water to flow through. As a result, fine-grained particles would be washed with water and transported upstream, slowly forming the void spaces in the levee foundation. This could especially happen if the levee is founded on paleo channels which comprises highly permeable and erodible sedimentary deposits. While generally the sand boils appear close to the toe, (Figure 2-6), visual detection of this mechanism may be harder as the sand boils may be found hundreds of meters away from the levee (Figure 2-7).

While burrows or sand boils can often be seen at the surface through visual inspection, internal piping or voids may not be visible and thus, a detection method capable of penetrating through the levee is needed to assess susceptibility of a levee to internal erosion. Additionally, a thorough assessment of the core and foundation soil types could also help identify soils which might be susceptible to internal erosion.

Figure 2-4 - The arrow indicates the location of a sand boil near the landside levee toe and the box indicates subsidence in levee crest due to loss of soil (Rutherford et al., 2016)

Figure 2-5 – View looking at exposed western edge of breach in a levee revealing the presence of animal burrows within the levee (Rutherford et al., 2016)

Figure 2-6 - Large sand boil network at levee toe near Olive Branch, IL (Rutherford et al., 2016)

Figure 2-7 - Sand boils approximately 1,200 feet landward of the levee with water still seeping through near Cairo, IL (Rutherford et al., 2016)

2.1.3 Surface erosion (Wet side)

Another common failure mechanism for levees is the erosion of soil on the water or wet side of the levees. Similar to the erosion of the land or dry side, soils on the wet side can be eroded due to the forces of flowing water. Providing adequate vegetative cover, proper compaction and

avoiding erodible soils are the main solutions to avoid this type of failure. One of the most comprehensive works on erodibility of different soil types is presented in Briaud (2008) where soils are categorized into six groups depending on their erodibility from very high erodibility to non-erosive (Figure 2-8). As can be seen, as the plasticity of the soil increases and/or the grain size decreases, soils can resist higher shear stresses and will erode at a slower rate. Therefore, depending on the expected water velocity, suitable levee construction material must be chosen.

Visual inspection may be helpful in detecting areas where surface erosion has started developing. However, many times the water may cover the erosion issues and it would be more advantageous to use non-destructive tools to assess the erodibility of soils and be able to make an assessment of the probability of erosion occurring for a given event.

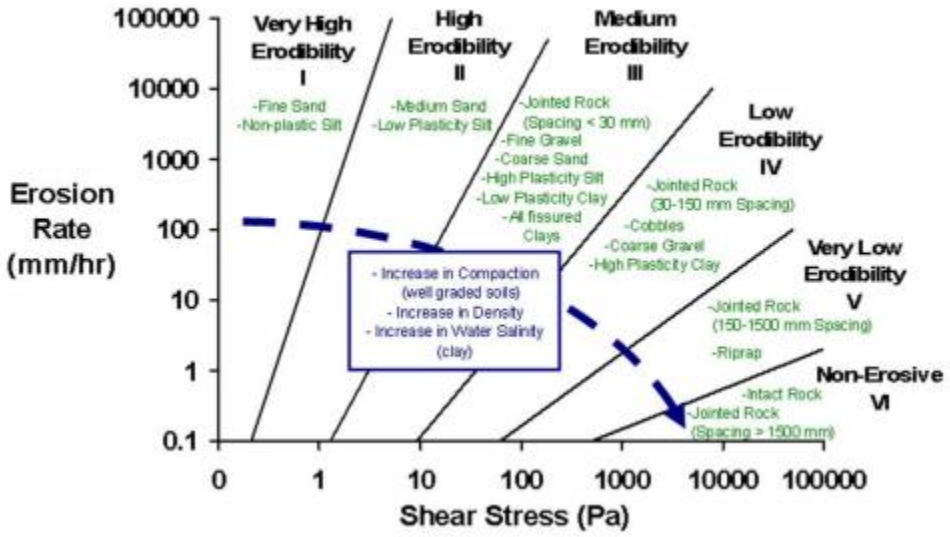

Figure 2-8 - Proposed erosion categories for soils and rocks based on shear stress (Briaud, 2008)

2.1.4 Sliding

Another failure mechanism threatening the stability of levees is failure due to sliding. In this process, the horizontal hydraulic pressure overcomes the shearing resistance provided at the interface of the levee's body and foundation and causes the levee to slide. This type of failure is likely to occur in levees where there is a sudden change of soil properties between the body and foundation materials. Although not very common, this phenomenon could occur for relatively tall levees where the levee's body is not connected adequately to the foundation. This type of failure can be prevented by increasing the bottom width of the levee and proper compaction of the bottom layer of the levee where it joins with the levee foundation.

As the sliding plane is unavailable for visual inspection, non-destructive test methods can be used to detect sharp contrast between the body and foundation materials. For example, sharp contrast between soil layers can be detected by an array of geophysical methods including seismic methods which are based on reflection and refraction.

2.1.5 Wave/Structural impacts

Wave impact is another process during which the levee structure will slowly deteriorate over time. Similar to other surface erosion processes, choosing the right soil and providing adequate vegetation could slow this process significantly.

Structural impacts are another cause of levee failures which may be due to the impact of boats or tree logs and other debris carried by the river during the flood. Such impacts may expose the core of the levee to the passing water and expedite the erosion. Any defects due to structural or wave impacts would be clear through visual inspection and no additional methods of detection are needed.

2.1.6 Liquefaction

Although there are not many documented cases for liquefaction in levees, it is another possible failure mechanism threatening levees. Generally, levees built using liquefiable soil or founded on liquefiable soil close to active faults are susceptible to liquefaction. One of the most interesting cases regarding levee liquefaction occurred in 1993 Kushiro-oki earthquake in northern Japan (Sasaki et al., 1995). The Kushiro river levees were underlain by a non-liquefiable peat layer. However, this highly compressible layer had subsided in a concave shape, creating a saturated zone in the levee as shown in Figure 2-9. Although liquefaction is a complex phenomenon, saturated sand layers subject to shaking have high liquefaction potential. To assess the liquefaction potential of a site, information about the potential seismic activity of the site and subsurface conditions are needed which cannot be obtained through visual inspection. However, non-destructive methods, such as Multi-Channel Analysis of Surface Waves (MASW) can confidently estimate the stiffness of subsurface layers which can be used to estimate liquefaction potential. Resistivity methods are also capable of distinguishing between sands and other fine-grained soils.

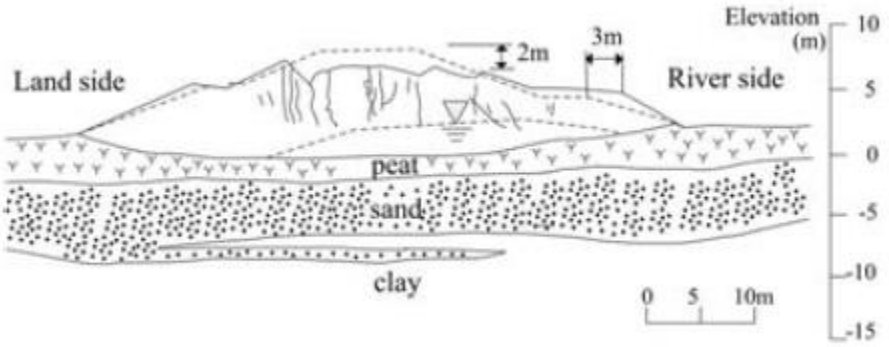

Figure 2-9 - Damaged levee of the Kushiro river (Sasaki et al., 1995)

2.1.7 Tree damage

Another potential threat to levee stability is the growth of larger plants such as trees on the levees. While under a normal climate trees may not damage the levee, severe climates such as storms could exert extreme forces on the tree and levee. If the tree gets uprooted, it will expose the levee's core and expedite the erosion process. Therefore, while grass vegetation is desired, it is often good practice to prevent trees from growing on top of the levees. Visual inspection methods would be adequate for detecting trees on levees, although it is difficult to identify the full extent of the root structure by this method.

2.1.8 Slope failure

Slope failure on the levee face can occur on the landside or waterside of the levee and reduce the thickness and/or height of the levee, ultimately reducing the stability. Slope failures can be the result of scour or overtopping erosion, seepage, desiccation cracking, rapid drawdown, earthquake loading, impacts, or simply low strength soil combined with the geometry of the levee slope. Scour and seepage are typically soil type dependent.

Factors such as insufficient compaction, desiccation cracking and rapid drawdown could increase the chances of slope failure. An example surface slide due to 2016 Midwest floods is shown in Figure 2-10. The exposed surface was immediately covered with plastic liner and sand bags to prevent further erosion until reconstruction finished.

In this case, non-destructive testing methods and visual methods are both required to examine the subsurface soil structure and the geometry of the slope in order to assess the risk of slope failure in levees.

Figure 2-10 -Surface slide covered with plastic liner and sandbags near Grand Tower, IL (Rutherford et al., 2016)

2.2 Detection and Evaluation Methods

There are currently numerous destructive and non-destructive methods available to detect anomalies and weak points within the ground. Although the data obtained through destructive methods is generally reliable and easier to use for geotechnical engineering purposes, it demands more time and money to obtain; these methods are also undesirable for levees in particular due to their destructive nature. As discussed, a large portion of the nation's levee system has little or no data regarding the current condition or design and the data that does exist is minimal in its consideration of subsurface defects. Therefore, it is critical to develop a low-cost, rapid and non-destructive testing framework to assess the condition of the aging levee systems and repair or reinforce these structures against future floods.

2.2.1 Non-destructive Assessment Methods

Non-destructive geophysical tests use electrical currents, electromagnetics and stress waves to "see" within the earth without drilling or punching holes. The tests are typically conducted from the ground surface and are used to image objects or soil layers to determine the engineering or geologic properties of the subsurface. Geophysical methods that can and have been applied to

levee evaluation include the Multi-channel Analysis of Surface Waves (MASW), P- and S-wave refraction, Ground Penetrating Radar (GPR), electromagnetics (EM), and capacitively coupled resistivity (CCR) (Hayashi and Konishi 2010, Lane et al. 2008, Inazaki and Sakamoto 2011, Kita et al. 2013, Mckenna et al. 2006). Each of these methods has distinct features that make them advantageous for detecting various defects within a levee system. For example, MASW and S-wave refraction provide a shear wave velocity (Vs) profile of the levee that is directly related to the shear modulus of the levee. This profile can be used to detect low density areas and strength related to weak spots within the levee and foundation system that could lead to failure. In addition, the Vs profile can be used to evaluate the liquefaction potential of various levee and foundation layers. The P-wave refraction method can determine the P-wave velocity profile of the levee and most importantly, it can be used to identify the line of saturation through the levee for liquefaction analysis and seepage monitoring. GPR can detect small buried objects, pipes, and other encroachments within the levee which can create weak spots and piping/seepage zones within the levee. EM and resistivity measurements can be used to infer the soil type of the levee and pick up changes in soil type with depth. Some of the most common geophysical methods will be described in more detail in the following subsections.

2.2.1.1 Electromagnetic surveys (EM)

Electromagnetic induction is a method to measure the apparent electrical conductivity of subsurface materials. Electrical conductivity is a measure of how well the soil conducts an electrical current. These measurements can be used to identify geologic materials and their locations. It can also be used for identifying buried metallic items. Conductivity values vary over several orders of magnitude depending on the type of material (Table 2-1). It is known that the amount of pore fluid present, the salinity of the pore fluid, the presence of conductive materials, and the amount of fracturing influence the conductivity measurements (Llopis and Simms, 2007).

Table 2-1 – conductivity and electrical resistivity values of some common rocks and minerals(Keller and Frischknecht, 1966)

Material	Resistivity, Ω-m	Conductivity, milliSiemens/m (mS/m)
Igneous and Metamorphic Rocks		
Granite	$5\times10^3 - 10^6$	0.001 – 0.2
Basalt	$10^3 - 10^6$	0.001 – 1
Slate	$6\times10^2 - 4\times10^7$	2.5×10^{-5} – 1.7
Marble	$10^2 - 2.5\times10^8$	4×10^{-6} – 10
Quartzite	$10^2 - 2\times10^8$	5×10^{-6} – 10
Sedimentary Rocks		
Sandstone	$8 - 4\times10^3$	0.25 – 125
Shale	$20 - 2\times10^3$	0.5 – 50
Limestone	$50 - 4\times10^2$	2.5 - 20
Soils and Waters		
Clay	1 – 1000	1 – 1000
Alluvium	10 – 800	1.25 – 100
Groundwater (fresh)	10 – 100	10 – 100
Sea water	0.2	5000

For measurement of soil conductivity through EM induction, a transmitter (Tx) and a receiver (Rx) coil separated by a distance are used. An alternating magnetic field is generated by the alternating current passed through the Tx coil. Eddy currents are inducted in the subsurface

conductive materials due to the formation of the magnetic field. In this setup, Rx coil detects the secondary magnetic field produced by the eddy currents as well as the primary field.

Typical EM systems record the quadrature phase, also known as the out-of-phase or imaginary component, and the quadrature component magnitude. The quadrature component is used to determine the apparent ground terrain conductivity. Anomalies such as filled-in abandoned channels, buried objects or voids typically produce conductivity readings which are different from the background values. The in-phase component is also very sensitive to metallic objects. Therefore, it can be very useful for locating buried metals such as metal rails, rebar, or electrical wires. However, a disadvantage is that if such materials are present and the object of the survey is not to locate such objects, these objects will interfere with the survey results significantly. Therefore, when planning a survey, it is important to avoid locations close to metallic fences, railroads, metallic gates, etc. to ensure the conductivity readings are from the subsurface geologic materials only. Additionally, although EM induced conductivity can be used to infer information regarding mineralogy, grain size, water content and anomalies, EM units require multiple passes at different frequencies and/or different coil distances to gather data at different depths.

Figure 2-11 - Geonics Ltd. EM34 EM induction instrument being towed by a vehicle collecting continuous data (Llopis and Simms, 2007)

The depth of investigation in EM induction systems varies considerably based on the array type, distance between the transmitter and receiver and the operating frequency (Llopis and Simms, 2007). For example, Llopis and Simms (2007) used Geonics Ltd. EM34 induction instruments for assessing levee conditions in the Feather River levees in California. They towed the coils on an electronically non-conductive sled at a walking distance to collect continuous data (Figure 2-11). The EM34 allowed for coil separations of 10, 20, or 40 m. Operating in the vertical dipole mode allowed for greater depths of investigation and less sensitivity to surface materials. This resulted in nominal depths of exploration of 15, 30 and 60 m for 10, 20 and 40 m coil

distances, respectively (McNeil, 1980).Dunbar et al. (2003) conducted EM surveys in Texas by towing a symmetric and coplanar dipole system on a helicopter above the levee at an altitude of 30 m. Using different frequencies, they gathered data up to the depth of 30 m. Although this method is more rapid than other geophysical methods, it did not provide a good resolution and it is relatively expensive compared to other non-destructive methods.

2.2.1.2 Ground Penetrating Radar (GPR)

Ground Penetrating Radar (GPR) is a geophysical method that images the subsurface using radar pulses. GPR transmits EM pulses (10-2000 MHz) (Davis and Annan, 1989) and the receiver antenna records the reflections. The penetration depth and resolution depend on conductivity of the materials and the signal frequency. In low conductivity materials such as dry sands, signals could penetrate up to 50 m while in conductive materials such as clays, they will penetrate only a few meters (Davis and Annan, 1989). Therefore, GPR is likely not the most effective option for levee assessment, as most levees are constructed using clays and are relatively high in water content.

2.2.1.3 Light Detection and Ranging technology (LiDAR)

LiDAR uses light in the form of a pulsed laser to measure ranges (variable distances) to the earth. These light pulses, combined with other data recorded by the system, can generate three-dimensional information about the shape of objects. These systems generally consist of a laser, a scanner and a GPS receiver (NOAA, 2017).

Palaseanu-Lovejoy et al. (2014) used LiDAR technology to create crest elevation profiles of levees in south Louisiana. They were able to identify abrupt changes in levee elevation and orientation. Using this data, they were also able to compare the levee height with the height requirements to withstand the 100-year flood. Surprisingly, only 5% of the crest points of the levees investigated passed the height requirement.

Unlike geophysical methods which provide information about the internal structure of the levee, LiDAR gives information about its geometry. This information can be used for assessing overtopping risk and slope stability analysis.

2.2.1.4 Multi-channel analysis of surface waves (MASW)

While resistivity methods characterize the subsurface by its resistance to current, surface waves use stress wave propagation to determine the stiffness of the ground below. The two types of seismic waves, whose motions are shown in Figure 2-12, are body waves, which propagate through the interior of a body, and surface waves, which propagate along a free surface. In geophysical testing, the two primary surface wave types are Rayleigh and Love.

Rayleigh waves were first predicted by their namesake, Lord Rayleigh, in 1885 (Strutt, 1885). In a homogeneous, elastic half-space with no free surface boundary condition, only compression and shear waves (body waves) can be produced. However, with the introduction of a free surface, non-dispersive Rayleigh waves are formed along that surface with displacements constrained to a depth of 1 – 2 times the wavelength of that wave. While Rayleigh waves are the only surface waves that can exist in a homogeneous half-space, A.E.H. Love predicted in 1911 that heterogeneous half-spaces allow the existence of what became known as Love waves (Love, 1911). Love waves can develop only in a half-space overlain by a layer of less stiff material and consist of horizontally polarized shear waves interacting with wave reflections at that layer boundary, whereas Rayleigh

waves form from the interaction of compression and vertically polarized shear waves (Love, 1927) (Ben-Menahem & Singh, 1981).

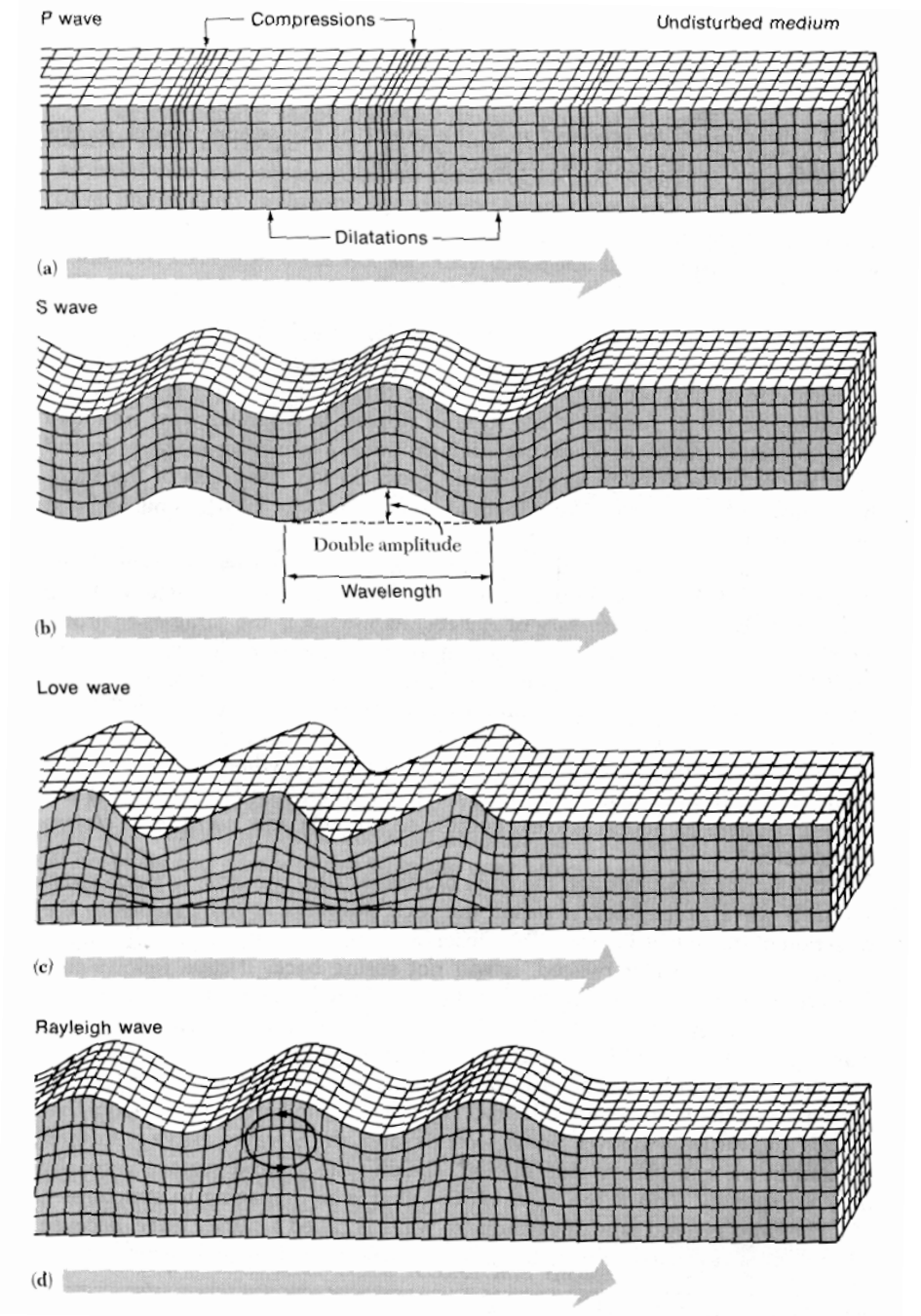

Figure 2-12 - Body and surface wave motions: (a) p-waves, (b) s-waves, (c) Love waves, (d) Rayleigh waves (Bolt, 1993).

Surface waves have long been of interest to seismologists for characterization of the interior of the Earth, though it required the development of numerical methods and geotechnical instrumentation before near-surface applications became popular. Van der Poel (1951) performed one of the first documented applications of surface waves using a generator with eccentric weights

and oscillograms to calculate dynamic Young's moduli and assess the rigidity of construction layers in roads. The first solutions to the surface wave inversion problems on theoretical dispersion curves came about in the 1950s with advances in computation, but dispersion curve fitting would not be developed until Nazarian and Stokoe (1983) did it manually by trial and error (Thomson, 1950).

The Steady-state Rayleigh method developed by Jones (1962) became the first engineering site characterization method. This simple method consisted of a single receiver in line with a vibrating seismic source that generated waves in ultrasonic frequencies to assess the thickness and elasticity of, at first, concrete slabs and, later, soil columns using lower frequencies. By moving the receiver away from the source with a constant frequency, wavelengths and phase velocities for that frequency could be calculated and by repeating the process for multiple frequencies, a composite dispersion curve could be obtained. Jones tested soils with both Rayleigh and Love waves and recognized the necessity of changing the source configuration to generate the desired waves, i.e. a vertically vibrating source generates Rayleigh waves and a horizontally vibrating source generates Love waves.

Surface wave methods became much more common with the development of the Spectral Analysis of Surface Waves (SASW) in the 1970s and 1980s (Nazarian & Stokoe II, 1983) (Heisey & Stokoe II, 1982). This two receiver approach, illustrated in Figure 2-13, yields a dispersion curve by estimating travel times for surface waves over a limited frequency range. By varying the receiver spacing, a composite dispersion curve over a larger testing range can be obtained. Despite its long and difficult testing procedure, SASW became much more popular in civil engineering site characterization.

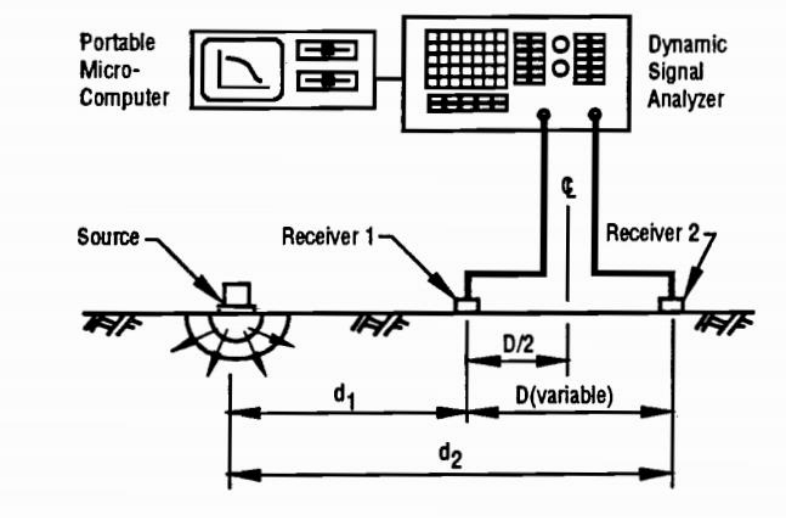

Figure 2-13 - SASW testing schematic (Rix, et al., 1991).

In 1987, Gabriels et al. (1987) demonstrated the first application of multichannel surface wave methods, however, until advances in computing and signal processing were made, SASW remained the primary surface wave testing method. In the early 2000s, the Multichannel Analysis of Surface Waves (MASW) became a robust and effective method for surface wave assessment and resulted in a boom in surface wave applications in civil engineering projects (Park, et al., 1999). MASW generally consists of a seismic source in line with a linear array of receivers, as

shown Figure 2-14. The MASW's use of multiple receivers results in faster data collection in the field and more robust data.

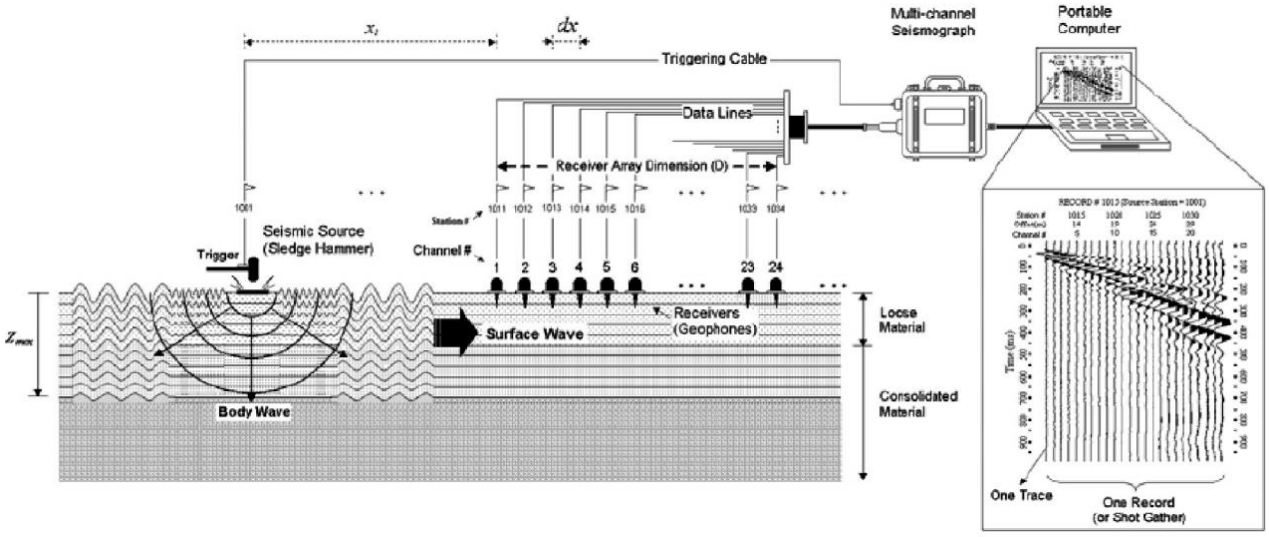

Figure 2-14 - MASW schematic showing the wave motion from source to receiver array to signal processing (Mohamed, et al., 2013)

After MASW data collection, several signal processing methods, usually transform based, can used to transform time-space domain data (field data) to another domain where phase velocities for given frequencies can be obtained resulting in a dispersion curve, an example of which is shown in Figure 2-15. Once a dispersion curve is obtained, that curve has to be processed to remove noise, undesired higher modes, and near- and far-field effects. Near-field effects are the result of interference from body waves and the surface wave front. Near the seismic source, the wavefield is a complicated mix of p-waves, s-waves, and surface waves because the various wave types have not yet separated and attenuated. Thus the body waves have an exaggerated influence on the displacements recorded by the receivers within 0.5 – 2 wavelengths of the source (Foti, et al., 2015). The other source of near-field effects is the shape of the surface wave wavefront. In the various surface wave methods, the expansion of surface waves is assumed to be planar, when it is actually cylindrical requiring the use of cylindrical coordinate beamformers rather than planar, at the cost of increased computing requirements (Zywicki & Rix, 2005). Near-field effects due to body wave interference are lessened in MASW by using relatively long source-offsets and longer arrays, both of which allow wavefronts to separate, attenuate and be identified in processing at the cost of high-frequency dispersion data. Far-field effects result from the wave losing energy with distance from the source and becoming indistinguishable from environmental noise.

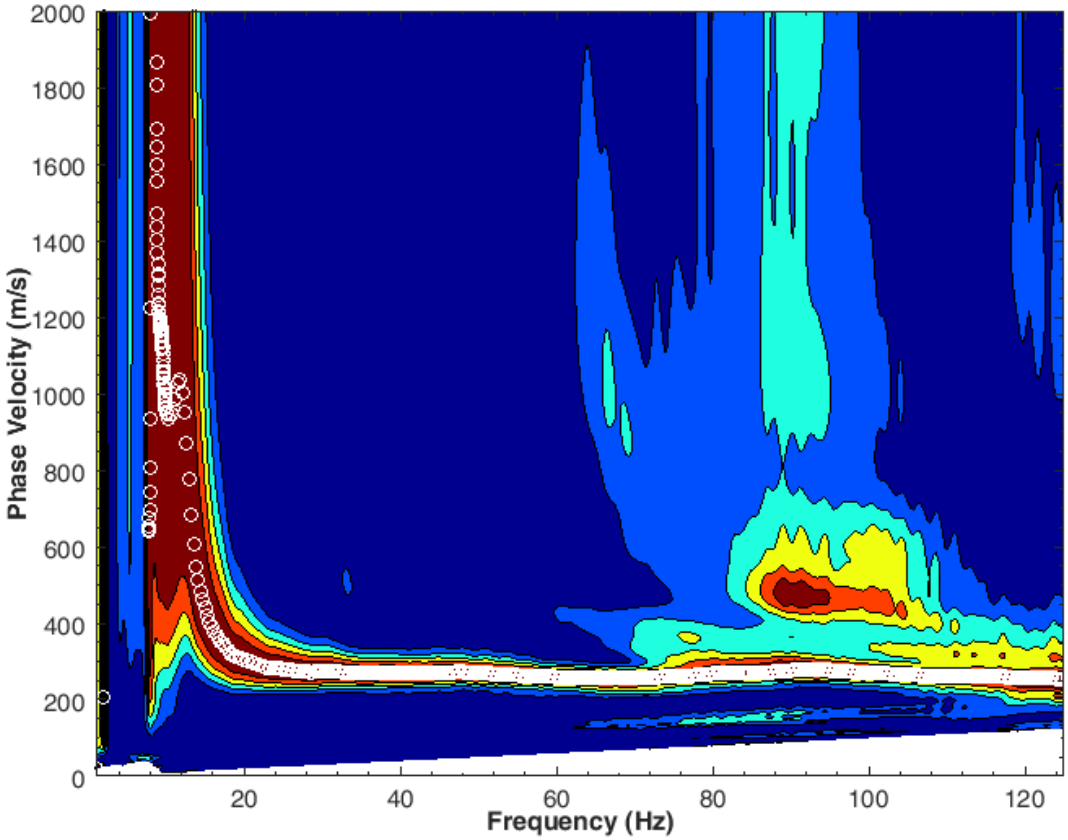

Figure 2-15 - Example dispersion curve from Kinion Lake Dam

Obtaining a subsurface shear wave velocity model requires forward modeling and the solution of an inversion problem, much like in resistivity methods. After higher modes and noise are removed, a variety of software can be used to process this curve and obtain ultimately obtain a shear wave profile. Generally, solving the inversion problem begins with a trial model for the site whose parameters are used to generate theoretical dispersion curves as shown in Figure 2-16. Through successive model iterations, the differences between the experimental and the theoretical are minimized. The most difficult part of MASW is not the data collection or the dispersion processing, but rather the interpretation and inversion. Inversion software using genetic algorithms to generate thousands of shear wave velocity models while keeping and modifying the best fitting models has become increasingly popular (Wathelet, 2008). The downside of this approach is that inversion problems are ill-posed and have an infinite number of solutions resulting in many possible model solutions and the need for large computational resources to generate these thousands of models. By using ground truth information (e.g. layer depths, material types, schematics) or loosely interpreting the dispersion curves, this initial solution space can be reduced yielding faster processing and better results.

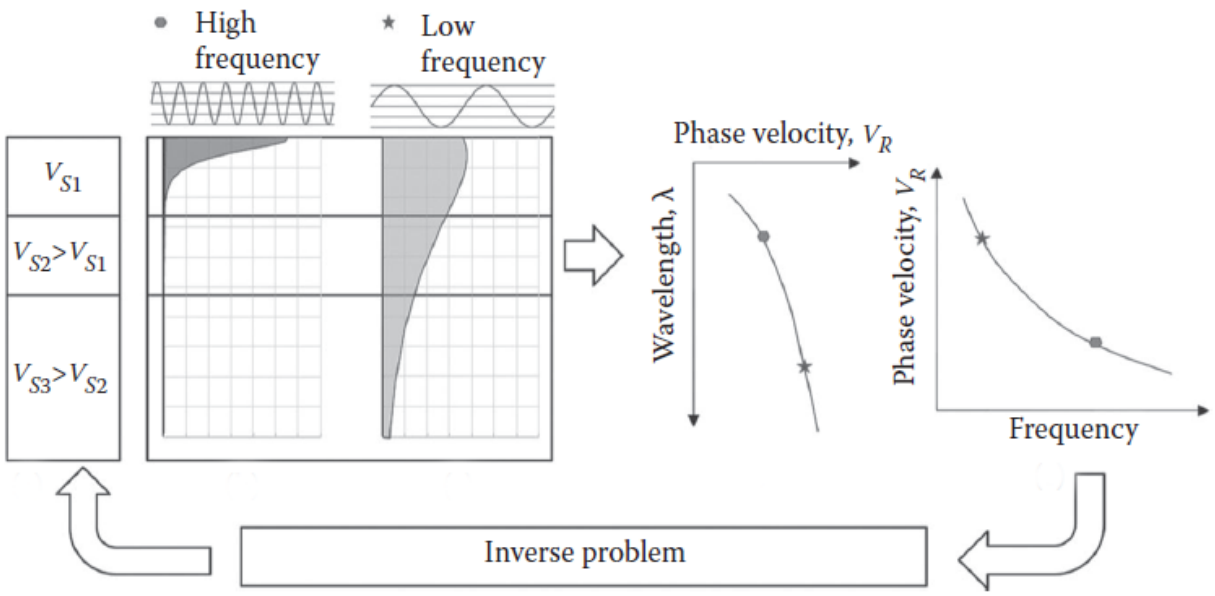

Figure 2-16 - General schematic for obtaining a Vs profile solution (modified from Foti et al. (2015))

Shear wave velocities are a proxy for and can be used to calculate the stiffness of the subsurface materials, allowing the detection of layer boundaries and anomalies. By performing MASW at multiple locations along an earthen structure, a pseudo-2D profile can be constructed, and deviations in shear wave velocities can identify bedrock intrusions, voids, and other features in the subsurface.

2.2.1.5 Electrical Resistivity Methods

Electrical resistivity is an intrinsic property that quantifies how strongly any given material opposes the flow of electrical current. The use of the electrical resistivity method has a long history in geophysical testing and it was made famous through the pioneering work of Conrad Schlumberger in France in 1912 (Dahlin, 2001).

Electrical resistivity measurements require at least four-electrodes, two current electrodes and two voltage potential electrodes. The arrangement of the electrodes and sequence of measurements is the array and many different arrays have been developed through the years. For example, to measure the electrical resistivity using a Wenner array (Figure 2-17 (a)), electrical current is passed between two external electrodes inserted into the ground (current electrodes) and then the resulting voltage potential is measured across two internal electrodes inserted into the ground (potential electrodes) (Herman, 2001; Loke, 1999). Some of the most common resistivity arrays are shown in Figure 2-17.

The ranges of resistivity corresponding to various materials consist of clays and shales at the less resistive end (10 – 100 Ω-m), gravels, sands and rock at the highly resistive end (800+ Ω-m), and silts and porous sedimentary rock in the middle (80-1000 Ω-m) (Palacky, 1987). However, the presence of water in more porous materials can make it much more difficult to interpret particular resistivity values as particular materials confidently. Rein, Hoffman, and Dietrich (2004) performed a long-term direct current (DC) resistivity monitory survey at two test sites to determine what site parameters most significantly affect resistivity measurements, concluding that water

saturation, soil temperatures, groundwater temperatures, and groundwater ion concentrations also affected resistivity measurements the most in decreasing significance.

In the DC electrical resistivity method, the electric current *I* is directly injected into the ground through a pair of electrodes and the resulting voltage *V* is measured between a second pair of electrodes. The impedance $Z = V/I$ is calculated which is then transformed into apparent resistivity ρ_a which is an indicator of the underlying resistivity structure ρ(r) of the earth. (Everette, 2013). The depth of a resistivity measurement depends on the distance between the current or sink electrodes and the distance from the voltage potential electrodes. Each measurement is called the apparent resistivity and is the measurement that would have been measured if the entire subsurface was uniform (Everett, 2013). A map of the apparent resistivity plotted at these locations is termed a pseudosection (Loke, 1999).

The Schlumberger array, shown in Figure 2-17(b), uses the outer two electrodes to complete the circuit and the internal distance to the two potential electrodes is varied to increase survey depth. Similarly, the Wenner array, shown in Figure 2-17 (a), uses the outermost electrodes to complete the circuit, however, all four electrodes are kept equidistant, requiring all four to be moved for deeper surveys, unlike in a Schlumberger array. Despite the longer testing time, Wenner arrays have been found to have the best signal response and horizontal resolution, though a more limited depth of investigation (Seaton & Burbey, 2002).

The third configuration is the dipole-dipole, shown in Figure 2-17(c), in which the two current-bearing electrodes are adjacent to one another and spaced equally to the potential measuring electrodes. The distance between these pairs can be varied to increase survey depth. Dipole-dipole arrays are more susceptible to noise, have lower signal-to-noise ratios, have better resolution particularly for dipping layers, and somewhat less depth resolutions than the alternatives (Dahlin & Bing, 2004).

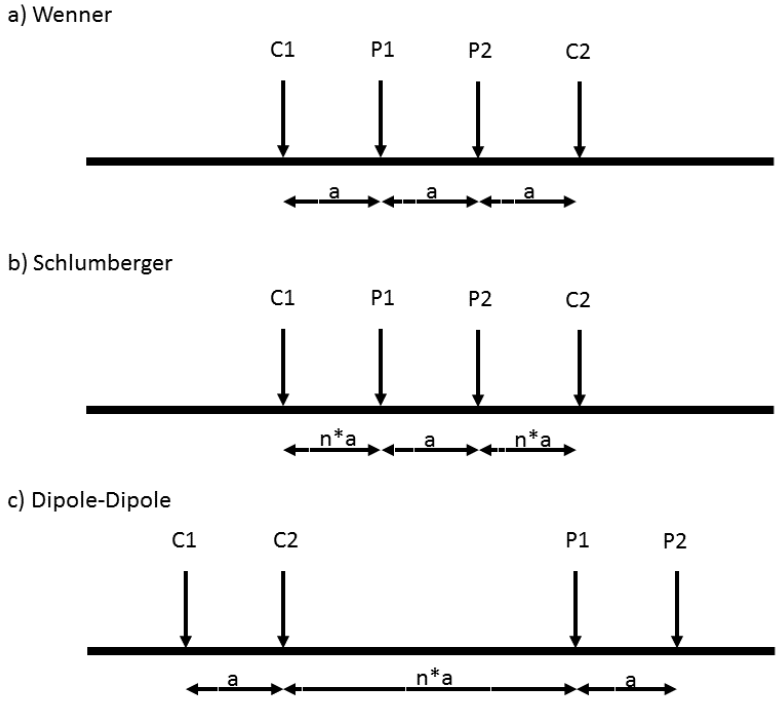

Figure 2-17 - DC array configurations: (a) Wenner, (b) Schlumberger, (c) Dipole-Dipole

Construction of a pseudosection using a dipole-dipole array (Figure 2-17(c)) is shown in Figure 2-18; where the measured apparent resistivity associated with current AB and potential electrode pairs PQ is plotted at the intersection of two 45° angles passing through the center of the electrode pairs. By moving the electrode pairs, apparent resistivity is measured at different depths and locations. (Everette, 2013). However, the pseudosection only provides a rough estimate of the true resistivity of the subsurface. Through a process called inversion, which requires complex mathematical calculations, true resistivity of the ground is obtained (Figure 2-19).

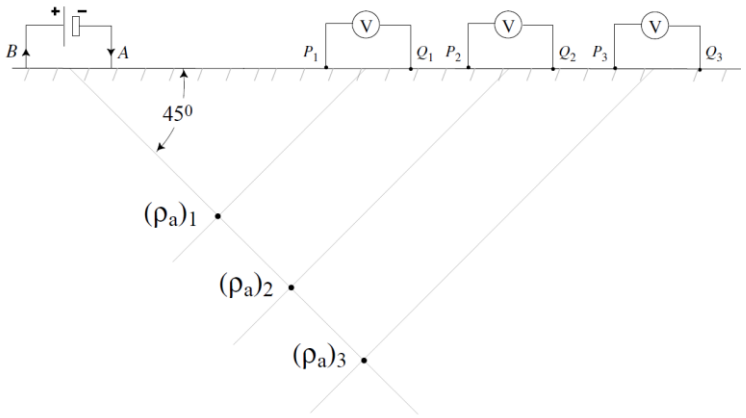

Figure 2-18 - Construction of a dipole-dipole resistivity pseudosection (Everette, 2013)

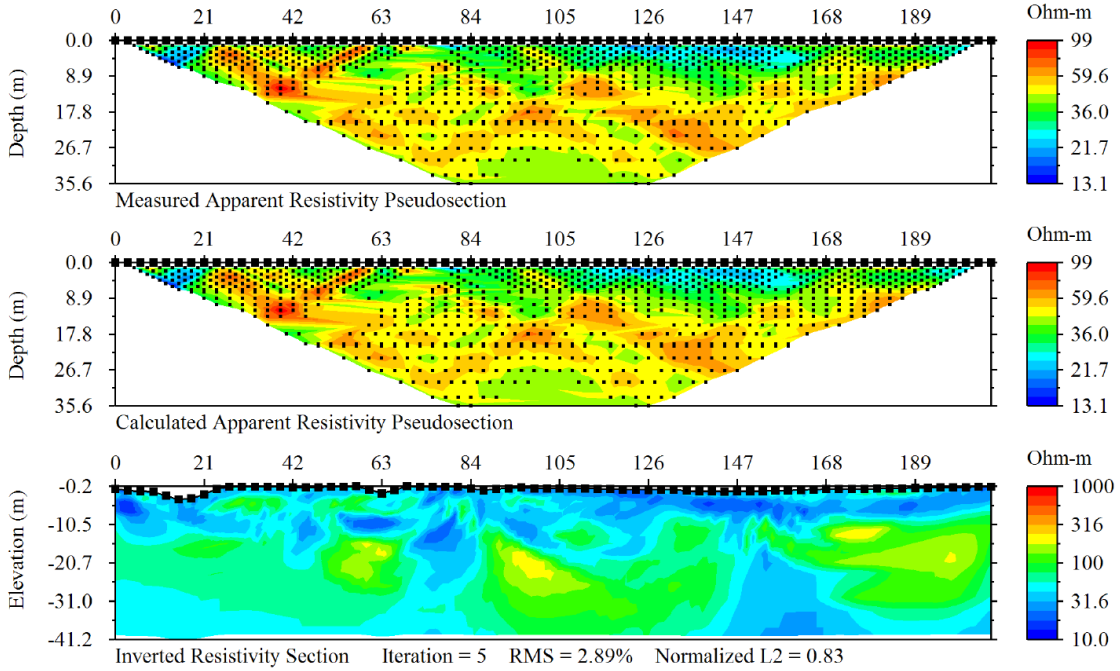

Figure 2-19 - measured apparent resistivity pseudosection for a hybrid Schlumberger – dipole-dipole electrode configuration (Top) along with the inverted resistivity image (Bottom). Middle image shows the calculated apparent resistivity based on the inverted cross section. (Everette, 2013)

2.2.1.5.1 Electrical resistivity Imaging (ERI)

2D DC surveys, also known as electrical resistivity imaging (ERI) allow continuous resistivity profiling along infrastructure like levees, dams, and roads. The typical setup consists of steel stakes attached to electrode cables connected to a resistivity meter, allowing long arrays of electrodes to induce current and measure potential in a semi-automated manner, proceeding from smallest spacing to largest, shown in Figure 2-20. The entire staked array can then be moved forward, resulting in longer 2D profiles. Alternatively, multiple electrode cables can be used in a line and once one set of electrodes is no longer needed, it can be moved to the end, extending the survey distance, as seen in Figure 2-21 (Dahlin, 1996). This reliance on computer-controlled multiple electrode systems allows much faster data collection over larger areas.

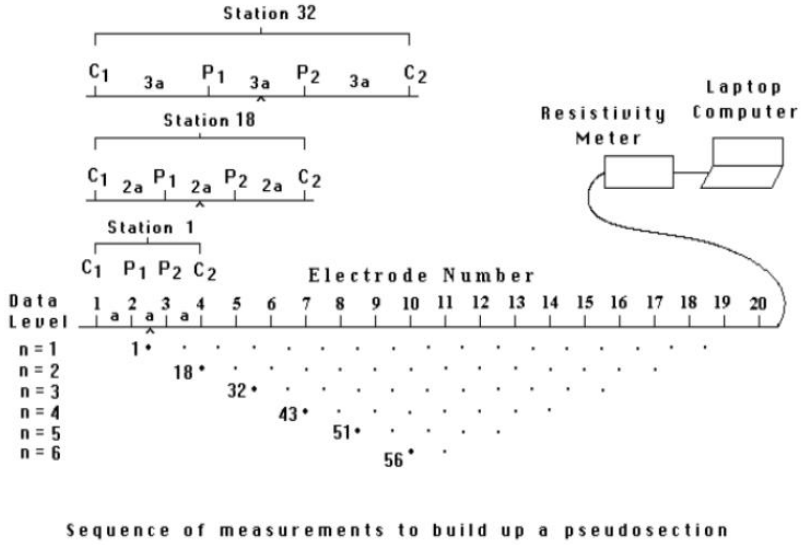

Figure 2-20 - Using a set of electrodes and cables to survey at different depths by varying the spacing (Loke, 1999)

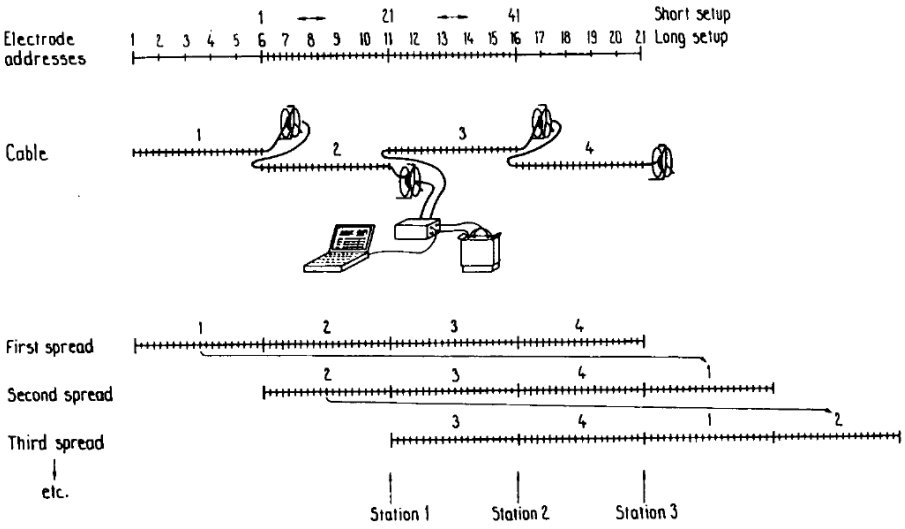

Figure 2-21 - ERI roll-along schematic (Dahlin, 1996)

2.2.1.5.2 Capacitively coupled resistivity (CCR)

Capacitively-coupled resistivity methods (CCR) solve many of the limitations inherent in traditional DC surveys by not requiring electrodes staked into the ground. In ERI surveys, this staking requirement makes testing pavements, gravelly surfaces, frozen terrain, and well compacted soils very difficult or even impossible. DC surveys also have difficulty with high surface resistivity values found on those same terrain types (Baines, et al., 2002). CCR uses a transmitter and receivers coupled in a dipole-dipole configuration. Using line antennas, these electrodes can be dragged along the ground manually (Figure 2-22) or by a vehicle (Figure 2-23) as a single unit enabling very rapid measurements over large distances (Timofeev, et al., 1994).

Obtaining a subsurface resistivity model requires first creating a pseudosection profile. This is normally done by locating an apparent resistivity value at the midpoint of the transmitter and the receiver and at a depth proportional to the distance between the two. The resulting pseudosection only approximates the true resistivity distribution below the surface and is mostly used to identify and remove unusually large or low values (Loke, 1999). After processing a pseudosection, a subsurface model can be obtained by use of a forward modeling program using either finite-difference or finite-element methods. In geophysical inversion problems, there exist infinite possible solutions that can result in the same apparent resistivity values. This requires some basic model assumptions and prior knowledge of the site to narrow the solution space and allow the software to calculate likely models.

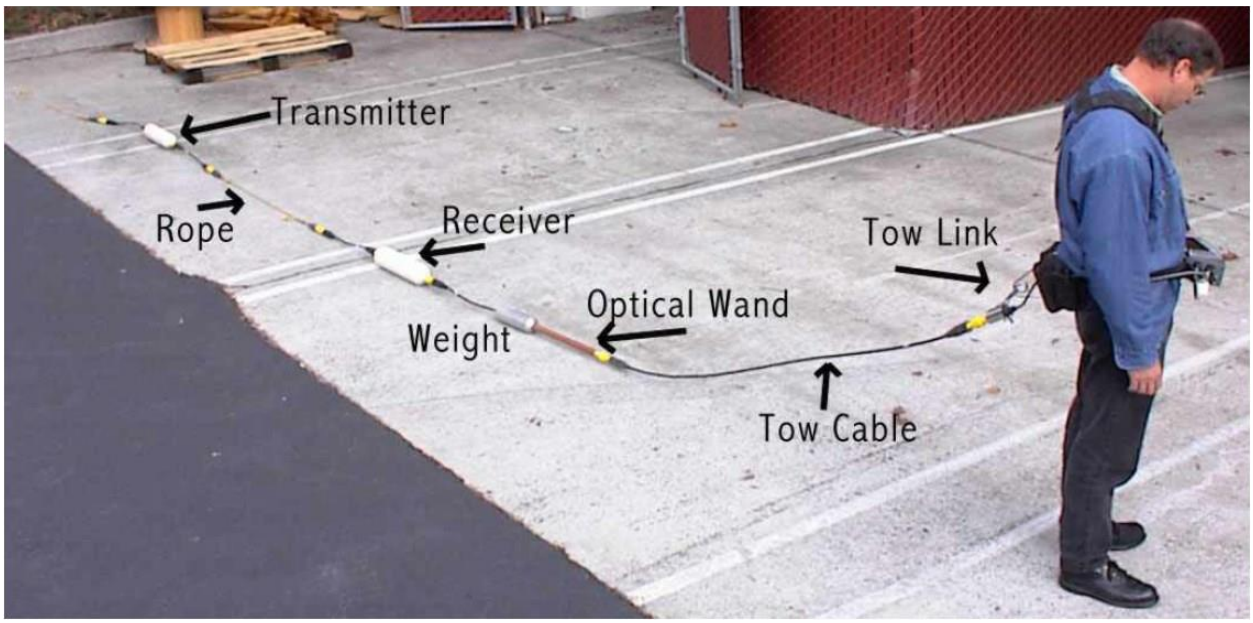

Figure 2-22 - Geometrics OhmMapper (Dipole-Dipole CCR configuration) towing setup (Geometrics, 2001)

Resistivity values are engineering values, themselves, but can be used with local ground truth information, such as bore logs, trenches and construction documentation to determine the underlying material types at a survey site. Resistivity methods are particularly effective at detecting the presence of water or shallow bedrock, since these materials represent very sharp contrasts compared to clays and silts.

Figure 2-23 - CCR used to measure electrical resistivity at the toe of a levee close to the Mel Price Lock and Dam in Edwardsville, IL

2.2.1.5.3 Previous Resistivity Studies Aimed at Determining Soil Type

There have been many attempts to identify soil type based on its resistivity magnitude. Piegari and Di Maio (2013) were able to derive an empirical relationship between soil resistivity and suction using a combination of Archie (1942) and Van Gnuchten (1980) models on a series of laboratory and field experiments. According to the field studies conducted by Besson et al (2004), electrical resistivity can be used to describe the structure of the tilled soil. Additionally, Seladji et al. (2010) investigated the effect of soil compaction on electrical resistivity in a series laboratory experiments. The authors focused on agricultural samples of clay and loam with organic content and analyzed the effect of soil microstructure, organic matter and saturation level on the measured electrical resistivity. While they were able to fit a model to their results, the results indicated a further need for investigation of low saturation soils and the effects of organic matter on the electrical resistivity of soil.

There have also been several efforts to relate field resistivity measurements to soil type or soil classifications. Two of the more significant studies were conducted by Kaufman and Hoekstra (2001) and Palacky (1987). Their results are summarized in Table 2-2.

Table 2-2- Resistivity ranges of different soil types

Soil Type	Soil Classification	Resistivity (Ω.cm) (Kaufman and Hoekstra, 2001)	Resistivity (Ω.cm) (Palacky, 1987)
CLAYS	CH	1,000-5,000	300-10,000
	CL	2,400-6,000	-
	OL	2,650-7,500	-
SILTS	ML	2,650-7,250	-
	SC	4,650-17,800	-
	MH	7,150-24,000	-
SAND	SM	9,600-45,250	47,500-1000,000
GRAVEL	GW	56,300-91,800	47,500-1,000,000
	GC	12,900-40,500	-
	GP	91,500-233,250	-

According to Kaufman and Hoekstra (2001), there are overlaps between many of the different soil types. Moreover, Palacky (1987) published a different range of values for similar soil types. He measured much lower resistivity values for clays, while his measured lower bound resistivity for sand surpassed the upper bound resistivity measured for sand by Kaufman and Hoekstra (2001). According to Palacky, gravels can have much higher resistivity compared to what was published by Kaufman and Hoekstra (2001). These two publications show some of the complexity of deriving soil type and geotechnical properties from electrical resistivity data measured in the field.

3 Methodological Approach

Many researchers have worked over the past seven decades to interpret the results of non-destructive geophysical testing methods for engineering purposes. Most of these researchers conclude that there is a need for more work in this area (Seladji et al., 2010, Samouelian et al., 2005, Piegari and Di Maio 2013). Based on the documented literature, electrical resistivity methods including ERI and CCR and seismic methods including MASW, and FWI were determined to be the most effective geophysical techniques for assessing levees and detecting potential subsurface defects. Therefore, the project focused on testing and analyzing the soils at two different sites (Kinion Lake Dam and the Mel-Price Wood River Levee System) using these particular methods.

As it is very challenging to understand the effect of various geotechnical parameters on electrical resistivity using field measurements where soils can be highly variable, the resistivity of different benchmark soils was first measured under controlled laboratory conditions. This laboratory investigation of resistivity provided the opportunity to examine the effect of temperature, water quality, soil type, density and water content to better understand the range of resistivity values possible for a particular soil. The methodology and details of the benchmark

materials used in this laboratory approach are described in the following section. The details of the two field studies including the setup, equipment, and methods used are also given below.

3.1 Laboratory Resistivity Testing

To measure the electrical resistivity of the soil, a Nilsson Resistance Meter Model 400 attached to a M.C. Miller Large Soil Box in a Wenner 4-electrode array (Figure 3-1) was used. According to ASTM G57 - 06(2012), the electrical resistivity of a soil specimen in this configuration is

$$\rho = R \cdot A/a \qquad (3\text{-}1)$$

where R is the electrical resistance measured between the two inner electrodes in Ohms (Ω), A is the cross-section of the soil specimen in cm^2 and a is the distance between the inner electrodes in cm. For the soil box used, the distance between the inner electrodes is 12.8 cm and the cross section is 12.8 cm^2 which gives the cross section to length ratio (A/a) of 1 cm. For this setup, the magnitude of the measured electrical resistance (R) in Ω is the same as the magnitude of its electrical resistivity (ρ) in Ω.cm. To ensure consistency in measurements and control over parameters such as density, water content and degree of saturation, the following procedures were followed.

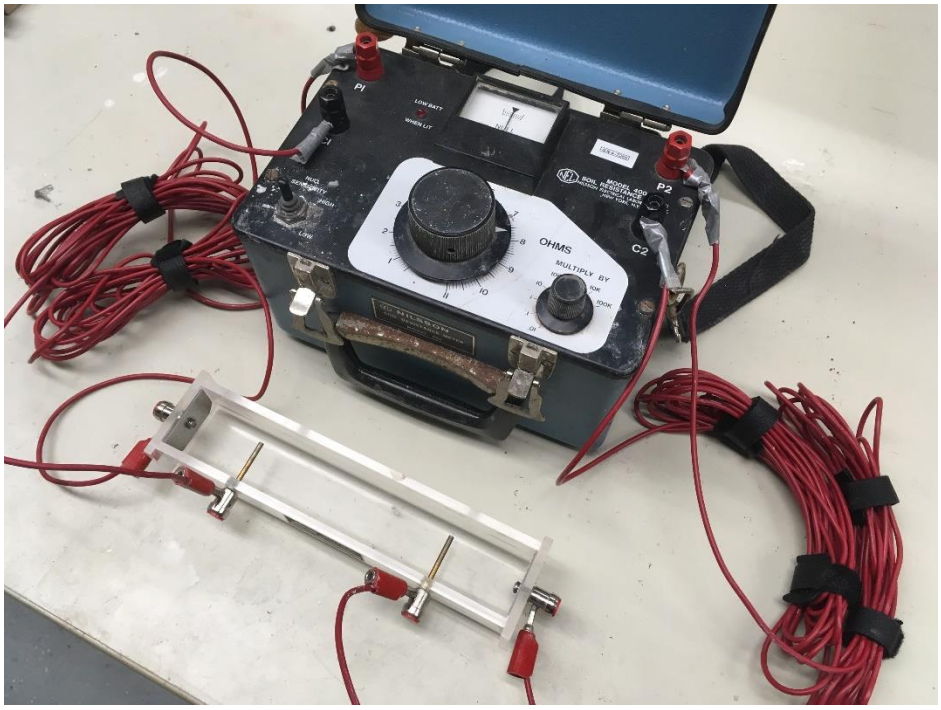

Figure 3-1 - Resistivity measurement setup

First, the water and dry soil mass were measured with a scale accurate to 0.01 g and were mixed thoroughly. The mixed soil was then sealed in a container and kept for at least 24 hours in a room with controlled temperature and humidity. To ensure the soil was at the target water content, it was weighed at the end of mixing and once more before the start of the test. A sample was also taken at the end of the test to verify the water content. Because of the many variables affecting electrical resistivity, it was critical to ensure that the specimen in the soil box was as uniformly placed as possible. To hit target densities, the total amount of the soil required to fill the box was calculated and placed in three equal layers. Once filled, the total weight of the soil box

was recorded for final density calculations and then the electrical resistivity and temperature of the specimen were measured simultaneously three times and then averaged. As soil temperature increases, its electrical resistivity decreases. Therefore, all of the resistivity values presented in this paper have been corrected to a common temperature of 15.5° C following Eq. 3.2 from ASTM G57-06 (2012)

$$\rho_{15.5}=\rho_t\ ((24.5+T)/40) \qquad (3\text{-}2)$$

where T is the temperature of the soil at the time of measurement and ρ_t is the resistivity of the soil at that temperature. $\rho_{15.5}$ is the corrected resistivity value at 15.5° C.

A total of nine different benchmark soils were made by mixing different portions of commercially available sand, Kaolin clay, Bentonite clay and red art clay. Deionized water was used for all of the tests to ensure repeatability. In Table 3-1, the composition of each benchmark soil is shown along with the measured index properties, as well as the range of densities and water contents in which each was tested. For the electrical resistivity measurements, each soil was tested at its loosest and densest possible compacted states corresponding to various water contents. Additional intermediate densities were also tested to obtain a representation of how electrical resistivity varies with density and water content. The dry density and corresponding water contents for the points tested are shown in Figure 3-2, where each benchmark soil is assigned a label according to its group symbol from USCS (ASTM D2487-11). The water content was varied from the driest possible state to a very wet state where electrical resistivity did not change with increased water content (AASHTO Standard T 288-12, 2012). The lowest tested water content for each soil type was limited by the equipment's maximum measurable electrical resistivity (1.1×106 Ω.cm) and was different for each soil type according to their physical properties. For example, the electrical resistivity of the poorly graded sand (SP) is measurable at a water content of 2% while the high plasticity silt (MH) required a water content of at least 6% for its electrical resistivity to be measurable using the current setup. The majority of soils in the field will likely be at water contents well above these thresholds.

Because it is known that the electrical resistivity of soil is a function of the resistivity of pore fluid, the effect of water composition was explored by comparing resistivity values for a common soil mixture with different water sources: distilled water, tap water from Arkansas, ground water from a well in Texas and ground water from a well in Arkansas. However, to ensure the consistency and reproducibility of the results for future studies, the remainder of the tests were carried out using deionized water.

As shown by Eq. 2, temperature is also known to affect the electrical resistance of different materials. In materials classified as conductors (e.g. copper), an increase in temperature is expected to increase the electrical resistance and in materials classified as insulators (e.g. glass), the opposite effect is observed. Since soils are mainly composed of insulators such as silicates, they are expected to have lower electrical resistivity at higher temperatures. To measure resistivity at different temperatures, the soil sample was compacted in the soil box, sealed and stored in a cold storage room until it reached the room temperature (5 °C), then it was removed from the room and tested continuously until it reached the ambient room temperature (21 °C). To measure electrical resistivity at higher temperatures, the sealed soil box was put in an oven at 30-40 °C for a short time. Once at equilibrium, the soil was removed and tested until it reached the ambient room temperatures again. It was important to cover the soil tightly between tests and while waiting to reach the target temperatures to avoid evaporation as much as possible.

Table 3-1 - Material description, index properties, and density and moisture conditions for the soils tested

Soil Type	Composition (% mass)				Index Properties							Testing range	
	Sand	Kaolinite	Bentonite	Red Art Clay	LL (%)	PL (%)	PI (%)	Gs	D_{90} (μm)	D_{50} (μm)	D_{10} (μm)	Bulk Density (kg/m^3) $\times 10^3$	w (%)
SP	100	0	0	0	-	-	-	2.67	850	440	240	1.63-2.00	2-20
SP-SM	90	10	0	0	-	-	-	2.66	800	380	100	1.12-2.11	4-16
SP-SC	90	8.5	1.5	0	-	-	-	2.64	780	375	80	0.98-2.10	3-12
SC	70	25.5	4.5	0	28	15	13	2.70	730	320	-	1.09-2.15	4-18
SM	70	30	0	0	26	15	11	2.64	750	330	-	1.03-2.11	10-15
CL-1	0	0	0	100	38	19	19	2.77	25.4	7.8	0.49	1.13-2.10	2-39
CH	0	85	15	0	72	33	39	2.62	6.6	0.4	-	1.15-1.82	10-60
CL-2	30	70	0	0	48	24	24	2.60	550	1.8	-	1.06-1.94	14-30
MH	0	100	0	0	62	32	30	2.61	5.9	0.4	-	1.06-1.60	6-70

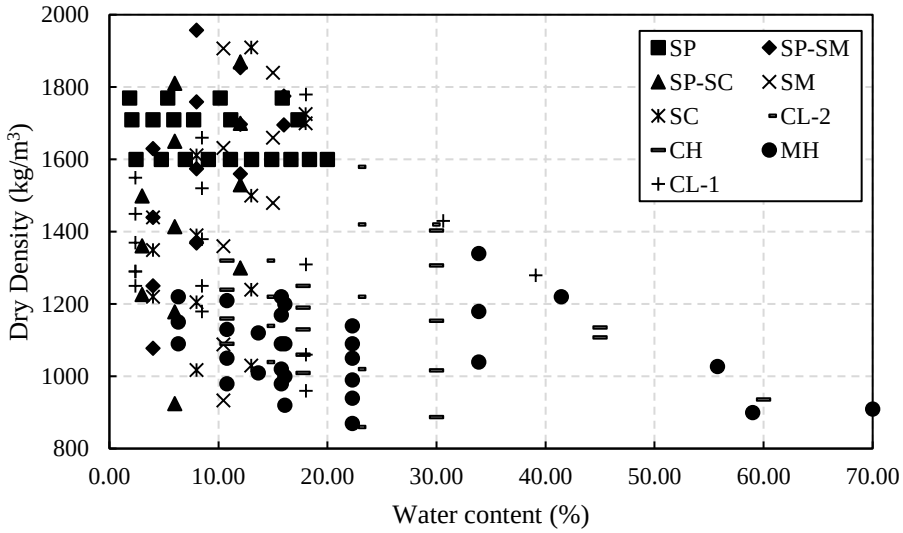

Figure 3-2 - Dry densities and corresponding water contents tested

3.2 Assessment of Kinion Lake Dam

3.2.1 Site Background

Kinion Lake Dam is a 342 meter long and 15 meter tall earthen dam located in Washington County, Arkansas (3-3). The local geology consists of an eroded plateau overlaying shales and sandstones with valleys cut into cherty limestone. Nearby bedrock outcrops consist of highly weathered limestone punctuated with fissures, joints, and caverns. This cherty limestone layer has an average thickness of 7 – 9 meters and the cherty gravel is typically filled with fines (NRCS,

2011).

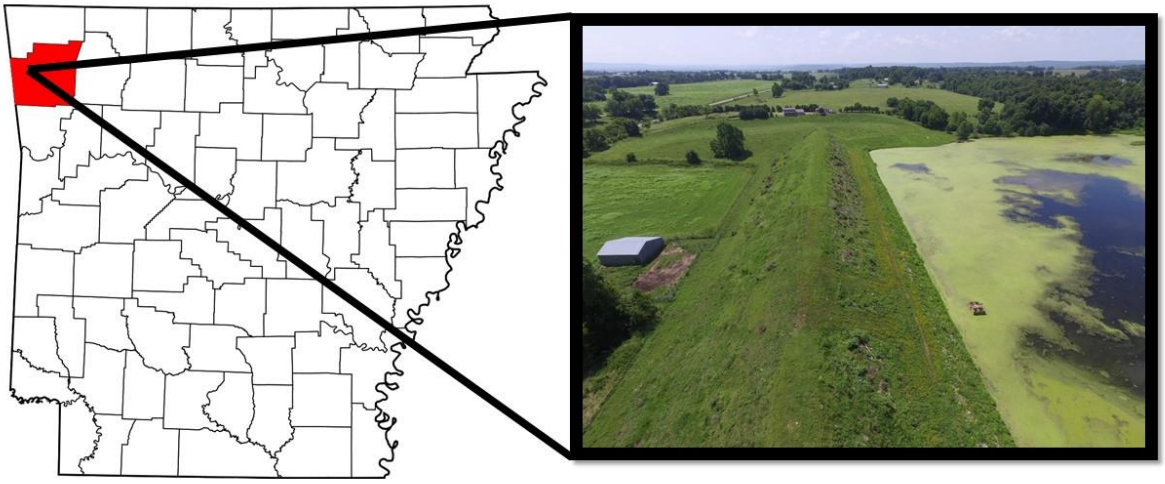

Figure 3-3. Location of Kinion Lake Dam in Washington County, Arkansas.

The dam was initially constructed in 1964 and immediately began experiencing seepage issues due to the local geology (NRCS, 2011). Prior to a 1969 drilling and grouting project, the structural integrity of the dam came under scrutiny as large sinkholes began forming, allowing large quantities of water to pass either through the dam, under the dam or through the abutments. This flow had the additional drawback of removing substantial quantities of fines from the interior of the dam and/or its foundation material (SCS, 1970). In 1969, Kinion Lake Dam was drilled and grouted in several locations along its length; however, it was unclear whether the grouting was successful because Kinion Lake experienced a severe drawdown due to a drought. Following the drought, seeps continued to form and in 1984, a foundation treatment consisting of backfilling the solution channels with high-plasticity clay and silt was performed and a foundation drain was installed (SCS, 1970). Even after these additional treatments, large seep areas continued to be documented, including a 20 feet wide seep that had broken the sod and jetted water six inches into the air. These seeps were in the same locations as those previously documented in the 1969 drilling report and the 1982 field inspection (NRCS, 2011). Additionally, the 1969 drilling explorations also located springs at the junction of the toe of the dam and the left abutment, seeps on the slope of the embankment, and a large spring with an estimated flow of 7500 liters per minute downstream (SCS, 1970).

Conclusions from the SCS (SCS, 1970), describe the bedrock under the dam as limestone with significant chert content and a general low resistance to weathering and ground water action. Solution cavities, infill of fines, and fractures made distinguishing between the bedrock and the gravelly soil overburden very difficult and somewhat ambiguous during drilling. This weathered bedrock foundation material allows almost unimpeded flow both through the dam and laterally, along cracks in the upper portion of the foundation. The bedrock profile under the dam, determined during the original 1963 evaluation, is shown in Figure 3-4. The contour of the bedrock was found

to be mostly level until inclining near the spillway, though some shallower regions were located at the 60, 140 and 180 m marks.

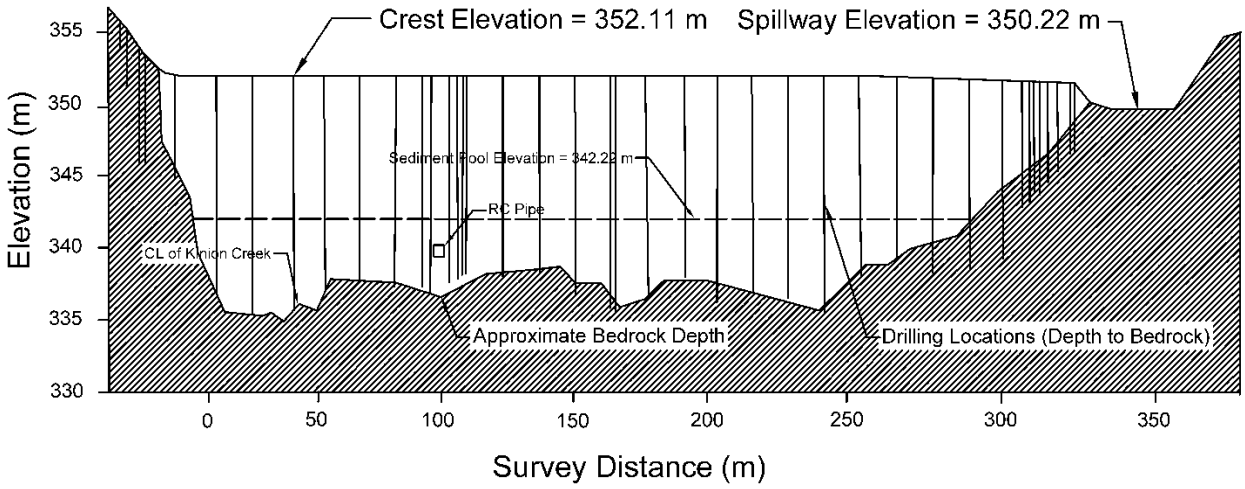

Figure 3-4. Bedrock profile modified from the 1963 drilling and grouting report showing depths to bedrock encountered during drilling (SCS, 1970).

3.2.2 Geophysical Investigation

The geophysical investigation of Kinion Lake Dam was conducted using a combination of geophysical methods including ERI, CCR, MASW, and FWI. The data were collected using each method over the period of approximately one year from July 2015 to March 2016. Data was collected along the centerline crest of the dam and along the downstream toe where seepage had been observed. The testing location along with testing parameters and data processing parameters are detailed for each method below.

Electrical resistivity is a quantification of how strongly a given material opposes the flow of electrical current. The electrical resistivity of earth materials can vary depending on the porosity, texture, degree of saturation, chemical makeup of the pore water, temperature, and clay content of the material (Kaufman & Hoekstra, 2001). However, in general resistivity values range from 10-20 Ohm-m for water, up to 75 Ohm-m for clays, from 26 – 240 Ohm-m for silts, 96 – 450 Ohm-m for sands and anything more resistive likely indicates an absence of water or an abundance of hard, resistive materials like gravels and rock (Kaufman & Hoekstra, 2001). As observed from these ranges, there is significant overlap between the different materials primarily depending on the degree of saturation of the material (Mofarraj, 2017).

Resistivity measurements are made in the field by inducing a current into the ground at one location and measuring the change in potential at another location. Traditional direct current ERI surveys are conducted using multiple stainless steel electrodes installed in the ground at a uniform spacing along a linear line for 2D surveys. Various measurements sequences including Wenner, Schlumberger, and dipole-dipole can be used in the field. The injection of current and measurement of voltage using multiple pairs of electrodes provides multiple readings of the apparent resistivity

of the materials at different depths. Through an inversion process, a model can be generated representing true resistivity with depth. CCR systems, on the other hand, are designed to be pulled along the ground rather than utilizing staked electrodes. The method works by inducing an alternating current via capacitive-coupling to the earth by a transmitting dipole and then measuring the potential using a receiving dipole. The measured voltage will be proportional to the resistivity of the earth between the two diploes and the current delivered by the transmitting dipole. The apparent measurement depth is determined by the dipole length and the distance between the receiver and the transmitter. Through an inversion process similar to what is used for ERI, the true resistivity with depth is determined. Testing at several sites has shown that the CCR response is nearly identical (within 2%) to that of a dipole-dipole DC resistivity measurement (Pellerin, et al., 2003). However, other work has shown differences between the two methods thought to be the result of violating assumptions (required low induction number, the source and receivers as line antennae rather than points, and effective dipole lengths) of the CCR theory (McNeill, 1980; Oldenborger, et al., 2013; Sapia, et al., 2017). One of the limitations of the CCR method (as seen in this dam investigation) is the shallower investigative depth of CCR (typically 6-15 meters versus 20 to >40 meters depth for ERI) (Asch, et al., 2008) but CCR typically provides better near surface resolution compared to ERI (Garman & Purcell, 2004).

Surface wave methods utilize the dispersive properties of surface waves (Rayleigh or Love) to determine the small strain shear wave velocity structure of the subsurface. Rayleigh waves have traditionally been the wave of choice for surface wave methods because Rayleigh waves are simpler to generate and sample in the field. However, Love wave use has increased significantly in the past decade. Love waves have been shown to provide more coherent data at difficult (i.e., shallow bedrock sites) sites and provide additional constraint to the inversion problem (Wood et al. 2014). Surface wave methods can broadly be split into two categories: (1) active source methods and (2) passive source methods. Active source methods are more commonly used for near surface site characterization whereas passive source methods are generally used for deep site characterization. Active source methods generally use a linear array of sensors to measure the phase velocity of waves emanating from a known source (typically located in-line with the array) and propagating past the receivers. By measuring the phase angles between sensors for a range of surface wave frequencies, an experimental dispersion curve is developed which relates surface wave velocity to frequency or wavelength. An inversion process is then used to develop the Shear Wave Velocity (Vs) profile at the site. This inversion process uses a numerical solution, which propagates Rayleigh or Love type surface waves over a layered half-space with each layer being assigned properties such as shear wave velocity, thickness, unit weight, and compression wave velocity. The numerical model solves for the theoretical dispersion of surface waves over this layered half-space. The theoretical dispersion curve is then compared to the experimental dispersion curve. Model parameters are updated until the theoretical dispersion curve matches the experimental dispersion curve for the site.

The MASW method (Park, et al., 1999) is an active source surface wave method that typically uses a linear array of 24-48 receivers to measure surface wave phase velocities in the field. Typically, a constant spacing between receivers is used along with a sledgehammer source to generate surface waves. Through a two dimensional transform such as the frequency-wavenumber transform, an experimental dispersion curve is developed. Several other dispersion analysis techniques exist (f-k, f-p, Park transform, beamformer) to process the raw signals recorded in the field. Despite the method used to generate the experimental dispersion curve, a fundamental or fundamental and higher mode inversion analysis is often used to match the experimental data and obtain a Vs profile. The Vs profile for the array is a function of the material over the lateral extent of the array. However, the 1D Vs profile generated from each analysis is considered to be more representative of the material located at the center of the array. To understand lateral variations in Vs using the MASW method, multiple tests are conducted by moving the receiver array forward or backward along a line and repeating the test. The multiple 1D Vs profiles are then stitched together along the survey line to create a pseudo 2D profile that describes the variation of Vs with depth and distance along the line. These pseudo 2D profiles can be particularly useful for mapping subsurface layers at a site. Typical shear wave velocity ranges include soft soils in the <180 m/s range, stiff soils between 180 and 360 m/s, highly weathered rock and dense soil between 360 and 760 m/s and weathered to fresh rock at anything greater than 760 m/s (ASCE, 2013).

3.2.3 Electrical Resistivity Imaging (ERI)

ERI surveys were performed from June 15-22, 2015, along the centerline crest and the downstream toe of Kinion Lake Dam using an AGI SuperSting R8/IP system. GPS locations for the electrode data were recorded and are shown in Figure 3-5. The dam crest survey consisted of a linear array of 112 electrodes at a 1.22 m spacing, while a 0.6 meter spacing was used on the downstream toe. To profile the entire dam while maintaining the higher resolution of close electrode spacing, a ¼ array (30 probes or 36 meter) roll along was conducted following each test setup. Testing was conducted using the Schlumberger and dipole-dipole configurations. The apparent resistivity data collected in the field was inverted using AGI EarthImager 2D CRP software. ERI data was collected and processed by the Natural Resources Conservation Service

(NRCS, 2016).

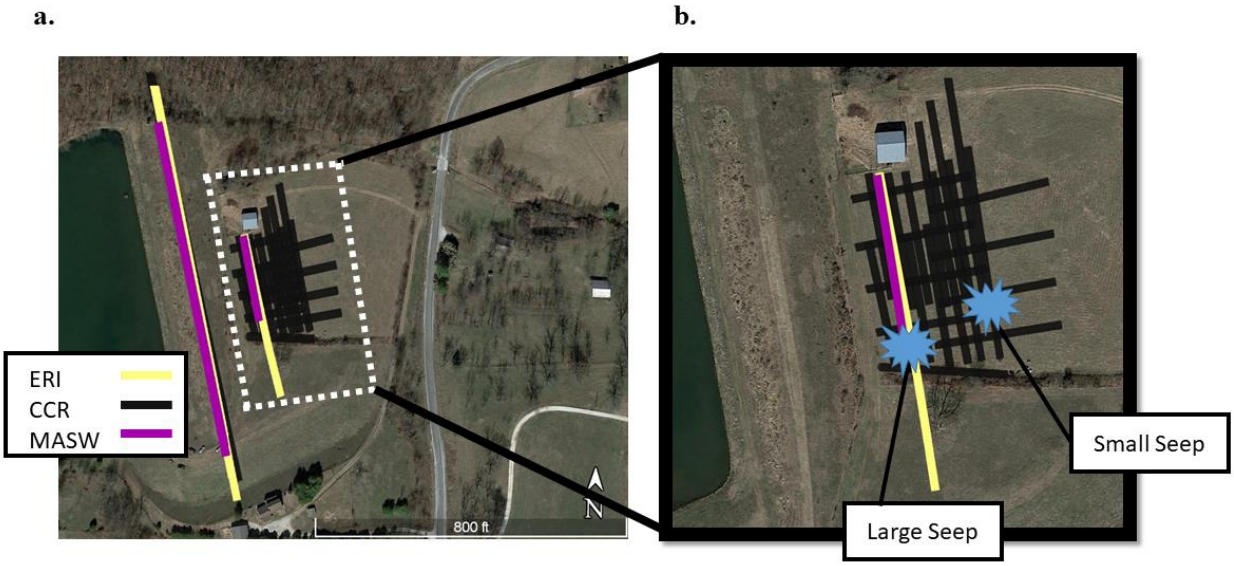

Figure 3-5. Survey locations for at Kinion Lake Dam lines a) Survey locations along the centerline crest of the dam and b) grid survey along the downstream toe (location of previous seepage is shown) (from Google Maps).

3.2.4 Capacitively Coupled Resistivity (CCR)

CCR surveys were performed on March 16, 2016 by University of Arkansas personnel, along the centerline crest of the dam using a Geometrics OhmMapper TR5 system (see Figure 3-6) which utilizes five receivers followed by a transmitter. The location of the operator was continuously recorded using a Trimble Geo7x GPS unit. To provide comprehensive measurements of the entire dam, dipole lengths of 5 meters and 10 meters in combination with rope lengths of 5 meter, 20 meter, 25 meter and 40 meter were utilized during testing. Short dipole lengths in combination with short rope lengths measure near surface materials while longer dipole lengths and longer ropes lengths measure deeper materials. A grid survey was also performed along the downstream toe of the dam (Figure 3-5b), overlapping with the previously performed ERI survey. A single

diploe length of 5 meters along with a rope length of 5 meters was utilized during testing.

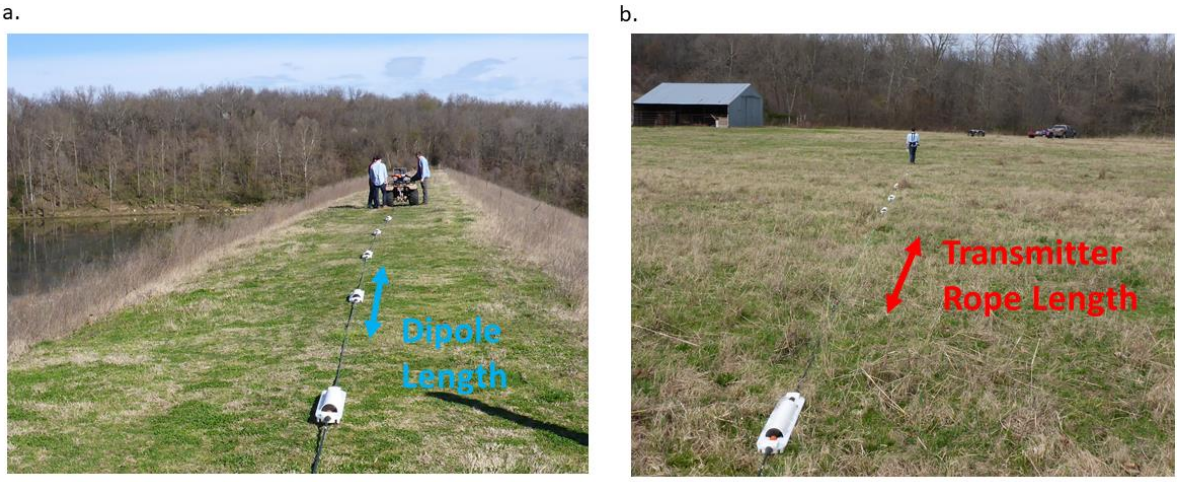

Figure 3-6. OhmMapper arrays: a) linear surveys pulled by ATV b) grid survey pulled by harness.

The raw OhmMapper data was first processed in Geometrics OhmImager to correct any metadata (rope-length, dipole length, operator offset) errors and to combine resistivity data for common locations before being exported to MagMap. MagMap was used to convert GPS data to UTM, remove dropouts and spikes from the apparent resistivity data, and export profile data for use in Res2dinv (Loke & Barker, 1996). Res2dinv uses a smoothness-constrained least-squares method incorporating damping factors to obtain an inversion solution (Loke & Barker, 1996). A 1.25 m cell size and large dataset optimization options (optimized Jacobian, fast, approximate Jacobian matrix calculation, and a sparse inversion) were utilized during the inversion.

3.2.5 Multichannel Analysis of Surface Waves (MASW)

MASW using Love and Rayleigh type surface waves, hereafter referred to as MASWL and MASWR, respectively, was performed along the crest of the dam and along the downstream toe on September 10th, and 15th, 2015, respectively. Testing was conducted by the University of Arkansas with testing locations shown in Figure 3-5. Surface waves were measured using a linear array of 48, 4.5 Hz vertical and horizontal geophones with a 1 m uniform spacing between geophones (a total array length of 47 m). The geophones were attached to a landstreamer system to increase the rate of testing. A sledgehammer source was used to generate Rayleigh waves (vertical hits, Figure 3-7a) and Love waves (horizontal hits, Figure 3-7b). For both tests, source positions of 10 meters and 1 meter from the first and last geophone, as well as at the quarter, half and three quarter points were utilized at each array location (i.e., a total of seven source positions for each array location). At each source position three sledgehammer blows were stacked to improve the signal-to-noise ratio of the data. After each setup, the array of receivers was pulled forward 24 meters, so that the first receiver would be located where the 24th receiver was located for the previous array (i.e., a 1/2 roll-a-along) resulting in ten setups total for the crest of the dam, and two setups along the downstream toe.

The experimental MASW data was processed using the frequency domain beamformer method in Matlab (Zywicki & Rix, 1999). Each 48 channel array was subdivided into 24, 24 channel sub-arrays each offset by one geophone (e.g. sub-arrays of channels 1 – 24, 2 – 25, 3 – 26, etc), allowing

for a dispersion curve to be obtained for every meter along the line, while reducing the number of array positions needed for testing. Offsets appropriate for MASW, (e.g. channels 1 – 24 include source locations of -10, -1, 36.5, 48, and 57 meters) were used for each subset of channels. Multiple source offsets are used as a means to: (1) identify potential near-field effects, (2) aid in selecting the fundamental mode of surface wave propagation, and (3) provide a robust means for estimating dispersion uncertainty (Cox & Wood, 2011). The maximum spectral peak in the frequency-wavenumber domain was picked automatically for each frequency to reduce user bias. Dispersion points clearly displaying near field effects, effective modes, or obvious inconsistencies were removed from the data. However, much of the "normal" dispersion scatter was left intact to estimate uncertainty. The composite dispersion curve was developed using all source offsets for a particular 24 channel subset. The data were divided into 50 frequency bins from 1-100 Hz using a log distribution. The mean and standard deviation were estimated for each data bin resulting in a mean experimental dispersion curve with an associated standard deviation. This mean dispersion curve was then inverted using the software package Geopsy (Wathelet, 2008). Multiple parameterization options (i.e., variations in the number of layers and potential thickness of those layers) were attempted for the datasets. The best parameterization was found to consist of 10 layers with each layer thickness allowed to range from 0-3 meters. The shear wave velocities of the layers were allowed to vary from 150 m/s to 3500 m/s. For each dispersion curve, 200000 Vs models were generated using the neighborhood algorithm in Geopsy. The goodness of fit was judged based on the misfit parameter (collective squared error between experimental and theoretical curves) and using visual inspection. The median of the 1000 best (lowest misfit) Vs profiles was taken as the 1D Vs profile for each sub-array. The individual 1D Vs profiles were combined together to develop pseudo 2D plots of the variation of shear wave velocity with distance along the line and depth.

3.2.6 Full Waveform Inversion (FWI)

The same seismic dataset collected for the MASWR was analyzed using the FWI method (Tran and McVay, 2012; Tran et al, 2013; and Tran and Luke, 2017). The method is based on a finite-difference solution of 2-D elastic wave equations to generate synthetic waveform data, and Gauss-Newton inversion technique to update material properties (Vs and Vp) until the difference between synthetic and field measured data is negligible. The MASWR dataset was recorded for 70 shots (10 landstreamer setups and 7 shots each setup), and 68 of them were used for the waveform analysis. The first and last shots (no receivers within 10 m from the shots) were removed, because the FWI method requires a dense source-receiver configuration. The total analyzed distance is 265 m along the dam.

To avoid incorrect local solutions, an appropriate initial model was developed with a consult of the spectral analysis of the measured data, waveform analysis was done in sequence of increasing frequencies (starting with low frequency data which requires a less detailed initial model). The 1-D initial model was established with Vs of 300 m/s on the surface and linearly increased to 900 m/s at 24 m depth, for the entire domain of 265 m (no lateral variation). The depth of 24 m was taken as about a half of the landstreamer length (47 m). The Vp initial model was generated from the Vs profile and a Poisson's ratio of 0.3. Two inversion runs were performed with central frequencies of 15 and 25 Hz, with the lower frequency run first. The bandwidth for each central frequency was 30 Hz with 15 Hz on each side. For example, with the central frequency of 25 Hz, measured signals from 10 to 40 Hz were considered, but signals lower than 10 Hz or higher than 40 Hz were removed by low- and high-pass filtering.

For inversion, the 24 m depth x 265 m length domain was divided into 6360 cells of 1.0 m x 1.0 m. The cell size of 1 m was selected to be the same as the geophone spacing. Vs and Vp of cells were updated simultaneously during inversion. The mass density throughout the domain was kept constant at 1800 kg/m3. Analyses at 15 Hz and 25 Hz were both stopped after 20 iterations, when the change of the least-squares error from one iteration to the next is small (less than 1%). It was found that Vs and Vp inverted results are very consistent. Therefore only Vs profile is included in this paper for comparison with other results.

3.3 Assessment of Mel-Price reach of Wood River Levee

3.3.1 Site Background

The Melvin Price reach of the Wood River Levee System is an approximately 4 km long and 10 meter tall earthen levee located along the Illinois side of the Mississippi River outside the town of Alton, as shown in Figure 3-7. The local geology consists of Mississippian St. Louis formation limestone bedrock at a depth of approximately 40 meters, overlain with approximately 30 meters of gravelly sand and topped with silty clay. Explorations in the area have found these layer thicknesses to be highly variable both along the length of the levee and perpendicular to it.

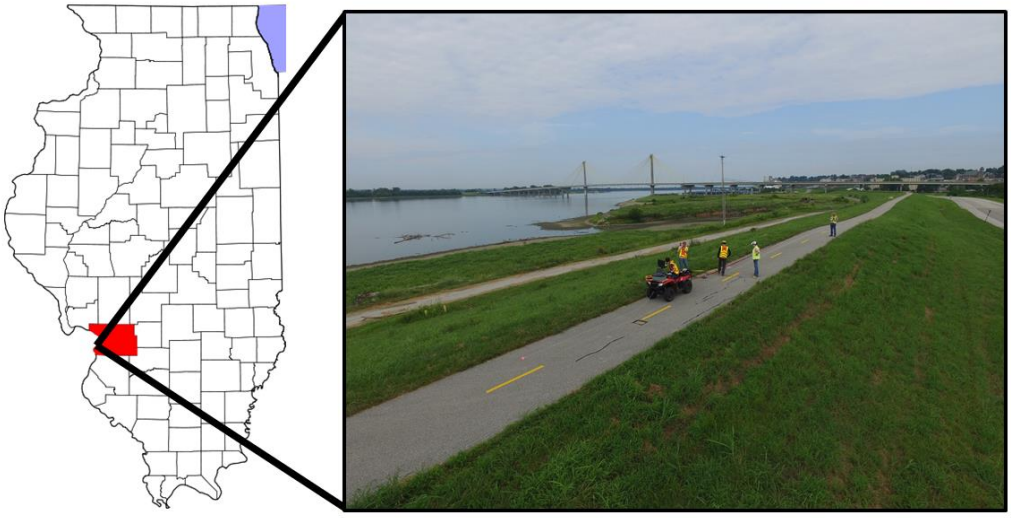

Figure 3-7. Location of the tested section of the Wood River Levee System in Madison County, Illinois

The Melvin-Price lock and dam was initially constructed in 1979 and opened in 1994 and served as a replacement of an older dam located two miles upriver (Shown in Figure 3-9). The typical section of the Melvin-Price Levee consists of a clay cap from the surface to a depth of approximately 2 m, a thin filter layer if needed, followed by a sand core layer from 3-10 m, as shown in Figure 3-9 (USACE 2016). The clay cap layer just covers the top and the riverside of the levee. This is common where clay material is scare and the major portion of the levee must be built of other material such as sand. In addition, if the difference in soil gradation between the clay cap and the sand core is great, there is a need for a filter layer to prevent migration of the fine material into the sand core.

After construction, a permanent pool of water began to form from Stations 0+00 to 115+24, effectively moving the river bank further inland. In 2009, clear flowing seepage was found on the dry-side of levee indicating significant amounts of under seepage below the levee. LIDAR and visual inspection identified numerous sand boils (the result of under seepage) between Stations 60+00 and 110+00, as shown in Figure 3-8. To remedy the under seepage and prevent possible erosion, the head differential between the river and the dry-side of the levee was reduced by establishing a permanent pond. While this ponding will reduce the rate of seepage, it removes the ability to visually monitor problem areas/boils. The existence of old river meanders and previous erosion are believe to contribute to the problems observed along the levee. An aerial photo taken in 1941, prior to the construction of the levee, indicates three river meanders crossing the current location of the levee. This figure illustrates the complex nature of this portion of the levee.

Figure 3-8. Melvin-Price Lock and Dam and Wood River Levee system. Levee centerline stationing and sand boil locations are shown (USACE, 2016).

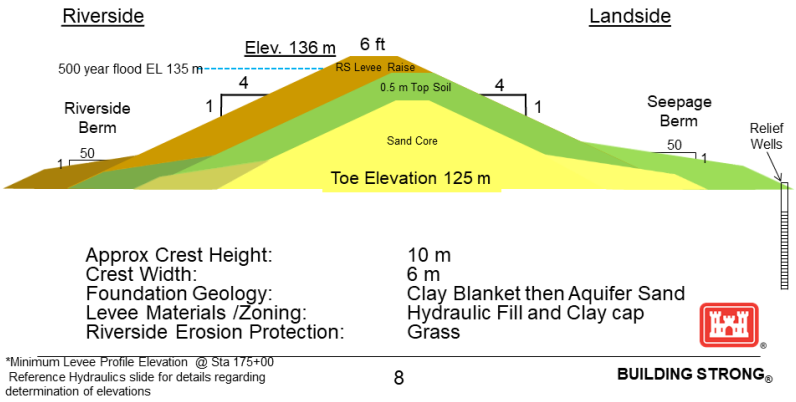

Figure 3-9-Typical levee section for the Mel-Price reach of the Wood River Levee System (USACE, 2016)

Figure 3-11-Aerial photo taken in 1941 of the future location of the Mel-Price reach of the Wood River levee with the levee stations overlaid.

3.3.2 Geophysical Investigation

The geophysical investigation of the Mel-Price Reach of the Wood River Levee system (referred to as the levee hereafter) was conducted using a combination of geophysical methods including CCR and MASW from August 8-11, 2016. Data was collected along the centerline crest

of the levee (which is defined as the top of levee hereafter), along the landside of the levee (opposite the river) where seepage and flooding had been observed, along a line formed by the previous CPT soundings and along portions of the bank of the river which is defined as riverside. The testing locations along with testing parameters and data processing parameters are detailed for each method below.

3.3.3 Capacitively-Coupled Resistivity (CCR)

CCR surveys were performed along the top, landside, and riverside of the levee using a Geometrics OhmMapper TR5 system. The GPS locations for the survey paths were recorded using a Trimble Geo7x GPS unit and are shown in Figure 3-10**.** Figure 3-10 represents the survey paths for the CCR along with the locations of the crossing utilities. The OhmMapper works by utilizing five receivers to detect current injected into the ground via a transmitter at varying rope lengths as shown in Figure 3-10. To provide comprehensive measurements of the entire levee, dipole lengths of 5 and 10 meters in combination with rope lengths of 2.5, 5, 20, 30 and 40 meters were utilized during testing. Varying the dipole and rope lengths allows the survey to assess materials at varying depths, i.e. short dipole lengths in combination with short rope lengths measure very near surface materials while longer dipole lengths and longer ropes lengths measure deeper materials.

Figure 3-10. Survey paths for MASW and CCR at Mel Price Reach of the Wood River Levee

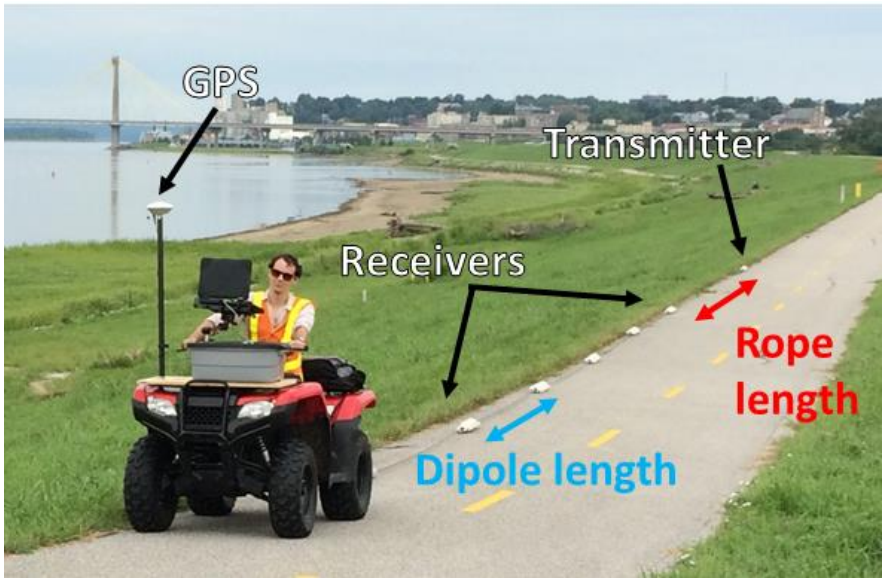

Figure 3-11. OhmMapper system pulled by ATV.

The raw OhmMapper data was first processed in Geometrics OhmImager to correct any metadata (rope-length, dipole length, operator offset) errors and to combine resistivity data for common locations before being exported to MagMap. MagMap was used to convert GPS data to UTM, remove dropouts and spikes from the apparent resistivity data, and export profile data for use in Res2dinv. Res2dinv uses a smoothness-constrained least-squares method incorporating damping factors to obtain an inversion solution (Loke & Barker, 1996). Res2dinv's large dataset optimization options (optimized Jacobian, fast, approximate Jacobian matrix calculation, and a sparse inversion) were utilized during the inversion. Profiles were ultimately generated using triangulation with linear interpolation, 0.5-meter vertical cell sizes and resistivity contours approximated material changes.

3.3.4 Multichannel Analysis of Surface Waves (MASW)

Similar to the CCR survey, MASW using Rayleigh type surface waves (V_R) was performed along the top, the landside, and the riverside of the levee. This testing was conducted by University of Arkansas personnel with the testing locations shown in Figure 3-10. Surface wave testing was conducted using a linear array of 24, 4.5 Hz vertical geophones with a uniform spacing between geophones of two meters (a total array length of 46 meters) as shown in Figure 3-12. The geophones were attached via a landstreamer system to increase the rate of testing. A sledgehammer source was used to generate Rayleigh waves. Source positions of 5, 10 and 20 meters from the first geophone were utilized at each array location (i.e., a total of three source positions for each array location). At each source position, three sledgehammer blows were stacked to improve the signal-to-noise ratio of the data. After each setup, the array of receivers was pulled forward to the next testing location. Testing locations were spaced at 30 meters for the top, 50 meters for the riverside of the levee, and 25 meters for the landside of the levee so that midpoints of each setup would be spaced at a consistent interval. A total of 202 MASW setups were conducted along different parts of the levee. Table 3-2 provides a summary of these testing locations. The locations and survey paths for each part of the MASW experiments are shown in Figure 3-10. Once the field tests were done, the following procedures were followed for analyzing MASW data sets.

Figure 3-12. MASW parameters on the CPT line.

The experimental MASW data was processed using the frequency domain beamformer method in Matlab combined with the multiple source offset method (Zywicki & Rix, 1999, Wood and Cox, 2011). Multiple source offsets are used as a means to: (1) identify potential near-field effects, (2) aid in selecting the fundamental mode of surface wave propagation, and (3) provide a robust means for estimating dispersion uncertainty (Cox & Wood, 2011). The maximum spectral peak in the frequency-wavenumber domain was picked automatically for each frequency to reduce user bias. Dispersion data points can be fundamental, effective and higher modes. Generally, the fundamental mode is the dominant for most frequencies of interest (Foti, 2014). In this investigation, the fundamental mode approach was used as the preferred mode for inversion process. Dispersion points from the field data clearly displaying near field effects, fundamental and higher modes, or obvious inconsistencies were removed from the data. However, much of the "normal" dispersion scatter was left intact to estimate uncertainty. In Figure 3-13a**,** the experimental dispersion data for station no. 96+00 along the landside of the levee is shown as an example. The dispersion data contains both fundamental and higher modes. The final experimental dispersion curve that was extracted from the raw data is shown in Figure 3-13b. The higher mode data and data effected by potential near field effects were removed in the final dispersion curve. For each station, the final dispersion data from all source offsets was divided into 100 frequency bins from 1-125 Hz using a log distribution. The mean and standard deviation was estimated for each data bin resulting in a mean experimental dispersion curve with associated standard deviation.

Table 3-2 Summary of the MASW surveys

Location	Number of MASW experiments	Total path length (m)	Estimated depth of exploration (m)
Top	108	3250	25
Landside	42	1025	30
Riverside 1	35	1700	25
Riverside 2	17	800	10

The mean dispersion curve was then inverted using the software package Geopsy (Wathelet, 2008). Multiple parameterization options (i.e., variations in the number of layers and potential thickness of those layers) were attempted for the datasets. The best parameterization was found to consist of 11 layers and extending to a depth between 10-30 meters with thicknesses increasing at a rate of 1.25 per layer (i.e. a layer ratio of 1.25 (Cox and Teague 2016). The shear wave velocities of the layers were allowed to vary from 100 m/s to 400 m/s in the top three meters, 100 m/s to 800 m/s in the next six meters, 100 m/s to 1000 m/s from 8 to 15 meters and then 100 m/s to 2000 m/s until bedrock or very hard material. These velocity ranges were chosen to match the material type as shown for a typical levee section in Figure 3-9.**Error! Reference source not found.** provided by USACE (2016). For each dispersion curve, 110,000 Vs models were searched using the neighborhood algorithm in Geopsy. The goodness of fit was judged based on the value of misfit parameter (collective squared error between experimental and theoretical curves) and by comparing the experimental and theoretical dispersion curves by eye. The median of the 1000 best (lowest misfit) Vs profiles was taken as the 1D Vs profile for each setup location. Shown in Figure 3-14 is the resulting 1000 best fit Vs profiles, median Vs profile, lowest misfit Vs profile, and the associated standard deviation for the station 96+00 for the landside of the levee as an example. The individual 1D Vs profiles were combined together to develop pseudo 2D plots of the variation of shear wave velocity with distance along the line and depth using triangulation with linear interpolation in the Surfer software (Surfer® 14 ,Golden Software, LLC*).*

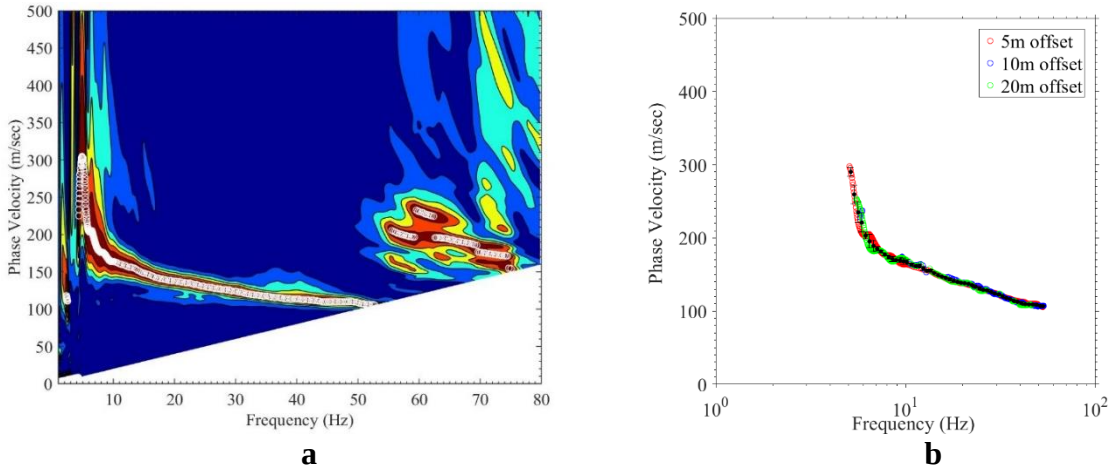

Figure 3-13. Typical experimental dispersion data points for station 96+00 for the landside of the levee a) Raw and b) Refined.

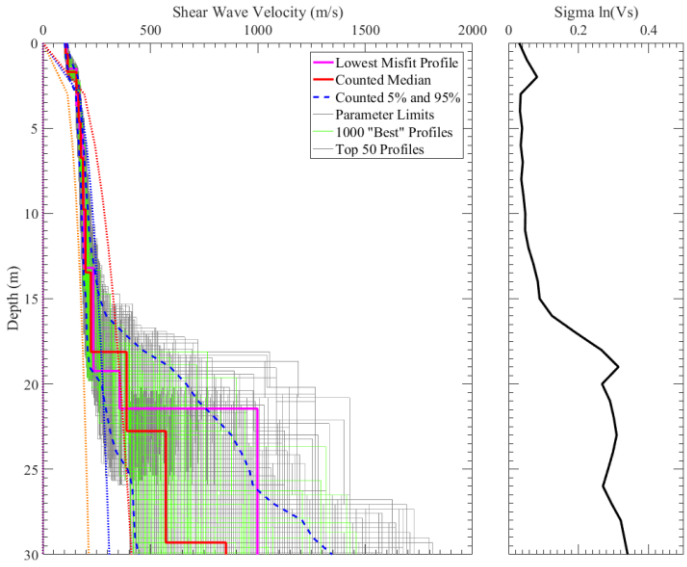

Figure 3-14. Result of inversion process for the station 96+00 located on the landside of the levee.

4 Results/ Findings

Following the methodologies described above, the laboratory and field studies were carried out over the course of two years. The laboratory resistivity findings are discussed first, followed by the results from the field studies at Kinion Lake Dam and the Mel-Price reach of the Wood River Levee.

4.1 Laboratory Resistivity Testing

As discussed several geotechnical parameters were examined to better understand their effects on the resistivity of different soils. Along with measuring the resistivity of different soil types according to the USCS, the effects of water composition, temperature, density, saturation and volumetric water content are also investigated.

4.1.1 Water composition

The variation of electrical resistivity for the SP soil using different water sources and saturations is presented in Table 4. Degree of saturation greatly influences the electrical resistivity, regardless of water composition; electrical resistivity changing from approximately 90,000 to 7,000 ohm.cm from 10% saturation to fully saturated condition. As shown in Table 4-1, deionized water results in the highest resistivity as it introduces the least amount of ions to the mixture. The smallest resistivity measurement was measured for the well water from Texas. Another interesting observation is that while pore water composition significantly affects the resistivity at low degrees of saturation, it does not seem to play a major role when the sand is saturated. As shown, using deionized water results in the highest resistivity measurements, which should be taken into account when natural soils are tested and compared to the benchmark samples.

Table 4-1 - Effect of water type on resistivity of sand (SP) (γd = 1600 kg/m3)

Water Type	Saturation (%)	Resistivity (Ω.cm)
Distilled Water	10	93000
Tap water - Arkansas	10	88000
Well water- Arkansas	10	80000
Well Water - Texas	10	75000
Distilled Water	100	7520
Tap water - Arkansas	100	7500
Well water- Arkansas	100	7400
Well Water - Texas	100	7110

4.1.2 Temperature

The effect of temperature on the resistivity of two different soil types (SP and SP-SM) is shown in Figure 4-1, where the points represent the laboratory measurements and the dotted line represents the prediction of Eq. 2 based on the resistivity estimate at 15.5 °C.

It can be seen that there are slight deviations from Eq. 2 for temperatures lower than 10 °C; however, the relationship works well for the ambient laboratory temperatures at which the rest of the measurements were taken in this study (15-23 °C).

Based on the data, a decrease in temperature from 20 °C to 5 °C can increase the resistivity by roughly 50%. Therefore, all of the values reported in the following sections have been transformed to the equivalent resistivity value at 15.5 °C using Eq. 2. Seeing the effect of temperature on electrical resistivity, it is recommended that the temperature in the field be approximated for any future studies aiming to interpret field measurements using laboratory data. The electrical resistivity data presented in the following section is the resistivity at 15.5 °C while in the field, a range of temperatures can be experienced depending on parameters such as seasonal and daily changes in solar radiation, slope orientation, thermal conductivity of soil, water content and vegetation cover (Florides & Kalogirou, 2005). Despite its complexity, there are several models available in the literature which can help estimate ground temperature at various depths in different seasons such as those presented by Mihalakakou et al. (1997) and Kusuda & Achenbach (1965).

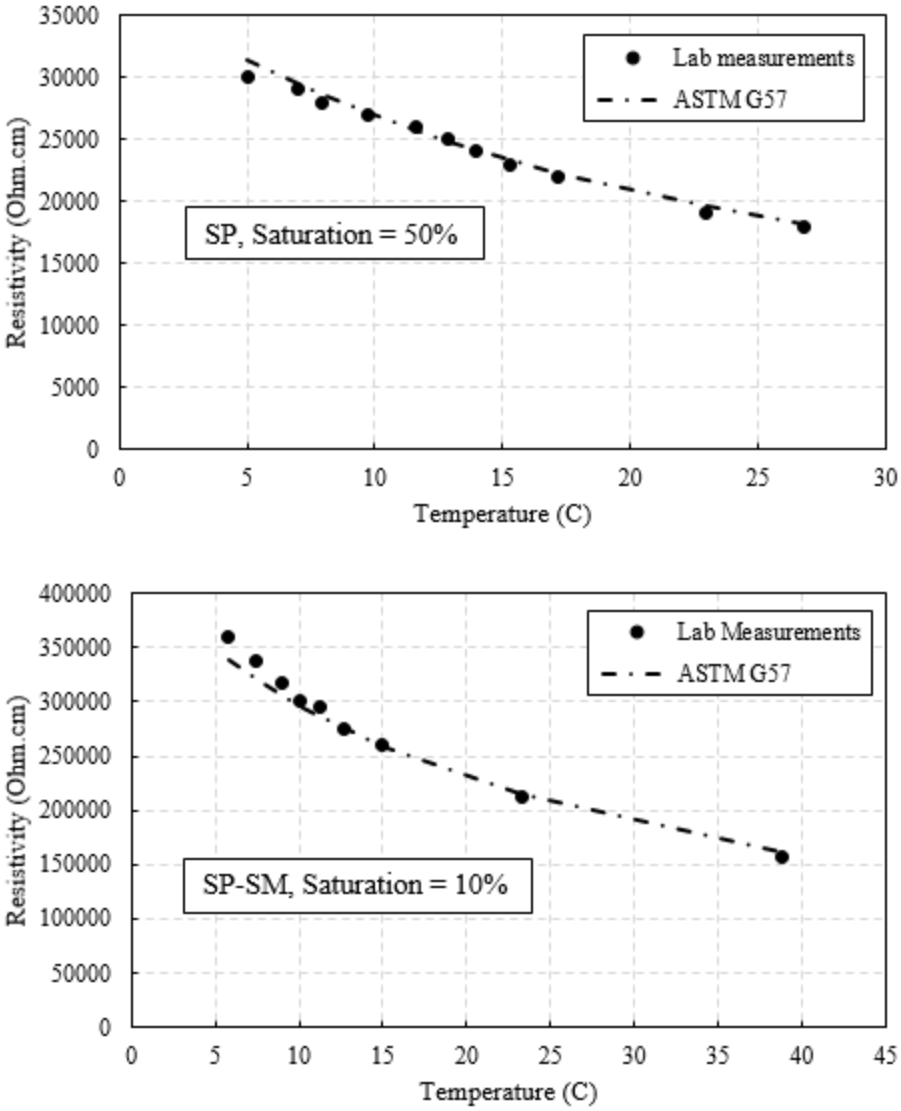

Figure 4-1 - Effect of temperature on resistivity

4.1.3 Degree of saturation, dry density, bulk density, and volumetric water content

As discussed, each soil was tested at various combinations of densities and water content, which resulted in several options for plotting the data. Resistivity values were plotted versus the degree of saturation, bulk density, dry density, and the volumetric water content to examine how the electrical resistivity measurements were influenced by moisture and density and to identify any trends (Figure 4-2). Plotting these various combinations was also important because of the large range of possible resistivity values for a given soil type.

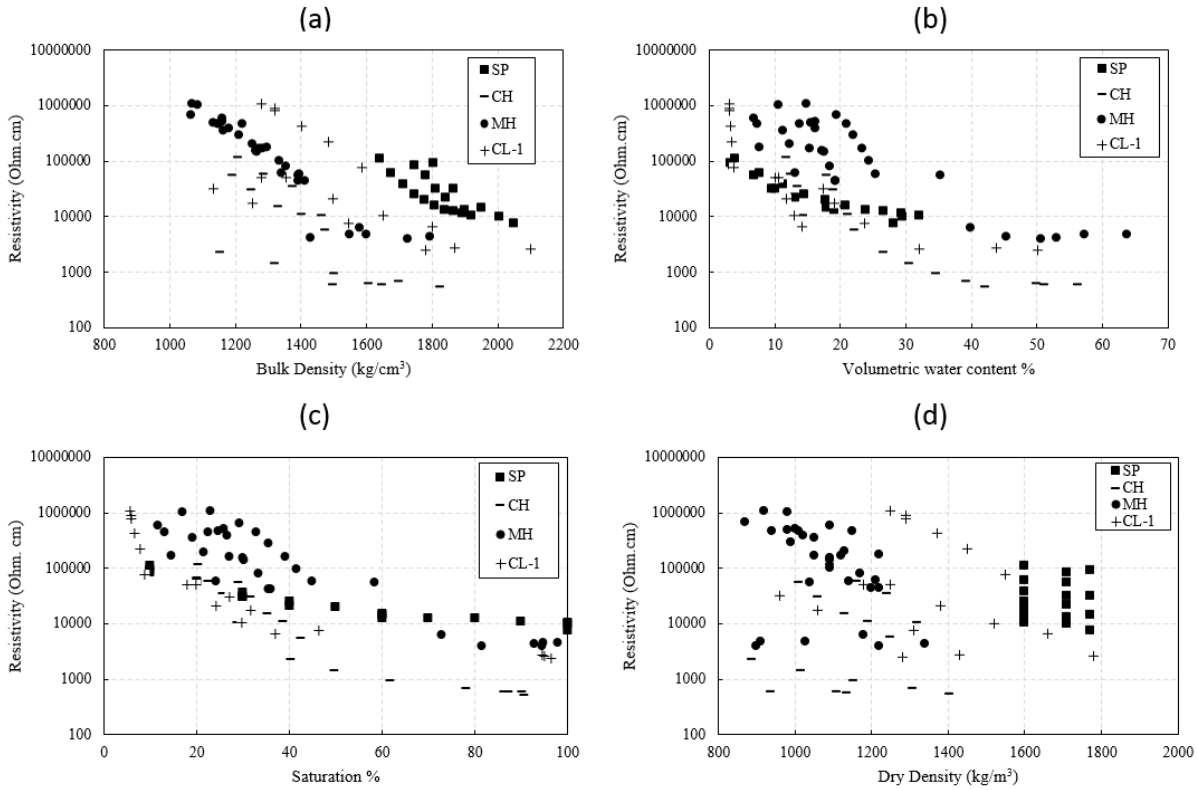

Figure 4-2 - Effect of bulk density (a), volumetric water content (b), saturation (c) and dry density (d) on resistivity of different soils

The bulk density and corresponding resistivity results for SP, CL-1, CH and MH soil types are displayed in Figure 4-2 (a). As can be seen, the non-plastic soil type (SP) lies in the upper right boundary of the plotted results while the soil type with highest PI (CH) occupies the lower left side of the plotted data and the MH and CL-1 soils occupy the area in between. The MH soil type has a higher PI than CL-1 (Table 3-1) and in Figure 4-2 (a) generally lies closer to the CH soil as compared to CL-1. Although some of these soils overlap each other in some locations, there appears to be a correlation between PI and the parameters plotted in Figure 4-2 (a). This likely indicates that bulk density could be used as a parameter for predicting soil type for soils that are not in a saturated condition. One disadvantage of this parameter from a field testing standpoint is that it would require some measure of in situ bulk density to single out a soil type, which requires another test to be conducted.

The relationship between resistivity and volumetric water content was also investigated (Figure 4-2 (b)). As can be seen, soils have a big range of resistivity for volumetric water contents below 25%. However, the effect of volumetric water content becomes limited on electrical resistivity for water contents above 30%. Although generally electrical resistivity decreases with an increase in volumetric water content, it cannot be concluded that the sample with lower electrical resistivity necessarily has higher volumetric water content. This is especially true for silts and clays where the minimum electrical resistivity (at saturation) is lower than the electrical resistivity of water alone. Moreover, it can be seen in Figure 4-2 (b) that the different soil types plot very close to each other when volumetric water content is used. Therefore, although volumetric water content provides a better correlation with resistivity in

comparison with dry density, it would still be hard to identify the type of soil based on this parameter.

As shown in Figure 4-2 (c), an increase in the degree of saturation leads to a decrease in resistivity for all soil types. Additionally, the minimum recorded resistivity for each soil (generally for degrees of saturation above 60%) decreases as its plasticity index (PI) increases. For example, the minimum resistivity observed for the high plasticity clay (CH) which has the highest PI is much lower than the minimum resistivity observed for the other soils tested. This trend could potentially help distinguish between high and low plasticity soils in saturated or close to saturated conditions.

The resistivity values were also plotted with the corresponding dry densities (Figure 4-2 (d)). It is evident from Figure 4-2 (d) that there is little correlation between dry density and the resistivity of soil since a soil's resistivity can vary several orders of magnitude at a specific dry density due to change in water content. Therefore, even if the dry density were known, it would be impossible to identify the soil based on its resistivity and dry density alone.

Although the dry density alone would not be a good indicator, it was proposed that a combination of degree of saturation and dry density might give the necessary information to distinguish between soil types. The effect of saturation and dry density on the resistivity of SP, CH, MH and CL-1 soils is shown in Figure 4-3. It shows that although the saturation is the major factor that affects resistivity, some soils are heavily influenced by their dry density (e.g. MH), whereas some are minimally affected by it (e.g. SP). Another important observation is that for each soil, there appears to be a limit saturation level above which the resistivity does not change significantly. At this level, dry density also does not affect the resistivity, which indicates that different densities could not be identified for a given soil in a saturated condition.

More importantly, these plots show that soil type could be narrowed down significantly if resistivity were known for the soil in its saturated condition. For example, a saturated sample with a resistivity value near or above 10,000 Ω.cm would likely be a sand and a saturated sample with a resistivity value below 1,000 Ω.cm would likely be a CH. This saturated condition could be assumed for soils below the water table and could perhaps be useful for non-destructive field-testing. The difference in the resistivity values for the saturated MH and the saturated CL-1 is not as well defined; however, the difference in the resistivity values at high and low saturation levels is drastically different. Therefore, identifying a particular soil is much more likely if resistivity values were known at two drastically different saturation levels (i.e. at perhaps 20% and 60% or

greater). While this is easy to do in the laboratory, it is not as practical in the field, especially for soils below the water table.

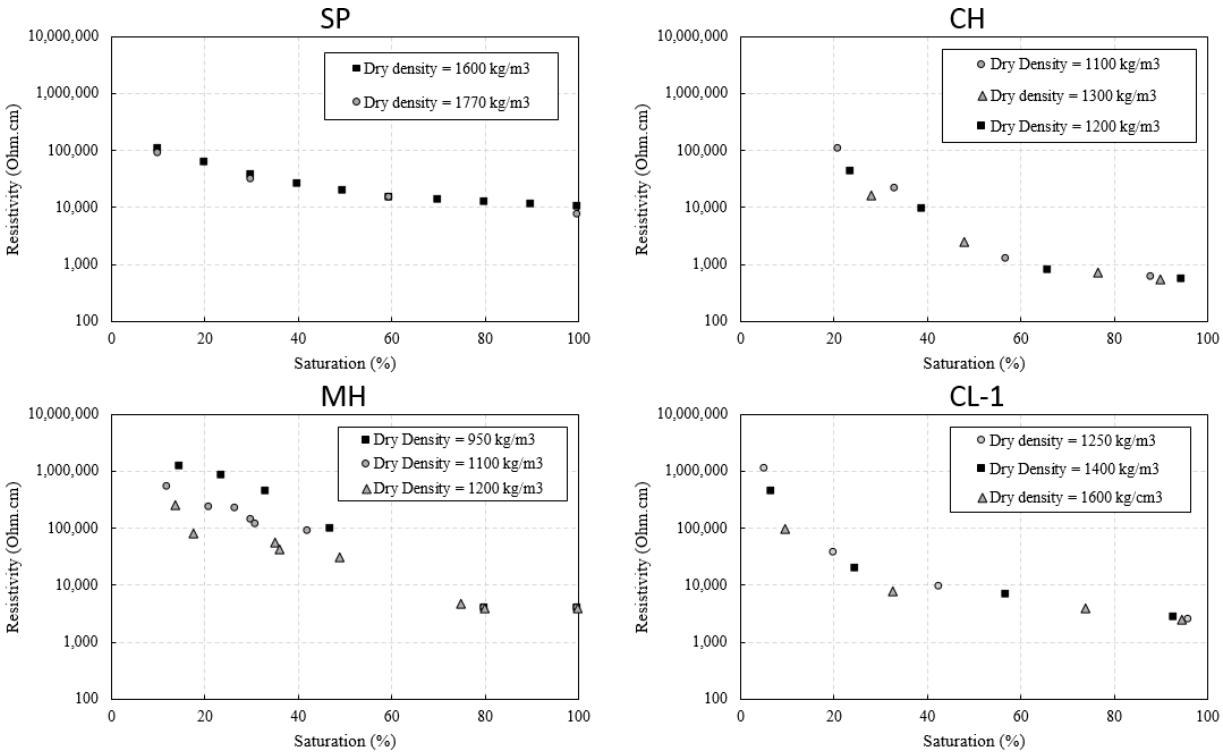

Figure 4-3 - Effect of saturation on different soil types at different dry densities

Although some correlation between each parameter and the measured resistivity is observed, the two parameters that were determined to be the most effective in identifying soil type were the degree of saturation and the bulk density. The best estimate of soil type can be made by using a combination of these two parameters and the corresponding resistivity values. To demonstrate this, the bulk density plot (Figure 4-2 (a)) was regenerated and the samples with the highest and lowest saturation values were identified using hollow markers and labels of the percent degree of saturation. While it was not true for all the soil types, highest and lowest saturations typically corresponded with some of the highest and lowest bulk densities. As shown in Figure 4-4, the regions for each of the various soil types is well defined with only a few samples as exceptions. The diagonally oriented zones move from right to left as PI increases. The results indicate that soil type can be greatly narrowed down and even possibly identified if even an estimate of the degree of saturation and/or bulk density can be made.

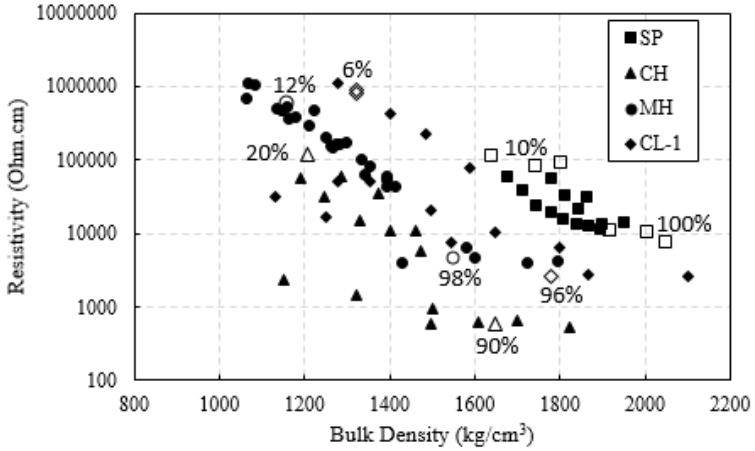

Figure 4-4 – Comparison of resistivity values and corresponding bulk density and saturation values (numbers inside the plotting area indicate degree of saturation for the hollowed out symbols)

As seen in Table 3-1, some soils were made by mixing different proportions of sand and Kaolin clay or sand, Kaolin clay and Bentonite clay to obtain the different major group classifications according to USCS. The resistivity measurements for SP,SP-SM, SM, MH and CL-2, i.e. Sand-Kaolin clay mixes, are shown in Figure 4-5. When resistivity is plotted as a function of bulk density, the SP soil type is somewhat separated from the other soils (Figure 4-5 (a)). Considering the samples with higher bulk densities, the resistivity values decrease as the fines content of the mixes increase. Figure 4-5 (b) shows that if the degree of saturation is known, it is possible to distinguish soil type using resistivity. As can be seen, if the soil is saturated under approximately 60%, the higher the fines content, the higher its electrical resistivity will be. However, close to saturation this relationship is inversed and soils with higher fines content show less electrical resistivity. This is because when Kaolin clay is relatively dry and in powder from, it has many air voids that increases the resistivity of the material. However, as the water content increases, ions will be able to travel more freely in the pore spaces, resulting in a lower resistivity. Therefore, the difference between the resistivity values of these mixes in a saturated condition is likely attributed to the difference in their mineralogy, while the difference in resistivity values in a drier condition is likely more related to the air void volume.

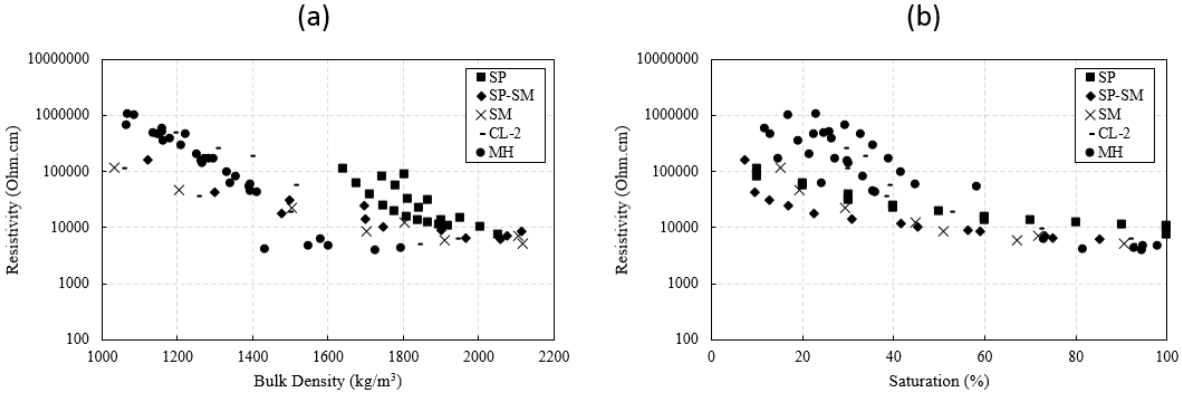

Figure 4-5 - Resistivity of Sand – Kaolin clay mixes with respect to bulk density (a) and degree of saturation (b)

The results for Sand-Kaolin clay-Bentonite clay mixes are displayed in Figure 4-6. A similar correlation is observed where SP (Sand) and CH (Kaolin clay-Bentonite clay) are the clear outliers at relatively high bulk densities and saturations. In general, for the bulk density data, higher plasticity soils tend to plot closer to the lower left corner while non-plastic soils plot to the upper right. Although a large number of benchmark samples were tested, it is important to examine these findings further using several natural soils.

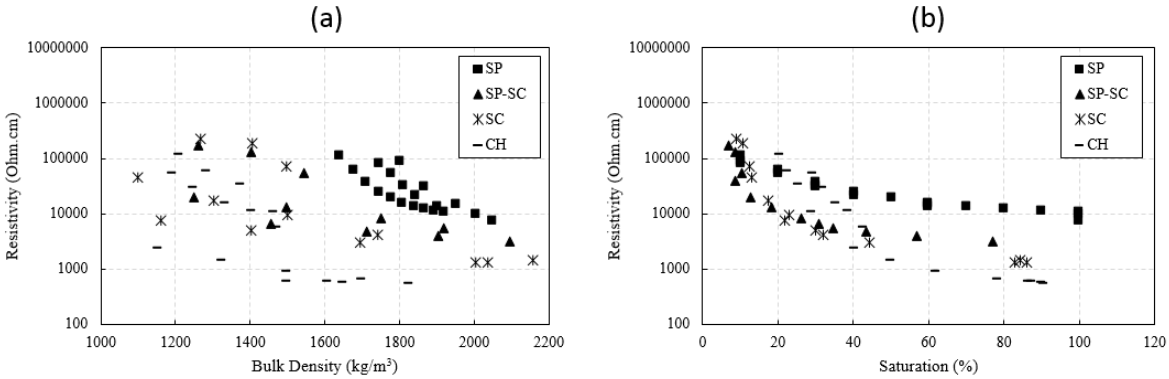

Figure 4-6 – Resistivity of Sand-Kaolin clay-Bentonite clay mixes with respect to bulk density (a) and degree of saturation (b)

4.1.4 Verification studies

Three cases were considered to assess the practicality of using the benchmark soil data in identifying soil types for natural field retrieved soil samples. For the first case, a clay sample obtained in Monticello, AR was considered. The soil was compacted in the soil box at the natural water content of 36.17 % to a bulk density of 1890 kg/m3, similar to the measured in situ bulk density (1878 kg/m3). The measured resistivity was 617 Ohm.cm. From Figure 4-2, it is evident that only a CH soil type has a resistivity lower than 1000 Ohm.cm. The sample indeed classified as a CH and neither water content nor density were necessary to determine the soil type for this sample because of the significantly low value of resistivity.

For the second case, a natural clay sample was tested at a water content of 8.35% and at densities of 1125.9 kg/m3 and 1415.37 kg/m3. The measured resistivities were 70,050 and 11,832, respectively for the two cases. Following the suggestions above, the sample was also tested at a higher water content of 36.01% and a bulk density of 1701.4 kg/m3 and the resistivity was found to be 1,504. Figure 4-7 shows these samples plotted with the benchmark sample results. The classification can be narrowed down to either a CL or CH based on the first two points. Considering the third point at the more saturated condition, the sample would likely be a CL. The sample actually classified as a CL, with a liquid limit of 36 and a plasticity index of 16. Therefore, the benchmark samples also appear to provide a means of identifying the classification for soils falling within the more difficult range. While the moisture content and densities can be varied for a field retrieved sample, examining a soil at different densities would be impractical in a single field study. These types of comparisons were simply made to examine the ability of the developed plots to capture soil type, similar to a blind study. As more and more natural samples are added in the future and adjustments are made to the relationships, it is likely that a clearer distinction could be made.

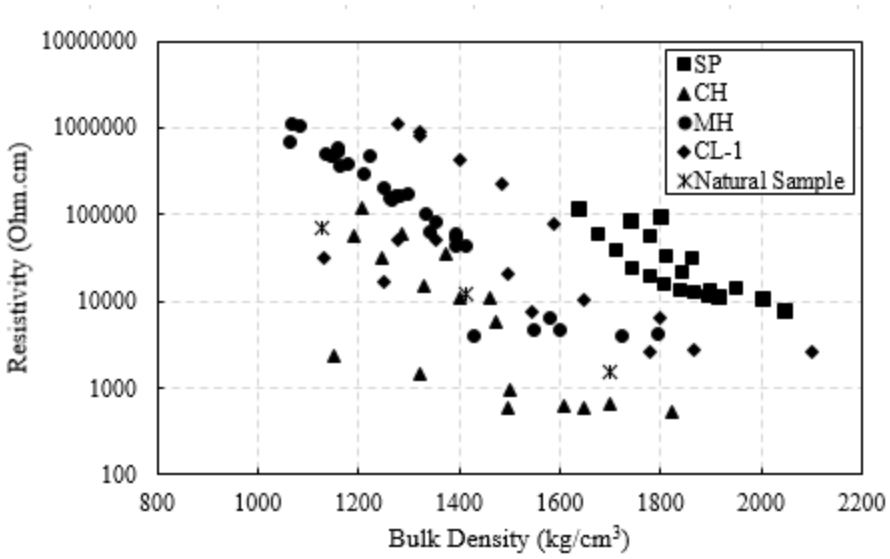

Figure 4-7 – Results of the natural soil sample plotted along with other major soil types

For the third case, a natural soil known as Hillside red clay (common in Arkansas) was investigated. This soil is generally a mixture of red clay and fragile cobbles of chert. The soil was sieved using a #10 sieve to separate the larger pieces of rock. The resulting sample had a fines content of 92.60%. The liquid limit was found to be 66 and the plasticity index was found to be 37, resulting in a USCS classification of CH. The resistivity of the soil was measured at a relatively high water content (+35%) The results of these tests along with the results obtained for other major soil types are presented in Figure 4-8.

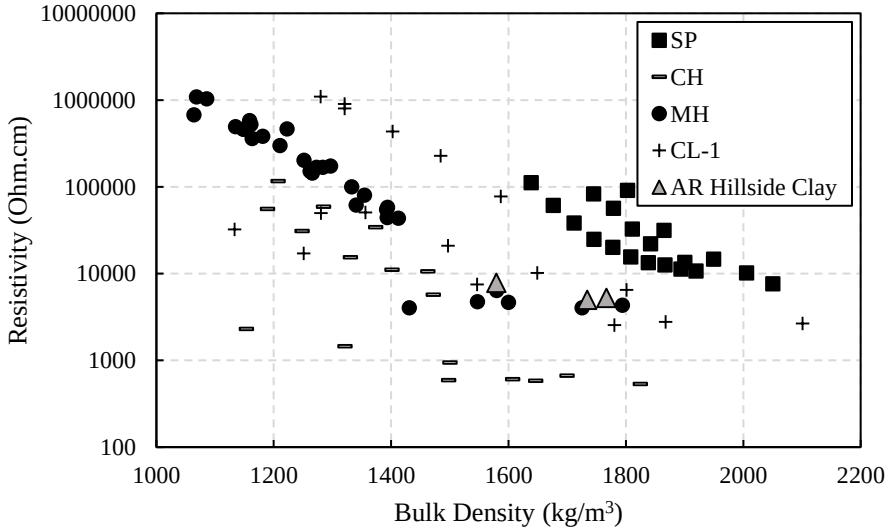

Figure 4-8 - Results of the Arkansas Hillside clay plotted along with other major soil types

Despite the CH classification, it can be seen that this soil overlaps the results of the MH benchmark sample. A comparison of the Atterberg limits of the three soils on the typical plasticity chart reveals that they are all very near the A-Line (Figure 4-9). However, one of the

main reasons this soil behaves like a MH according to the resistivity measurements may be due to the existence of small grains of chert mixed with the red clay.

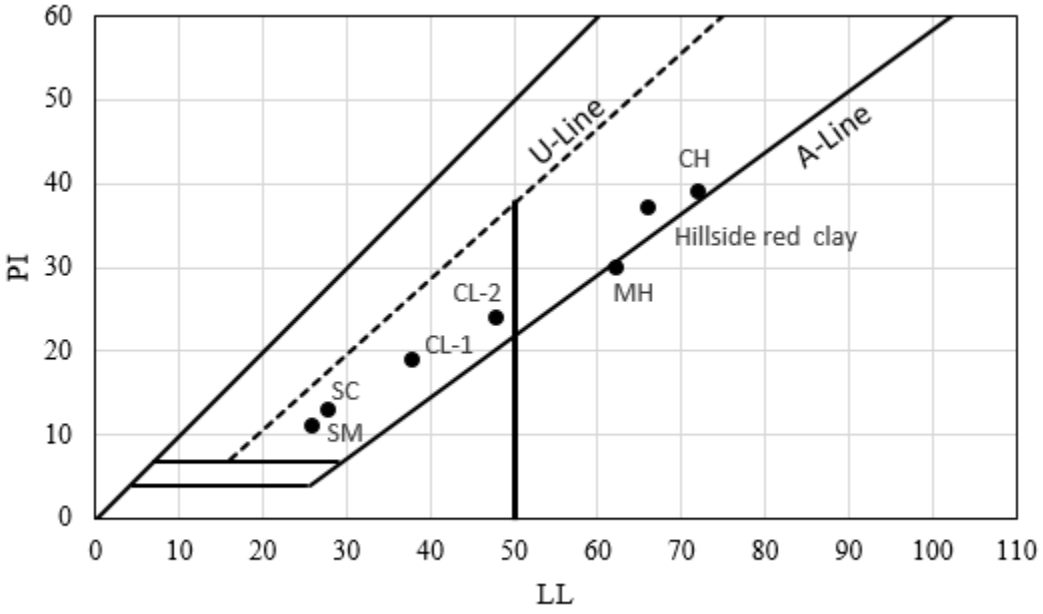

Figure 4-9 - Atterberg limits of different soil types used in this study

For the third case, two different sands, designated as SP-1 and SP-2, from Arkansas were tested at high and low water contents and densities. It was observed that these soils show higher resistivities (10,000-20,000 ohm.cm higher) compared to the benchmark SP sample when saturated. However, it is still evident from Figure 4-10 that these two cases lie closest to the benchmark SP sample compared to the other soil types. It is likely that the higher resistivity measurements may be due to slight difference in mineral composition, gradation and perhaps even fines content.

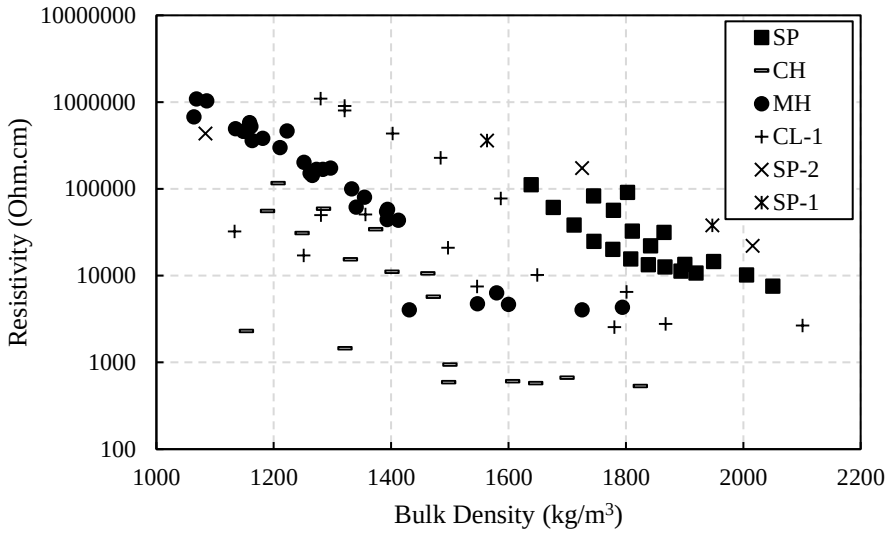

Figure 4-10 – Results of two different types of sands from Arkansas (SP-1 and SP-2) plotted along with other major soil types

4.1.5 Additional Considerations

As discussed, the only ML that could be sourced as a benchmark sample was a processed kaolin clay. This soil classified as ML with a liquid limit of 34 and a plasticity index of 6. The results are presented in Figure 4-11 along with the results of the CH benchmark soil. As shown in the figure, the processed kaolin clay is indistinguishable from the CH soil and appears very differently from the unprocessed kaolin (MH). Further analysis of the kaolin clays through Energy-dispersive X-ray spectroscopy (EDX) revealed that the unprocessed Kaolin was a sodium-potassium (Na^+-K^+) kaolinite with 25% sodium and 11% potassium cations while the processed Kaolin was a sodium-calcium (Na^+-Ca^{2+}) kaolin with 33% sodium and 24% calcium. Therefore, despite the similar name, mineralogicaly speaking they are different soils with different cation exchange capacities (CEC). The presence of Ca^{2+} cations in the processed kaolin likely causes the lower resistivity compared to the unprocessed kaolin. This finding reveals the importance of mineralogy in the measured resistivity of soils.

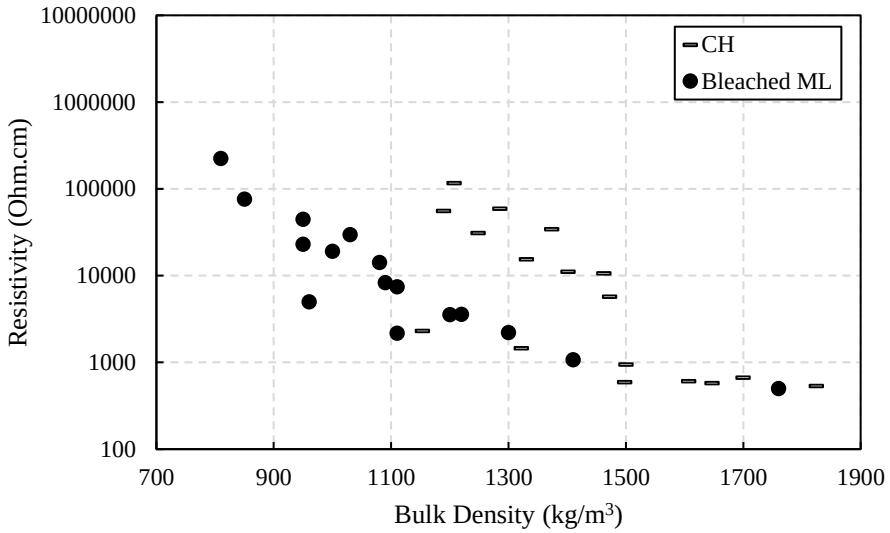

Figure 4-11 - Resistivity of processed Kaolin clay in comparison with the CH soil type

4.1.6 Application

After gaining an understanding of the effect of various parameters on the resistivity of soils, this knowledge needs to be applied to the interpretation of resistivity data collected in the field. As seen in Figure 4-2 and Table 4-1, when the soil is below the water table, the measured resistivity is not sensitive to the density, water content and water quality. Therefore, if the location of the water table is known, the soil type for soils below the water table can be distinguished. Under this condition, a chart in the format of Figure 4-12 shall be used to predict soil type. As can be seen, most of the soil types tested can be easily distinguished based on their resistivities under saturated conditions.

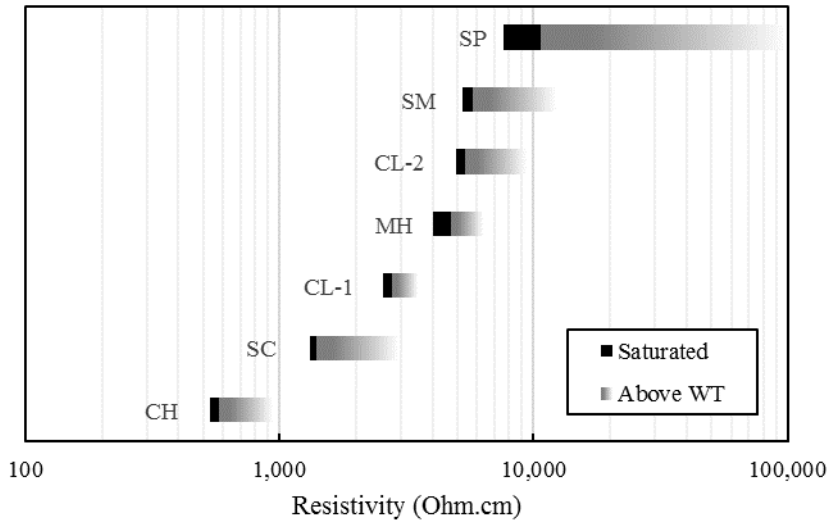

Figure 4-12 - Expected resistivity for different soil types above water table (up to approximately 25m)

Distinguishing soil types above the water table is more challenging due to the broader range of water content and the increased effect of density on resistivity. Moreover, matric suction will cause water to rise above the water table at different heights depending on the soil type and particle sizes. However, several steps could be taken to simplify this part as well. For example, it is known that water does not rise in sands more than one meter (for typical gradations in nature), while clays may remain at water contents close to saturation for tens of meters above the water table (Fredlund et al., 2012). It should be noted that other phenomenon such as rain, flooding, extreme heat or humidity could alter the moisture content of these soils and should be carefully considered when planning a resistivity survey. Therefore, under normal conditions and having known the depth of water table, sands should show the whole range of their resistivity in the first meter above the water table (10^4-10^5 ohm.cm); any sand more than one meter above the water table is likely to have a resistivity in the order of 10^5 ohm.cm. However, clays hold water contents close to saturation tens of meters above the water table and the actual height depends on their soil water characteristics curve (SWCC). As can be seen in the generic SWCC plots presented in Figure 4-13, clays can be assumed saturated up to 10 meters above the water table (98 kPa suction) and the suction decreases gradually above 10 meters although they still maintain a relatively high water content up to 100 meters (980 kPa suction) above the water table. As water tables deeper than 25 meters are hardly encountered unless it is extreme desert conditions, the results in Figure 33 were plotted for the depth of 25 meters to make it more applicable to typical field studies conducted for geotechnical purposes.

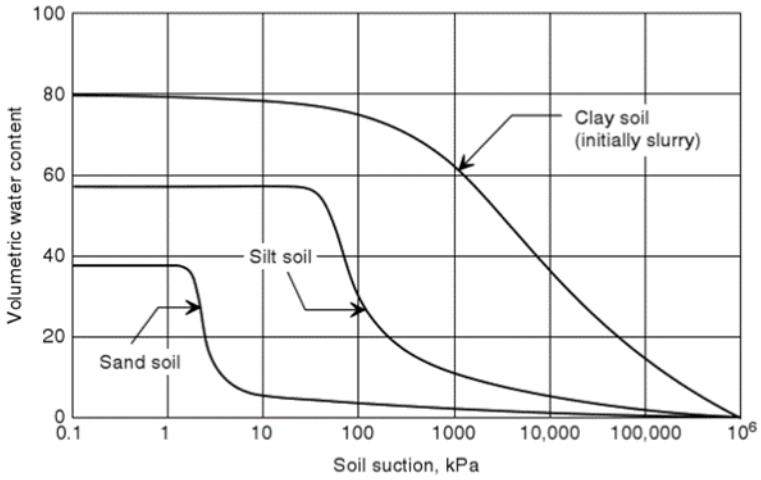

Figure 4-13 - Comparative desorption SWCCs for sand, silt, and clay soils (Fredlund et al., 2012)

Therefore, it is safe to use charts similar to Figure 4-12 to discern different soil types up to 25 meters above the water table. While most of the tested soil types do not have any overlap in their range of resistivities, some such as CL-2, MH and SM do. A closer look at the composition of these soils (Table 3-1) shows that they are all composed of Kaolinite. Therefore, resistivity is consistent for similar minerals and can perhaps give information about the mineral present.

4.1.7 Conclusions

Parameters such as temperature, saturation, volumetric water content, dry density, bulk density, and mineralogy (i.e. soil classification) were shown to influence electrical resistivity

measurements. Laboratory tests on the benchmark samples allowed for a better understanding of the effects of each of these parameters on the measured resistivity, so that the plots developed could be used to predict soil type for natural samples and for non-destructive field studies. Not only do the laboratory findings improve field estimates of soil type, they also impact several standardized laboratory tests routinely performed for material characterization. Temperature and density were shown to influence the resistivity measured, and thus these parameters should be controlled or corrected for in order to provide comparative results.

For the field applications, the results indicate that an estimate of the degree of saturation in conjunction with electrical resistivity measurements offer the best estimate of soil type. While previous literature has shown that the quantity of water present highly influences the resistivity measurement, this work has identified the specific threshold at which the water begins to control the measurement. This finding strongly impacts the assessment of subsurface soils using electrical resistivity. Soils below the water table (i.e. fully saturated or 100% saturation) can easily be distinguished based on their resistivity alone. The laboratory results also showed that soils with a degree of saturation above a threshold of 60% still showed a similar resistivity value to fully saturated samples, improving the ability to identify soils in zones above the water table. However, uncertainty in interpretation increases above the water table as the soils can have a broader range of electrical resistivity depending on water content and density. As more natural samples and sites are tested and added to the database, a statistical analysis may be able to further improve estimates of soil type for samples above the water table.

4.2 Kinion Lake Dam

Based on the 1969 drilling report, Kinion Lake Dam consists of three distinct layers: 10 – 12 meters of soft soil, 1 – 5 meters of cherty gravel and cobbles and at 13 – 15 meters below the surface, a fractured limestone bedrock layer (Natural Resource Conservation Service, 2011). This layering is used as ground-truth to estimate the accuracy of each of the geophysical methods at identifying the depth of bedrock across the dam and also at identifying any unique features along the cross section. In addition, intra- and inter- method comparisons will be discussed to understand the variability between the results of each method. The implications of the results will be discussed in regards to their impact on Kinion Lake Dam and on the use of the methods for dam evaluations in general.

4.2.1 Crest of Dam

The 2D results of the surface wave and resistivity surveys are shown in Figure 4-14. Figure 4-14a and Figure 4-14b represent the raw pseudo 2D dispersion curves for MASWR and MASWL, Figure 4-14c and Figure 4-14d represent the pseudo 2D Vs results developed from data in Figure 4-14a and Figure 4-14b, respectively, Figure 4-14e represents the full waveform inversion Vs results, and Figure 4-14f and Figure 4-14g represent the CCR and ERI results, respectively. For each subplot, a dotted black is included that represents the interpreted depth to bedrock from the 1969 drilling report. Examining the dispersion plots for MASWR and MASWL in Figure 4-14a and Figure 4-14b, which are plotted in terms of pseudo depth (i.e., experimental wavelength divided by 2, which approximates depth), reveals a generalized three layer system similar to that described in the NRCS drilling report. Comparing the two plots, a strong velocity increase is observed in the Love wave dispersion data 1-2 meters below the bedrock depth estimated using the 1969 drilling report. A similar velocity increase is observed in the Rayleigh wave dispersion

data at a slightly higher depth than observed for the Love wave data. This difference is likely caused by the differences in the dispersion properties of Rayleigh versus Love waves (i.e., wavelength/2 is only a rough estimate of depth and the dispersion properties of the waves are different). Although these plots can be used independently in the assessment of variability across the dam, the true layer thickness and shear wave velocities must be obtained from an inversion process. The primary use of these plots was to develop the inversion parameterization for the site by providing general estimates of initial depths and shear wave velocities of the subsurface.

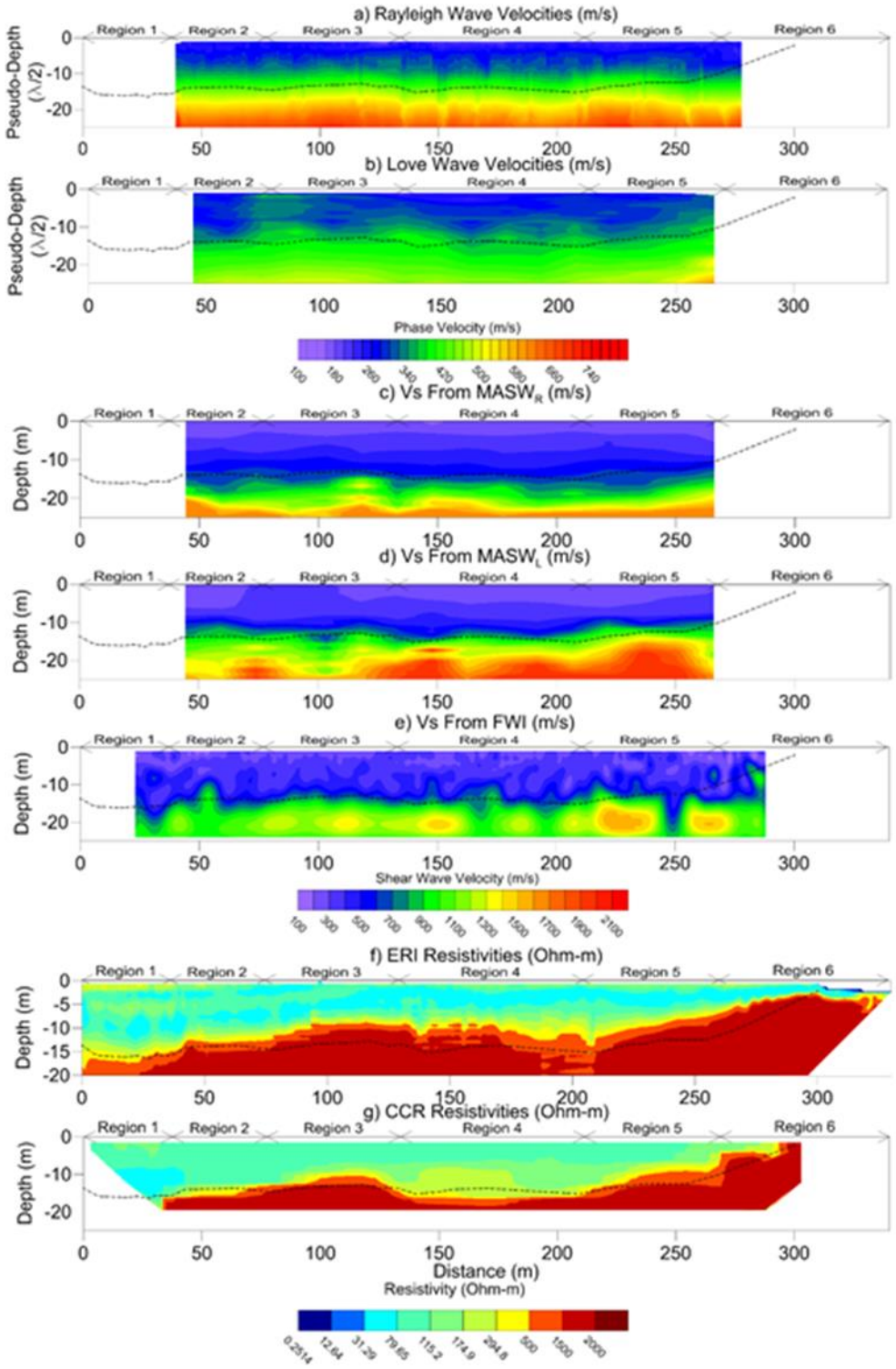

Figure 4-14. 2D Profiles for the crest of Kinion Lake Dam: a) Rayleigh wave dispersion velocities, b) Love wave dispersion velocities, c) MASW$_R$ Vs, d) MASW$_L$ Vs , e) FWI Vs, f) ERI resistivities, and g) CCR resistivities. The dashed line represents the bedrock line determined from the drilling and grouting report. The labeled regions are areas of interest discussed in the text.

Comparing the three 2D Vs profiles in Figure 4-14c-4-14e for the MASWR, MASWL, and FWI, respectively, a 10 – 11 meter top layer, a 1.5 – 5 meter transition layer and a stiffer bedrock layer at variable depths (11-14 meters) below the surface can be observed in each plot, with shear wave velocities corresponding to a stiff soil, soft rock, and rock, respectively (ASCE, 2013) This resulting system agrees fairly well with the drilling report; however, the MASWR Vs results indicate a bedrock depth approximately one meter deeper and the MASWL Vs results indicate a bedrock depth approximately one meter shallower than the drilling report. In addition, the MASWR Vs results indicate a thicker weathered rock layer than observed in the MASWL results. These differences are likely caused by the difference in the experimental dispersion curves generated from each wave type. As shown in Figure 4-15a, where typical Love and Rayleigh dispersion images for the dam crest are shown, the Love wave dispersion image has a significant mode jump from 15-23 Hz, while the Rayleigh dispersion images, shown in Figure 4-15b, were smooth and fundamental mode throughout. This frequency range corresponds to a depth of 10-15 meters below the dam and is critical to resolving the bedrock depth. Therefore, having poor data in this region results in more uncertainty in the MASWL Vs information generated in that region. The FWI Vs results match the bedrock depth from the drilling report best (less than 1 meter difference), but it results in a much more variable contour (i.e., sharp increases and decreases in bedrock depth). The MASW results indicate more subdued and consistent bedrock depth below the dam. The fluctuation of Vs values from MASW are muted (less extreme) because the results represent averaging over large volumes, whereas Vs values from the FWI are quite localized (cells). These FWI undulations could be real features under the dam or noise artifacts; however, without additional information is it difficult to confirm either. The FWI may provide a higher resolution image, identifying mores subsurface features than using the MASW profiles.

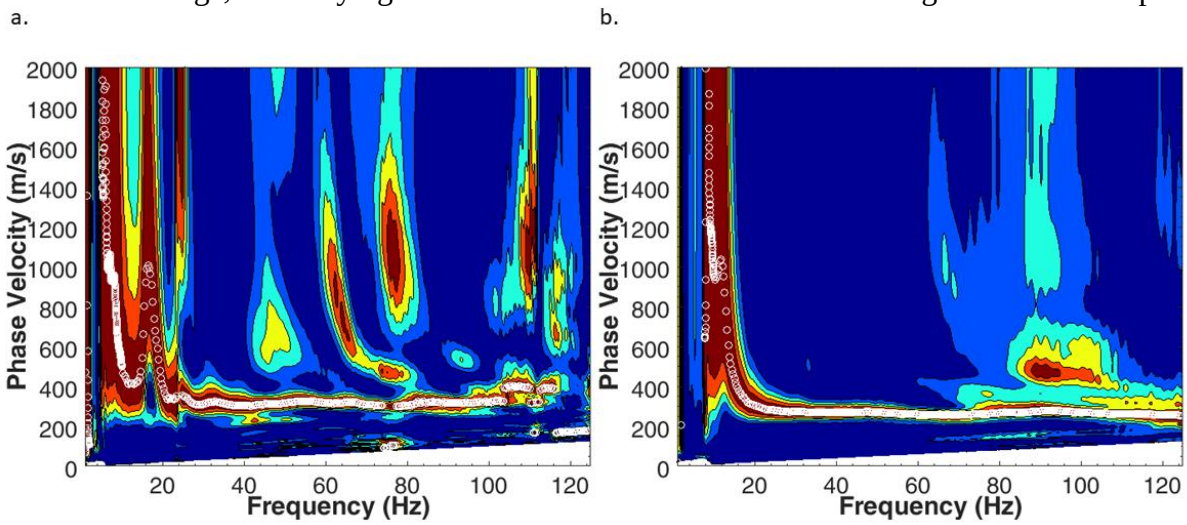

Figure 4-15. Typical a) Love wave and b) Rayleigh wave dispersion images for the crest of Kinion Lake Dam.

Comparing the results from the Vs methods in more detail, plots of the percent differences between the 2D Vs profiles developed using each surface wave method are shown in Figure 4-16. For Figure 8a, the percent difference between the MASWR and MASWL Vs is shown. For the top 10-12 meters of the cross section (i.e., the stiff soil), the two methods are generally within 5 – 10%, with the MASWR Vs generally greater than the MASWL Vs. However, in the weathered rock and rock layers below 10 meters, the differences become greater with MASWL Vs typically being 25

– 50% greater than MASWR Vs. This highlights one of the limitation of surface wave methods in that resolving the velocity of the half space in the model (i.e., bedrock in this case) is often difficult due to a lack of long wavelength information (Wood et al. 2014). The percent differences between the MASWR Vs and the FWI Vs results and the MASWL Vs and the FWI Vs results are shown in Figure 4-16b and Figure 4-16c, respectively. Comparing the MASWR Vs and FWI Vs results, the values are typically within 10 – 20% of one another with larger variations (up to +/- 40%) occurring in somewhat randomly distributed locations. Comparing the MASWL Vs and FWI Vs results, the MASWL Vs is 0 – 25% higher than the FWI beyond 20 meters in depth, and generally 0 – 25% lower in the top 10 meters. The difference between MASWL Vs and FWI Vs are similar to those observed between the two MASW approaches, which makes sense given the FWI and MASWR were derived from the same raw dataset.

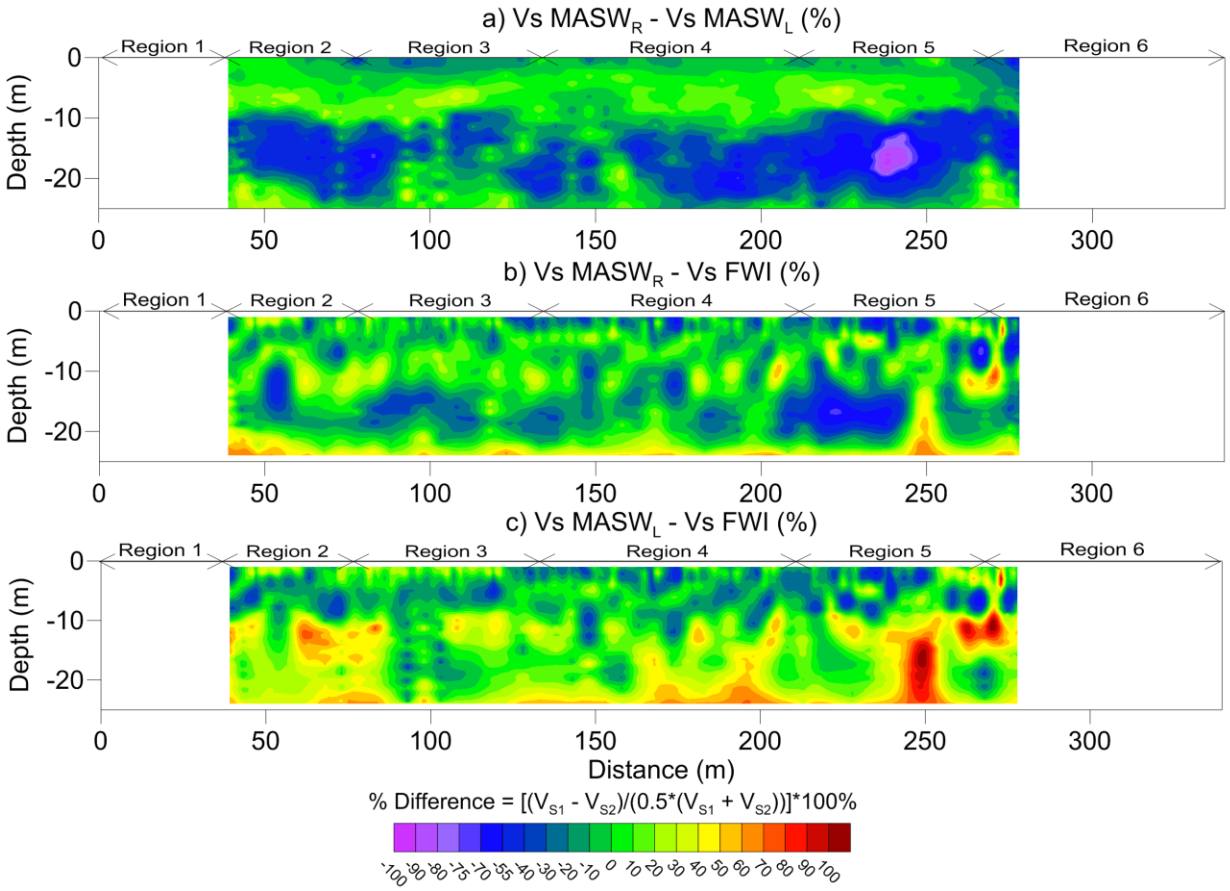

Figure 4-16. Crest percent difference plots for a) Rayleigh and Love inversions, b) FWI and Rayleigh inversions, and c) FWI and Love inversions.

Overall, surface wave methods seem more appropriate for determining the general stiffness and layering at a location, rather than detecting small features. The discrepancies in the surface wave data are likely a combination of resolution limitations and uncertainty in the inversion process. In practice, vertical resolution for MASW surveys is generally twice the receiver spacing, or in this case, two meters, putting the resulting bedrock depths within this resolution window. However, as with any surface geophysical method resolution ability decreases with depth below the surface. The horizontal resolution for MASW surveys is usually taken to be 10% of the array

length, or in this case 2.4 meters. This results in smaller, lateral features being obscured, reinforcing the conclusion that MASW is best suited to more general subsurface profiling.

The resistivity results from the ERI and CCR surveys are shown in Figure 4-14f and Figure 4-14g, respectively. In general, the survey results indicate a similar three-layer system as observed in both the surface wave results and the 1969 drilling report. These three layers, in descending order, have resistivities corresponding to clays/silts, soil-filled fractured rock, and unfractured rock (Kaufman & Hoekstra, 2001), matching the soil and rock descriptions in the drilling report well. For the CCR results, a high-resistivity bedrock layer is observed at an average of 15 meters below the surface, which is 1 - 2 meters lower than the drilling report, but with a similar bedrock profile. The ERI results, conversely, show a high-resistivity layer 1 – 2 meter shallower than the depth shown on the drilling report. The primary differences between the two methods, shown in Figure 6 occurs within Region 4, where the CCR results indicate that bedrock is approximately 1-2 meter deeper than what is indicated on the drilling report, while the ERI indicates bedrock is approximately 3-4 meters higher.. This anomaly in Region 4 was not observed in any of the surface wave results indicating the feature is likely not related to a major change in stiffness in the region (i.e., i.e., not a soil filled region). Given the CCR survey was completed on March 16, 2016, following a wet winter, whereas the ERI survey was completed during a dry summer, on June 22, 2015, the difference in resistivities is likely due to a difference in the quantity of water present in the area during each survey. Similar changes in resistivity were observed by Inazaki and Hayashi (2011) due to seasonal water level variations. These differences may also represent significant internal erosion that has occurred in that region. Internal seepage can result in the removal of fines which promotes more rapid changes in water content as the water elevation in the lake changes. Lower resistivity values would be measured when water levels are higher (higher water content) and higher resistivity values would be measured when water levels are lower (lower water content) due to the inability of the bedrock to retain the ground water. This type of fluctuation seems likely when comparing the specific and relative resistivity differences, as shown in Figure 4-17. The resistivity in the middle and bedrock layers of the March CCR survey are much lower, suggesting lower water contents in the top two layers in the summer. Finally, this internal erosion is supported by the approximate surface elevation of the lake outlet (7-10 meters below the crest of dam), which corresponds to the depths at which this highly variable restivity zone occurs. The detection of potential internal erosion based on seasonal differences highlights the necessicity of resistivity monitoring or at least the use of multiple surveys in different seasons for determining seepage issues.

Comparing the resistivity and Vs results, the primary differences between the methods are the depths at which layers are resolved in the subsurface, though each method is typically within 1 – 2 meters of the depths determined using the drilling report. This depth variability is likely due to the complex geology, specifically the second transition layer, which the drilling investigation found very difficult to distinguish from the bedrock. This transition layer combined with seasonal variations and resolution limitations inherent to the methods used likely led to the variations observed in the data. Seasonal precipitation variations and potential internal erosion are likely responsible for the OhmMapper results over-estimating bedrock depth relative to the drilling report and the ERI results under-estimating the bedrock depth primarily due to the difference in moisture content when the two tests were conducted. Overall, the use of multiple resistivity tests in different

seasons seems useful for detecting this transition layer and the potential internal erosion for the earthen dam.

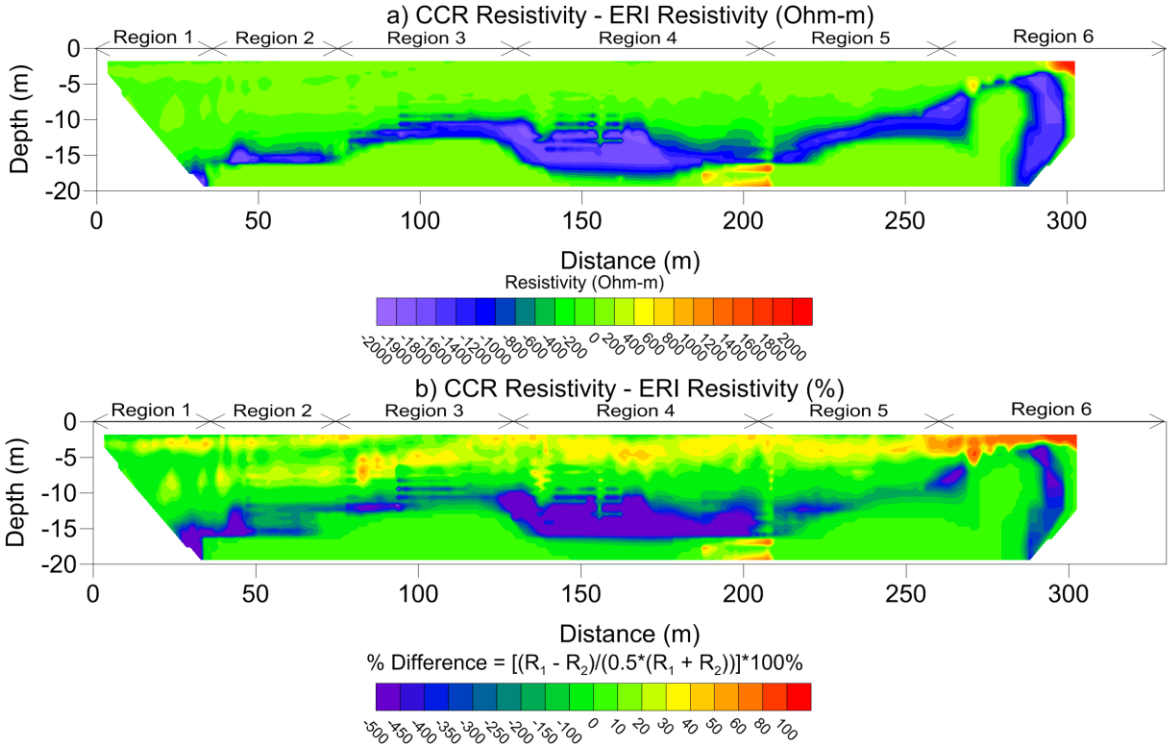

Figure 4-17. Actual (Ohm-m) and relative (%) resistivity differences between the OhmMapper and ERI profiles along the crest.

4.2.2 Toe

The downstream toe of Kinion Lake Dam was the most extensively tested location and featured the most complex subsurface layering (see Figure 3-5b). The results of a single survey line for the Love wave dispersion velocity profile (Figure 4-18a), MASWL Vs profile (Figure 4-18b), and the CCR and ERI profiles are shown in Figures 4-18c and 4-18d, respectively. Although traditional MASWR was conducted along the same line shown in Figure 4-18 (See Figure 3-5 above), the results were of very poor quality. Example dispersion curves from the MASWL and MASWR are shown in Figure 4-19a and 4-19b, respectively. The Love wave dispersion curve has a smooth high quality fundamental mode trend, while the Rayleigh wave dispersion curve has no useable trend with only small sections of the curve which potentially could be useable data. Given this very poor quality Rayleigh wave dispersion data, Love type surface waves seem much better suited for these shallow bedrock sites. Comparing the 2D profiles in Figure 4-18, a valley type bedrock profile is observed for each of the methods with only the ERI line extending far enough to resolve both edges of the valley. The bedrock layer resolved in the profiles starts near the surface in Region 1, is within 5 meters of the surface in Region 2, and is quickly sloping downward, extending beyond the maximum investigation depths (7 – 10 meters) in Region 3. In addition, the resistivity results (both CCR and ERI), indicate a low resistivity zone in Region 4 from about 2 meters deep

extending down to the bedrock, which could indicate an area of high water content (clays/silts). This feature is very likely the previously documented seepage locations.

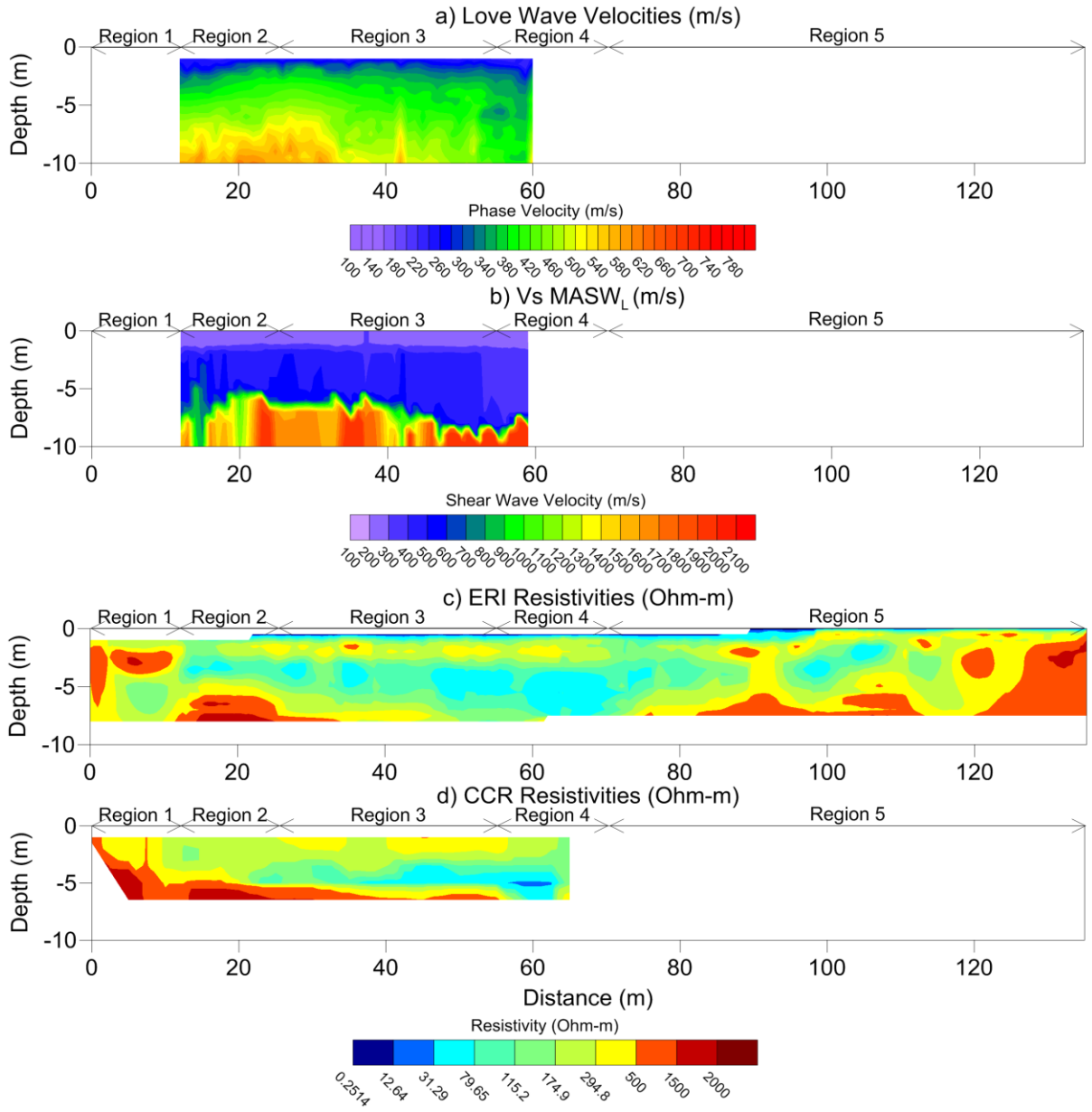

Figure 4-17. Profiles along the dry-side toe of Kinion Lake Dam: a) love wave velocities, b) shear wave velocities from the Love wave inversion, c) CCR resistivities, and d) ERI resistivities. The regions are areas of interest discussed in the text.

To image this subsurface valley feature in more detail, 2D horizontal slides of resistivity extending from 1 meter to 6.7 meters below the surface are shown in Figure 4-20, which were created using the multiple CCR lines collected along the toe. In the plots, a bedrock layer is observed that is shallower at the North end of the site but deeper, or at least less resistive toward

the Southwest corner indicating a valley feature that extends perpendicular away from the dam. The low point of the valley (observed in Figure 4-20h), is the location of the largest seep observed during large precipitation events. Based on the investigation from the dam crest, the region of suspected internal erosion in the dam (Region 4) lines up very well with the location of the subsurface valley observed at the toe of the dam. This may represent a seepage channel flowing from the lake, through Region 4 of the dam and through the subsurface valley at the downstream toe. The fairly low resistivity values in this location may indicate actual water presence or the deposition of fines from the interior of the dam.

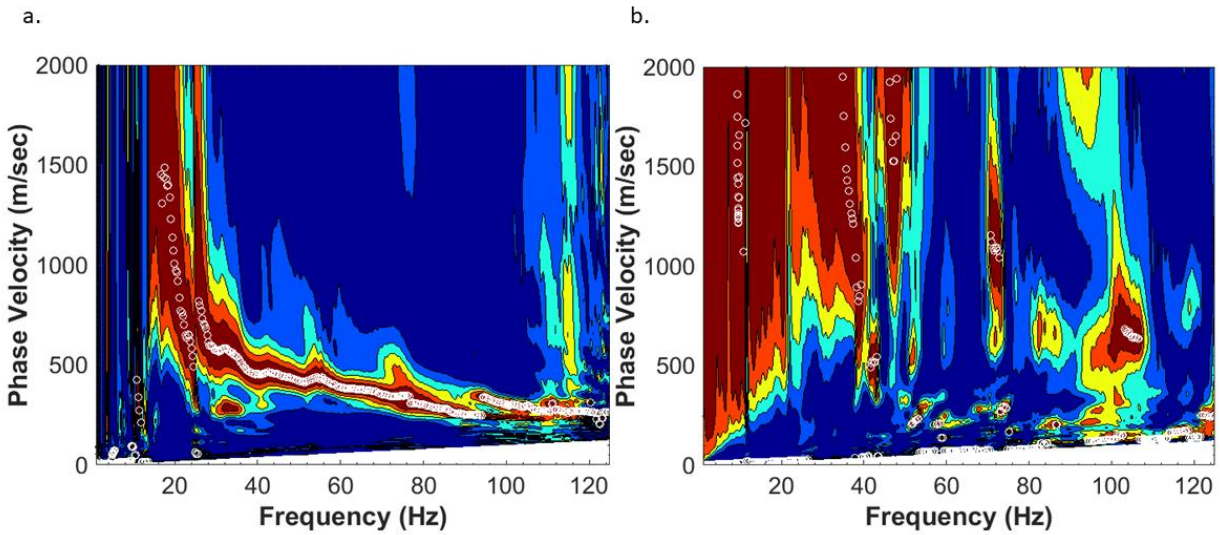

Figure 4-18. Typical a) Love wave and b) Rayleigh wave dispersion images from the toe of Kinion Lake Dam.

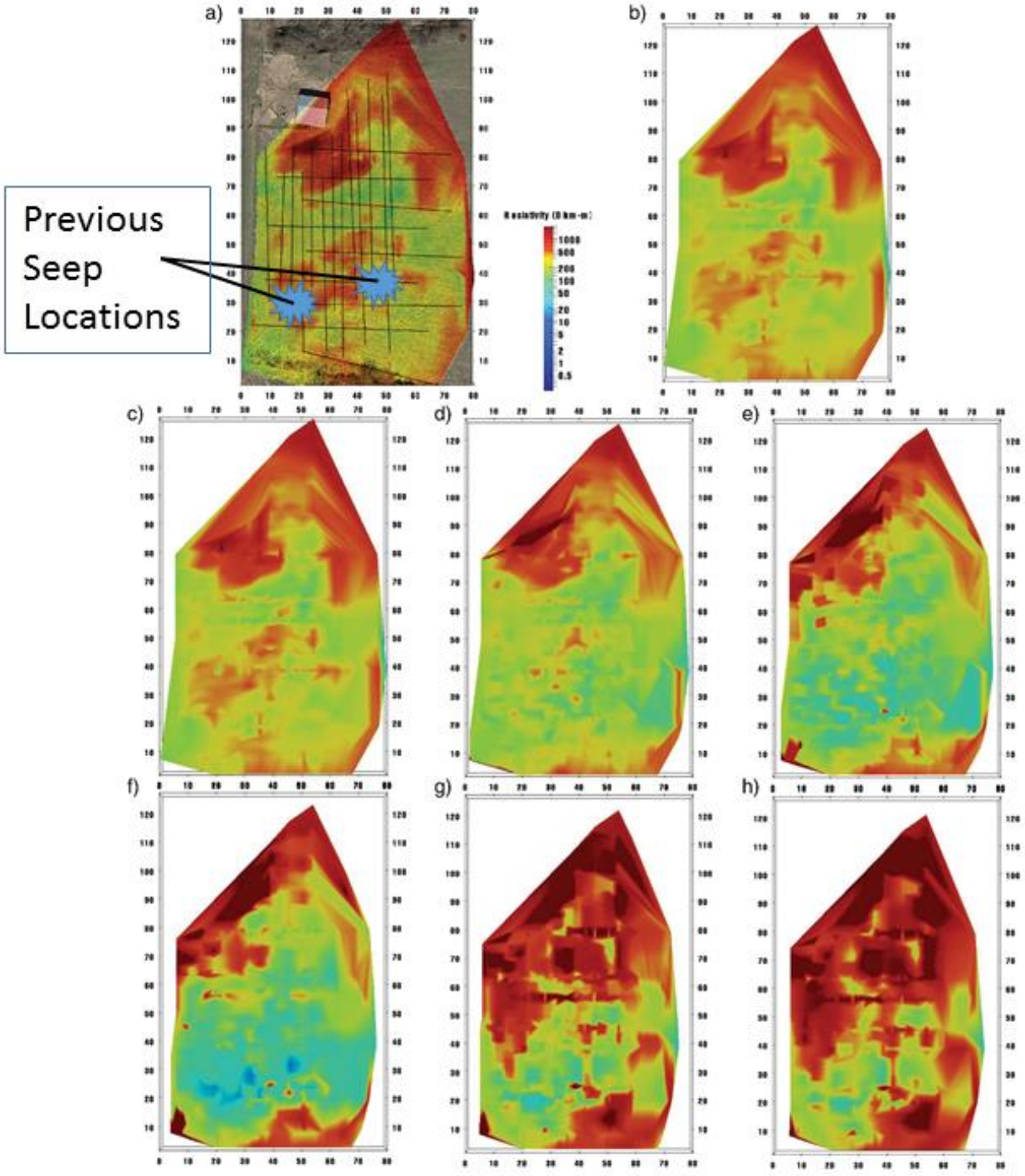

Figure 4-19. Crossections of the toe of Kinion Lake Dam at various depths: a) 0 meters with map overlay, b) -1 m, c) -2 m, d) -3 m, e) -4 m, f) -5 m, g) -6 m, h) -6.7 m.

4.2.3 Conclusions

MASW, FWI, ERI and CCR surveys were conducted along the crest and the downstream toe of Kinion Lake Dam. The bedrock layer below the dam was resolved using each of the methods within 1-2 meters of the location determined from a previous drilling program. However, the presence of a weather bedrock layer lead to some difference between the methods and ambiguity regarding the location of bedrock beneath the crest of the dam. $MASW_R$ and FWI was determined to be more effective for locations with bedrock at depth (the dam itself), whereas $MASW_L$ was determined to be more effective for locations with shallow and complex bedrock (along the toe). An area of potential internal erosion was observed along the southern edge of the dam (around 130 – 210 meters along the survey lines). The detection of this erosion was possible by comparing resistivity profiles made in different seasons (wet versus dry seasons), corresponding to different water levels in Kinion Lake. A subsurface valley feature was also imaged along the downstream toe of the dam perpendicular to the region of potential internal erosion in the dam. The deepest point in the valley was also the location of the large seep that occurs along the downstream toe during large precipitation events. The location of these regions could be a seepage channel which promotes internal erosion of the dam.

4.3 Mel-Price reach of Wood River Levee

The processed data from the MASW and CCR surveys are used for soil characterization and are compared with existing information including Standard Penetration Test (SPT), Cone Penetration Test (CPT) and general stratigraphy for the levee. In addition, empirical correlation between the shear wave velocity (Vs) and SPT raw blow count (N) are developed using co-located boreholes and shear wave velocity profiles. The results of this investigation are discussed in the following sections and their general application and direct applications to the Mel-Price Levee section are discussed in detail.

4.3.1 General observation

Figure 4-20 represent Rayleigh wave phase velocity (VR) variation (before completing the inversion process) with pseudo depth (wavelength divided by 2) and station number for the top of the levee. Each point in this figure corresponds to a raw Rayleigh wave velocity recorded in the field. The plot is used to identify any significant variations in the sub-surface prior to the inversion process. Based on Figure 4-20 and general information regarding the levee structure, the top of the levee generally consists of a four-layer system: soft clay, soft sand, medium-dense sand, and very dense sand/gravel. Examining the lateral variation in V_R in Figure 4-20, there is a sharp increase in Rayleigh wave phase velocity that corresponds to the location of utilities which cross the levee (labeled in Figure 4-20). The most noticeable increase in V_R is near station 50+00 (labeled as 1 in Figure 4-20), which matches the location of the old pump station and pipe. Moreover near station 80+00, the top 6 meters of soil around the Flood Gate has a higher V_R than its surrounding areas indicating better compaction or a different material type than present at other sections of the levee.

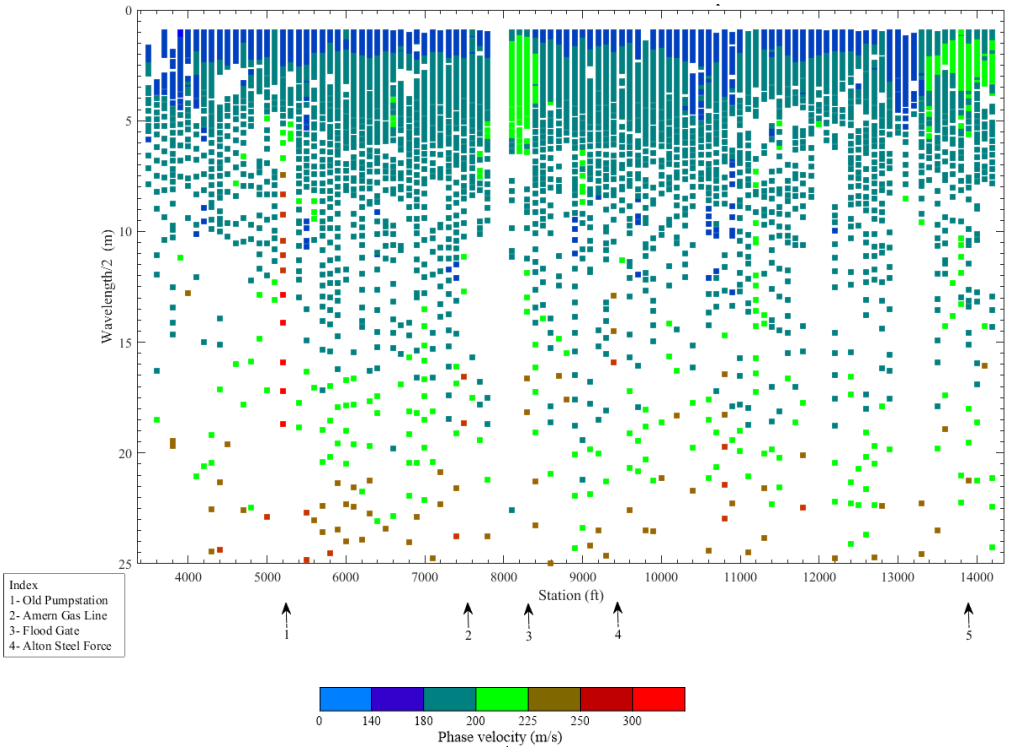

Figure 4-20 2D cross section of the top of the Me-Price levee section with Rayleigh wave phase velocity versus puedeo depth (wavelength/2).

4.3.2 Landside of the Levee

Figure 4-21 represents the 2D Vs and resistivity profiles for the landside of the levee along with a current aerial image of the levee. The blue points on the Google Earth image indicate the positions of the MASW testing locations along the landside portion of the levee. The ranges of resistivity and shear wave velocity that correspond to different soil types are indicated along with the color scales in Figure 4-21. The Vs ranges are based on reference Vs profiles (see Equation 4.1) for different material types presented by Lin et al. (2014), and the SPT blow count information from the boreholes along the survey line. Equation 1 solves for overburden stress-corrected shear wave velocity.

$$V_S = V_{SR} \times (\frac{\sigma_0'}{P_a})^{n_s} \quad (4.1)$$

where V_S is the overburden stress-corrected shear wave velocity, V_{SR} is the reference shear wave velocity at 1 atm effective mean stress, σ_0' is the initial effective mean stress, P_a is the reference stress of 1 atm, and n_s is the exponent of normalized effective mean stress. V_{SR} and n_s values are provided for a number of different soil types and densities ranging from soft clay to dense gravel. These curves provide reasonable bounds for various soil types and densities as a function of overburden stress.

Soil type along the landside cross section was also estimated based on resistivity. However, based on the laboratory resistivity testing, it is difficult to define soil type based on solely on resistivity without a-prior knowledge of the soil saturation. Therefore, information from the available boreholes were used as a guide to define the specific resistivity correlation for this site. Comparison of the classification results from the borehole logs and laboratory define ranges are similar when the soil is considered near saturation, which is very likely considering the static water

level for the landside profile was very near the ground surface. The same procedures were followed for determination of the shear wave velocity and resistivity ranges for the other sections of the levee (top and riverside). However, no invasive information was available for the top of the levee cross section.

In Figure 4-21, the information from the four boreholes is shown along with the Vs and resistivity 2D cross sections. The numbers to the right of the boreholes for 2D Vs cross section in Figure 4-21c are the average raw SPT-N values for each layers. Based on the Vs cross section, the subsurface consists of five soil layers. A 2-3 m thick soft clay layer at surface, a soft sand layer from 3-14 m, a medium dense sand layer extends from the base of soft sand to depths ranging from 22-25 m, followed by a dense sand layer between 27-30 m depth, underlain by very dense material. The thickness of the various layers is fairly uniform across the cross section varying by up to 2-4 meters at discrete locations. Overall, the Vs cross section is in good agreement with the borehole information indicating Vs can provide a good estimate of SPT N value and soil type/density especially when some a-prior information is available.

The 2D resistivity cross section along with USCS soil classification based on borehole logs is shown in Figure 4-21a**.** The resistivity results indicate the subsurface consists of a three-layer system that includes a top layer of lean clay from the surface to depth of about 2-3m, underlain by a thin silty sand layer from 3-4m, and finally a poorly graded sand up to a depth of 10 m. Overall, the CCR soil classifications are in good agreement with the Vs and borehole results, but the resistivity only provides valuable information up to 10m depth. One limitation of the CCR technique is it is only capable of mapping near-surface layering. However, the CCR method was able to resolve the silty sand layer, which was not resolvable using surface wave methods.

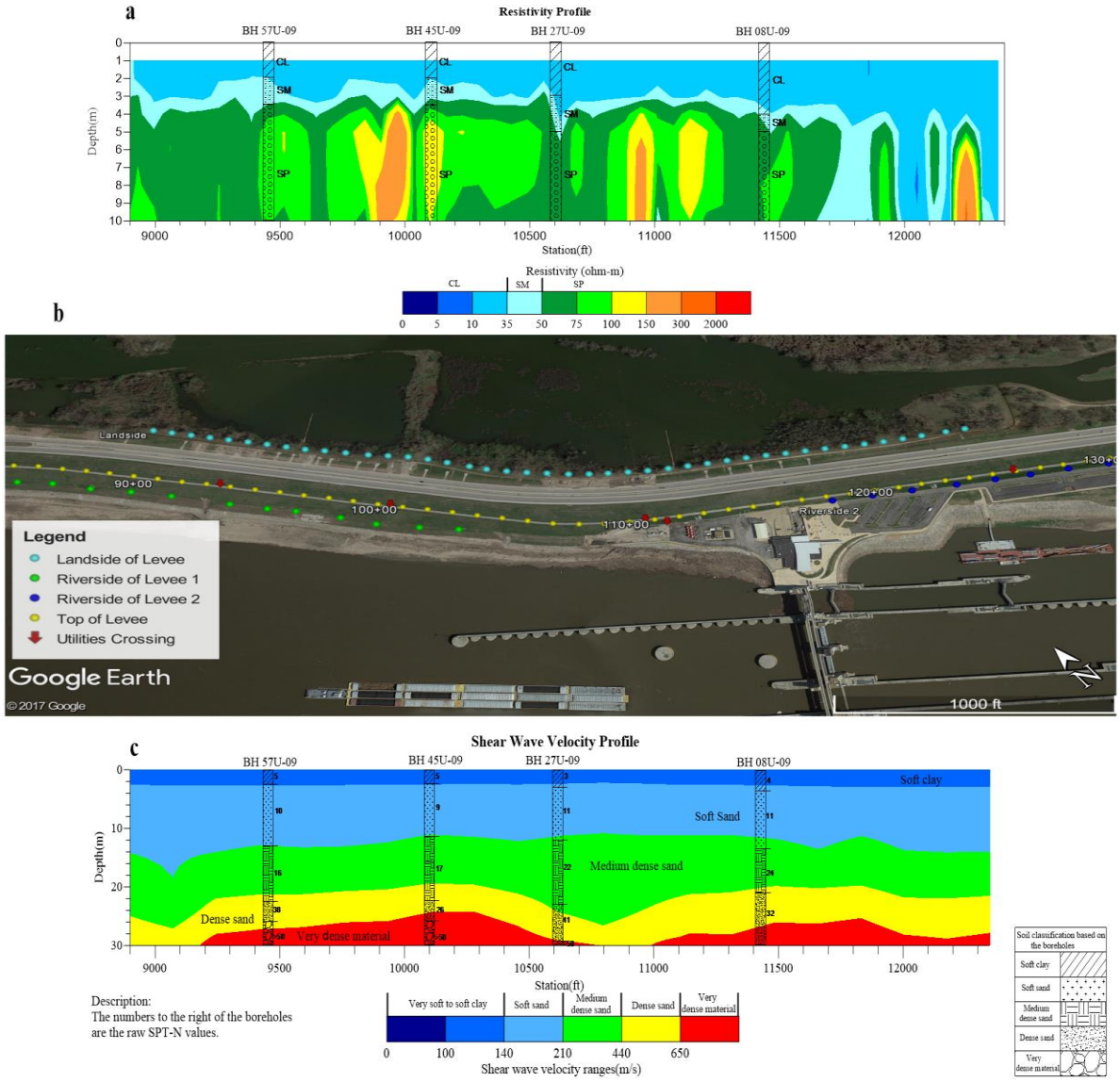

Figure 4-21-2D cross section for the landside of the levee, a) 2D CCR cross section b) Current Google Earth image c) 2D Vs cross section

4.3.3 Top of the levee

The most extensive MASW and CCR testing was performed on the top of the levee (as shown in Table 3-2). The 2D Vs and resistivity cross sections for the top of the levee along with an aerial image taken in 1941 are shown in Figure 4-22. The ranges of resistivity and shear wave velocity that correspond to different soil types (colors) were chosen using a similar procedure to the landside. However, a higher Vs range was chosen for the clay layer due to the increased overburden stress for deeper clay layer in the cross section.

Based on the 2D Vs cross section for the top of the levee (Figure 4-22c), the subsurface consists of a 5-layer system that includes a 2-3 m soft clay layer at the surface, a soft sand layer from 3-8m, a discontinuous soft clay layer from 8-12m, a soft sand layer from 17-22m, and finally a medium dense sand layer.

Examining the lateral variability of the cross section in Figure 4-22c, the first area of interest is the surface clay layer, which appears to be discontinuous along the cross section. However, these discontinuities are likely the result of better compaction in parts of the levee, which increase the shear wave velocity to a level similar to the underlying sand layer. Vs is generally insensitive to soil type. Therefore, different materials with similar Vs cannot be distinguished. The validity of this presumption is examined further using the resistivity results.

The second areas of interest are the discontinuities in the deeper clay layer between 8-12 meters. The existence or lack of existence of this clay layer along the cross section is clearly visible in the experimental dispersion curves and 1D Vs profiles along the levee as shown in Figure 4-23. Experimental dispersion curves from Station 40+00 (no clay layer present) and Station 108+00 (clay layer present) are compared in Figure 4-25a. For Station 40+00, the experimental dispersion curve is clearly normal dispersive (i.e., the phase velocity continually increases as frequency decreases) resulting in a constantly increasing shear wave velocity with depth as shown in Figure 4-25b. However, Station 108+00 has considerable drop in phase velocity for frequencies between 7-20Hz (i.e., an inversion) resulting in a velocity inversion in the shear wave velocity profile (i.e., a soft layer between two stiffer layers), as shown in Figure 4-23b. The Vs of this softer layer corresponds well with the reference velocity for a soft clay, which matches with the generalized layering for the area. Examining the locations along the cross section where these discontinuities occur, they appear to correspond quite well with the location of the old river meanders from the 1941 aerial image for the area. This indicates the deeper clay layer and in some cases the medium dense sand layer may have been eroded by the old river meanders. These sections where the clay layer disappear are potential problem areas of the levee for piping and might be the areas of interest for improvements or further investigations. Several sections not associated with old river meander from the 1941 aerial image (stations 35+00 to 45+00, 82+00 to 85+00, and 120+00 to 125+00) appear to also have no clay layer present in the subsurface. The reason for this is unknown, but based on the experimental data the clay layer is unlikely to exist in these areas or has a significantly higher stiffness than other parts of the cross section. Although, the clay layer was able to be resolved using surface wave methods, the exact thickness of the clay may vary from that shown in Figure 4-25c do to a lower resolution ability as depth below the surface increases.

Also in Figure 4-22c, two sharp increases in Vs are observed along the cross section at Stations 53+50, and 76+00. These anomalies are clearly observed in the experimental dispersion curves, which are shown in Figure 4-25a. Also included in the Figure 4-25a is a typical experimental dispersion curve from Station 108+00 for comparison. For frequencies greater than 20 Hz (shallow depths), all of the dispersion curves are very similar. However, for frequencies less than 20 Hz, the phase velocity of the dispersion curves corresponding to the anomalies (Station 52+00 and 75+00) increases rapidly at higher frequencies than the typical dispersion curve (Station 108+00), indicating a much stiffer layer is present closer to the surface than typically encountered in the cross section. This sharp increase in Vs at shallow depths is mirrored in the Vs profiles for Stations 52+00 and 76+00 as shown in Figure 4-24b. The location of these anomalies corresponds very well with the location of major utilities crossing the levee including a pump station pipe, and the Ameren Gas Line. This emphasizes the abilities of surface wave methods to resolve these relatively small targets at depth and detect major inclusions crossing a levee.

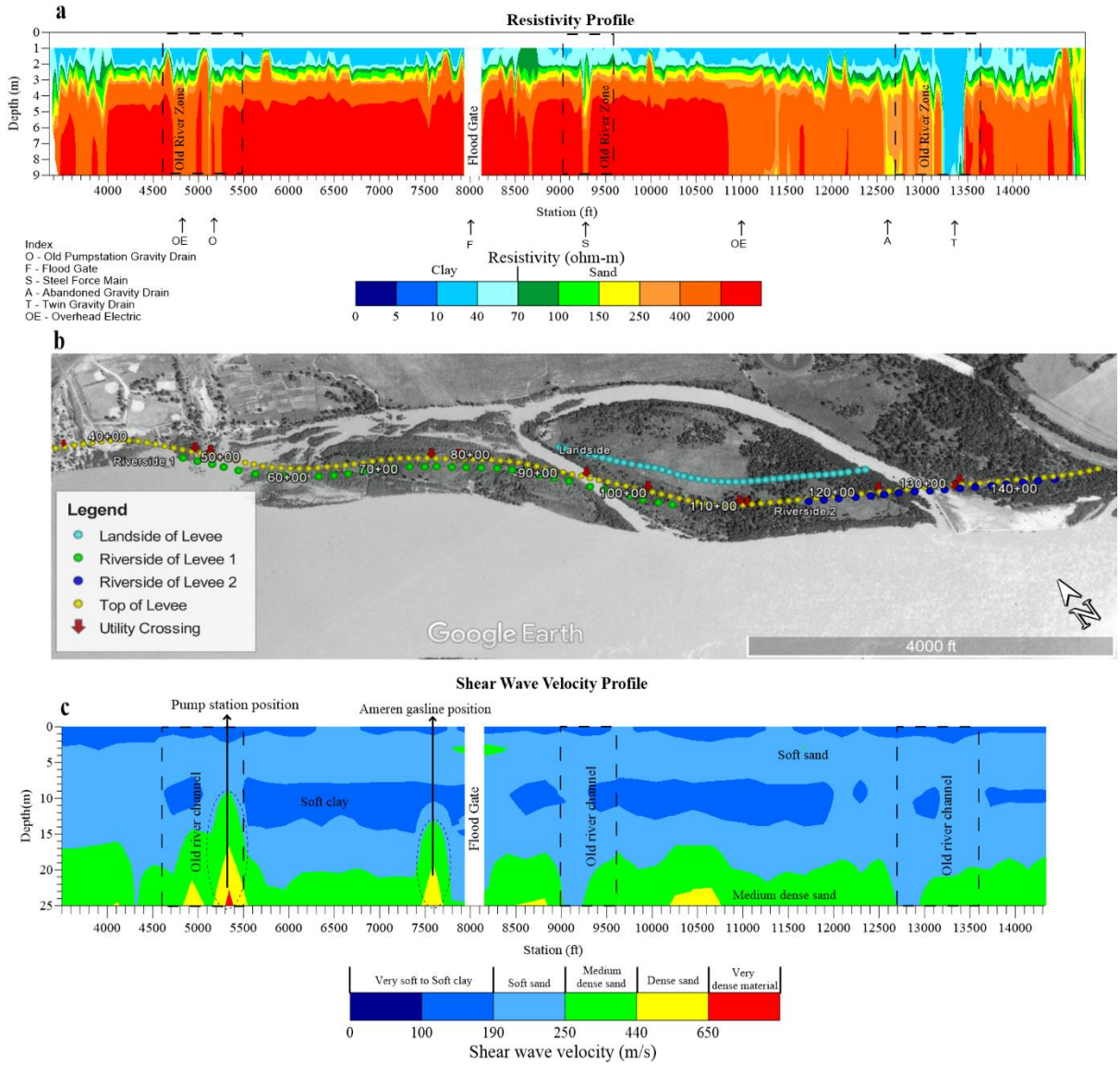

Figure 4-22- 2D cross section for the top of the levee, a) 2D CCR cross section b) 1941 Google Earth view c) 2D Vs cross section

The results of the CCR survey for the top of levee along with the locations of the old river channel and utility crossings are presented in Figure 4-22a. Based on the CCR survey which only provides information for the top 9 m, the top of levee consists of two layers: a clay layer from the surface to a depth of approximately 2-3 m, followed by a sand layer from 3-9m. Beyond the general layering, there a number of areas of interest. First an area of very low resistivity extending from the surface down to the 9 m is observed at Station 133+00, which corresponds with the location of a twin gravity drain crossing the levee. This low resistivity section likely occurred due to the presence of metal in the twin gravity drain. Another possibility is that seepage paths around the twin gravity drain led to low resistivity values. Two other lower resistive areas are observed in the cross section at Stations 50+00 and 93+00 which, match the location the old river channel. These areas are observed as areas of slightly lower resistivity from 3-9 m than the surrounding area. This slightly lower resistivity may be due to lack of the deeper clay layer in the area. The slightly lower

resistivity from 3-9 meters is observed from Station 35+00 to 40+00 and believe to be the result of no clay layer being present at 10 meters below the surface. The lower resistivity section from Station 108+00 to 145+00 is likely the result of a geometry change in the levee at that point rather than changes in the subsurface. In general, the areas of low resistivity match well with the results from the Vs cross section, but are not as clear in resolving the subsurface features in most cases. Overall, the 2D resistivity cross section is generally consistent with the results of the 2D Vs cross section with both methods providing independent verification anomalies in the levee.

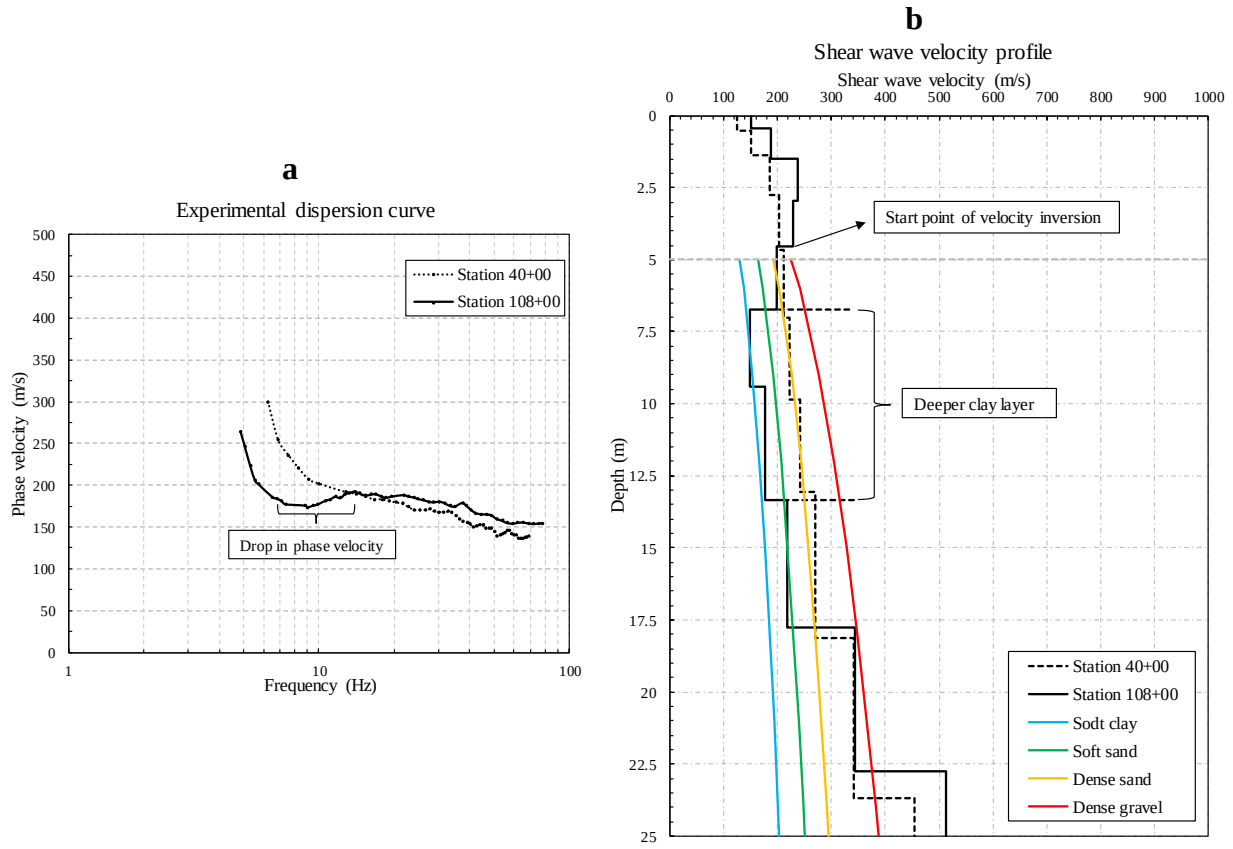

Figure 4-23-Experimental dispersion curves and shear wave velocity profiles for the top of levee a) Dispersion curves for the stations 40+00 and 108+00 b)Shear wave velocity profiles for the stations 40+00 and 108+00 along with reference Vs profiles from Lin et al. (2014).

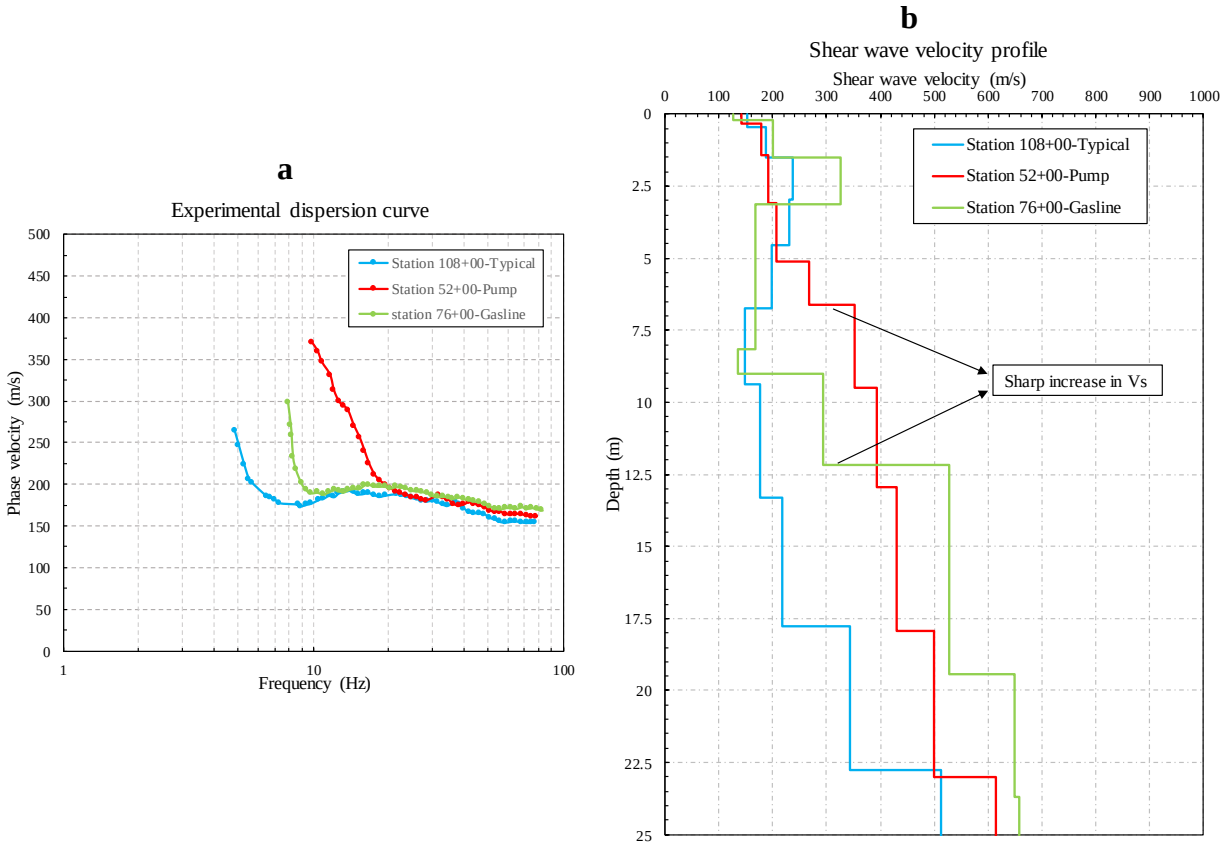

Figure 4-24-Sharp increase in Vs profiles for the top of the levee, a) Dispersion curves for the stations 100+80,52+00, and 76+00 b) Shear wave velocity profiles for the stations 100+80,52+00, and 76+00

4.3.4 Riverside

In Figure 4-25, the results of the MASW and CCR surveys for the riverside of the levee along with the current Google earth image are shown. The MASW survey was performed in two different paths, Riverside levee 1 and Riverside levee 2, as shown in the Google Earth image. In Figure 4-25c, the MASW survey for the riverside levee 2 only provides information up to a depth of 10 m due to the low resolution of the Rayleigh wave dispersion curve data at long wavelengths (low frequencies). The 2D Vs cross section for the riverside levee 1 indicates that the subsurface mainly consists of two layers: a soft soil layer from surface to approximately 16 m depth, overlain by a medium dense sand layer. However, based on the results of 2D Vs cross section for the riverside of levee 2, there is a soft clay layer at surface in that portion of the levee. The lack of a surface clay layer in the MASW results of riverside levee 1 is probably a consequence of testing along the asphalt road at the toe. The higher velocity of the asphalt and base likely shadow the minor difference between the sand and clay layers. This is confirmed later by the resistivity results.

Unlike the 2D Vs cross section for the riverside levee 1, the results of the CCR in Figure 4-25a show a thin clay layer (approximately 2 m thick) at the surface. Generally, the results from the CCR are much noisy than other parts of the levee. This makes it difficult to characterize the material below the top clay layer, but two sections (Station 96+00 and 130+00) with lower resistivity values match up fairly well with the location of the old river meander zones. The third old river meander zone at Station 50+00 indicates a higher resistivity than nearby sections. There

is a possibility that the low resistive areas are indicators of high water content or internal seepage paths in the levee. However, due to the poor quality of the CCR data for these sections, there is a need for further investigations to determine the reason behind the low resistivity values.

Figure 4-26 shows the results of the cone penetration test for the CPT-526-08 located close to the Station 94+00 for the riverside of the levee. The results of the CPT sounding reveal a generalized two-layer system; a clay layer from the surface up to about 2m depth, followed by a sand layer. This confirms the results of the CCR and MASW surveys, but there are some discrepancies in the results that are likely caused by the poor quality experimental datasets.

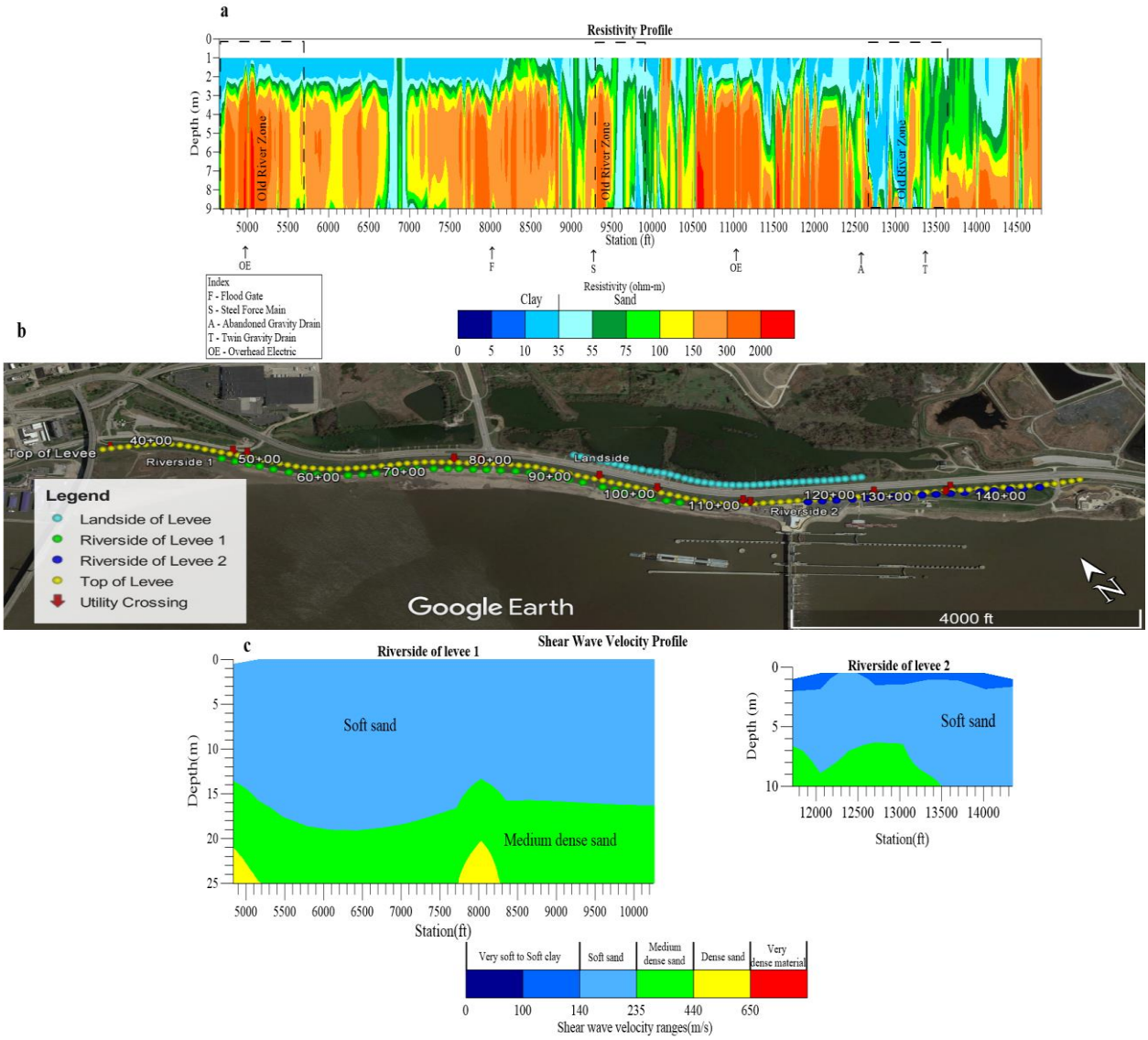

Figure 4-25- 2D cross section for the riverside of the levee a) 2D CCR cross section b) Current Google Earth image c) 2D Vs cross section

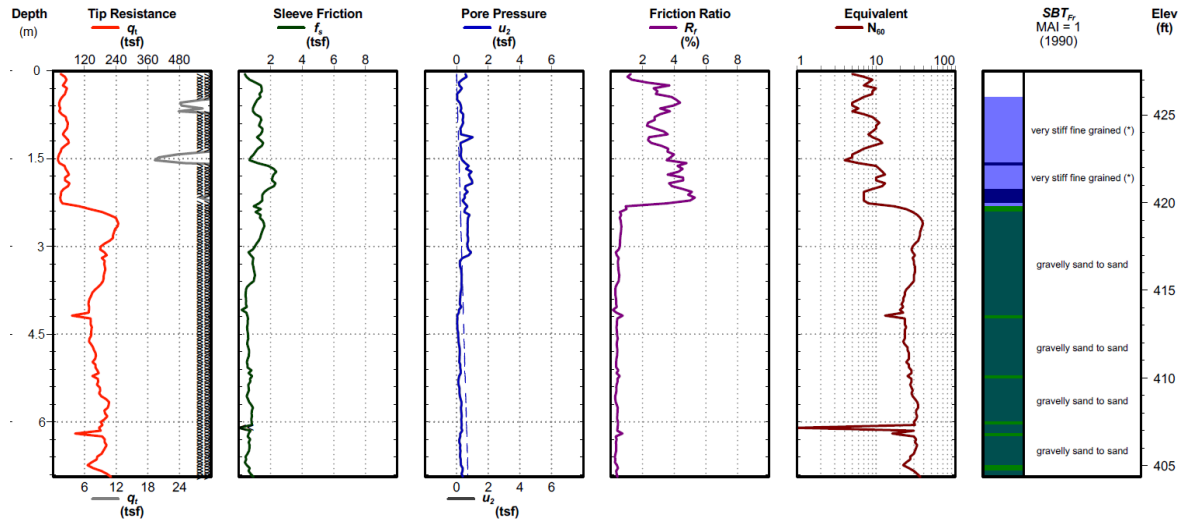

Figure 4-26- Cone penetration test result for the CPT-526-08 for the riverside of the levee

4.3.5 Combination of the MASW surveys for the top and landside

The combined results of the 2D MASW surveys for the top and the landside of the levee are presented in Figure 4-27. The elevation difference between the top and the landside of the levee, which is about 7 m, was considered for plotting the combined 2D MASW profile image. As shown in Figure 4-27, the 2D Vs cross section for the top and the landside are consistent, with slight differences in predicting the location and thickness of the clay layer. The deeper clay layer in the 2D Vs cross section for the top of levee matches the clay layer in the 2D Vs cross section for the landside; however, a thicker clay layer was resolved for the top of the levee survey compared to the landside survey. This is likely a result of the reduced resolution of surface wave methods at depth and the non-unique nature of the inversion process.

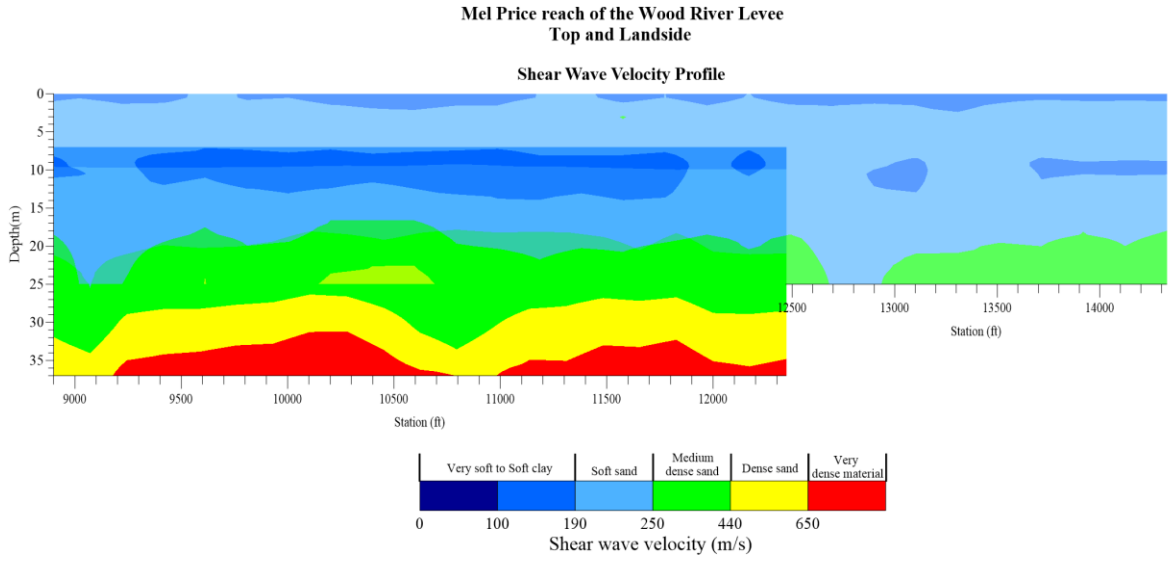

Figure 4-27- Combined 2D Vs cross section for the top and the landside of the levee

4.3.6 Empirical correlation between the raw N-SPT and Vs for the landside of levee

Many studies have been conducted in an attempt to correlate raw N-SPT with shear wave velocity (Fabbrocino, S., Lanzano, G., Forte, G., de Magistris, F. S., & Fabbrocino, G. , 2015), (Athanasopoulos, 1970), (Akin, M. K., Kramer, S. L., & Topal, T., 2011) and most of them have used power-type function, like Equation 2 as the most suitable one for data regression.

$$V_S = a \times (N_{SPT})^b \tag{4-2}$$

where a and b are regression coefficients. Regarding the parameters affecting the raw SPT-N value and shear wave velocity of soil deposits, this kind of correlations are typically site specific. The information from all types of soil that includes 181 pairs of data for the landside of the levee were used to develop the N-Vs correlation. Figure 4- represents the best-fit empirical correlation between the raw N-SPT value and related shear wave velocity by a power law function along with the lower and upper bounds. The R^2 of 0.827 for 181 pairs of data is an indicator of reliable correlation.

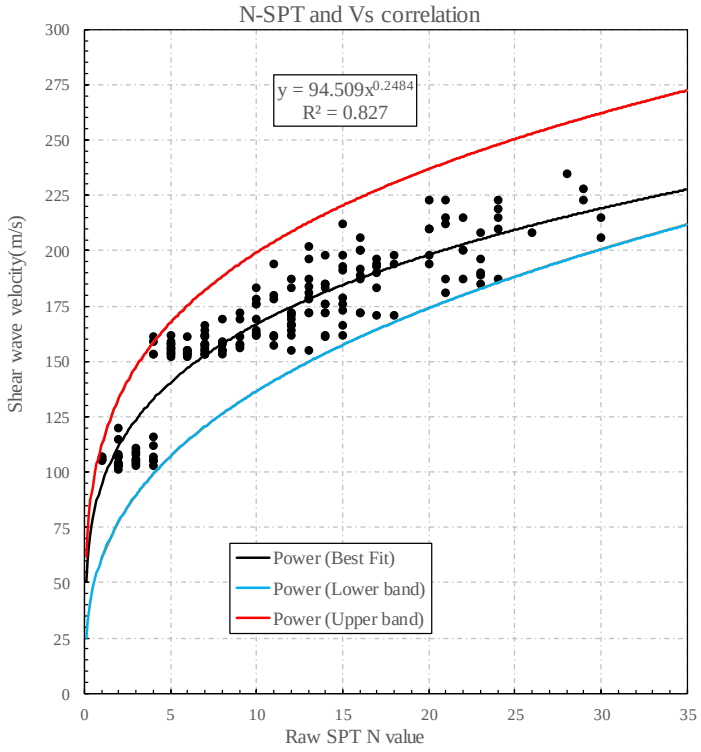

Figure 4-29- Correlation between the N-SPT and Vs for the landside of the levee

In order to evaluate the reliability of the proposed correlation, the normal consistency ratio (Cd, see Equation 4-3), which is defined as a difference between the estimated and measured shear wave velocity to measured raw N-SPT value, is calculated and the results are shown in Figure 4-28.

$$Cd = \frac{(Vs_{measured} - Vs_{estimated})}{SPT - N} \tag{4-3}$$

From Figure 4-28, the average Cd value is close to zero, indicating that the estimated V_S values are very close to the measured values for N values greater than 5. For N values less than 5 the

performance of the correlation is diminished likely due variability in the N values in the very soft materials. Overall, the proposed correlation can be used to estimate raw SPT-N value from the continuous shear wave velocity information from the study area in order to determine soil strength for design.

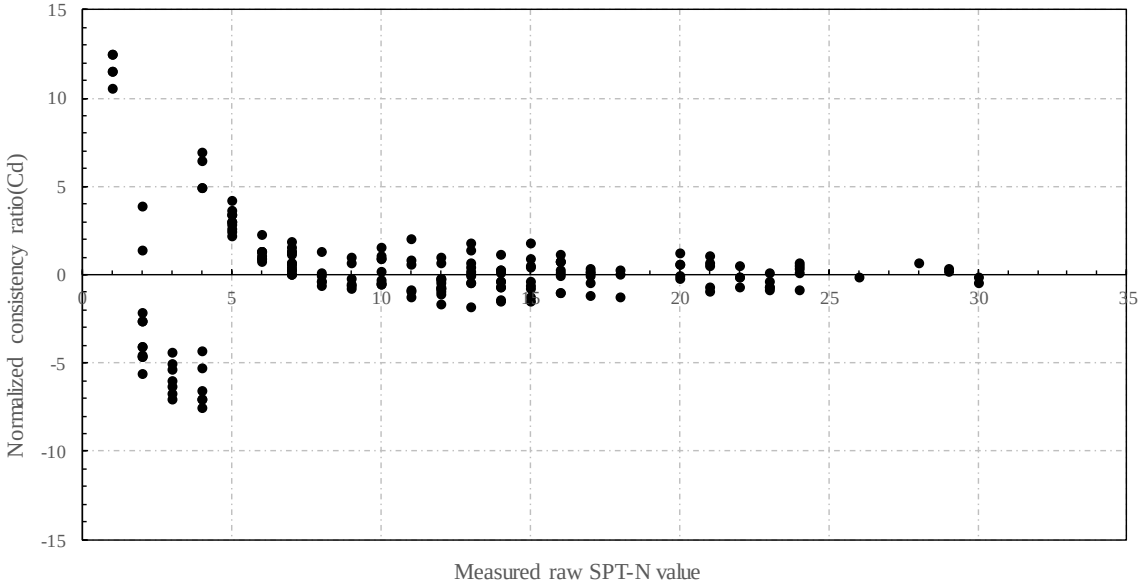

Figure 4-28- Normal consistency ratio (Cd) for the proposed N-Vs correlation

4.3.7 Conclusion

MASW and CCR surveys were performed for over 6800 m along the top, landside and riverside of the Mel Price Reach of the Wood River Levee with the goal of mapping near-surface structure and providing information regarding potential problem areas along the levee. Comparison of the results obtained from the geophysical surveys with in-situ tests (SPT and CPT) indicates a good consistency between invasive and non-invasive tests. The MASW survey provides valuable information about soil stiffness, which is in good agreement with N values from the SPT tests. The CCR soil classification results match closely with the results from the CPT soundings and laboratory tests from the boring logs. These two geotechnical properties (soil type and soil density) are the main parameters affecting the breaching and overtopping failure potential. In addition, the results from the MASW and CCR surveys for the top of the levee were able to resolve several potential problem areas where old river meanders were present or where utilities were crossing the levee. Therefore, the combination of MASW and CCR surveys is a powerful technique for rapid and non-invasive levee assessment.

5 Impacts/ Benefits of Implementation

Based on the research described in this report, there are a number of impacts and benefits of the research. The core impact of the research revolves around the ability to use geophysical methods to rapidly and cost-effectively evaluate levees. Based on the two sites tested during the study, the project team was able to test between 5-10 km of levee per day demonstrating the

relatively rapid assessment process of testing using resistivity and surface wave methods. Through both the laboratory and field testing, we were able to demonstrate the ability to identify soil type and in-situ stiffness based on both resistivity and shear wave velocity derived from the testing methods. This allows for basic evaluations to be made regarding the risk associated with the levee. Moreover, we are able to show through the field tests the ability to detect a number of common defects which can lead to failure in levees. Each of the specific impacts/benefits of the research are described below in detail.

- **Detection of Internal Erosion using Resistivity:** the work at Kinion Lake Dam where resistivity measurements were made during both wet and dry seasons demonstrated the ability to detect internal erosion of earthen levees and dams. Internal erosion is often a primary failure mechanism for both levees and earthen dams. The ability to detect it before failure occurs provides a significant benefit to levee and earthen dam owners. It is recommend that if yearly evaluations are conducted that they take place on a staggered schedule to allow testing to be conducted during different seasons to better resolve potential internal erosion in the levee or earthen dam.
- **Advantages of Love Wave Testing:** based on work at Kinion Lake Dam, Love wave surface wave testing was shown to be much more effective at resolving subsurface layering at shallow bedrock sites than traditional Rayleigh wave surface wave testing. Rayleigh wave surface wave testing was shown to be completely ineffective at these shallow bedrock sites. It is recommend that future investigations where shallow bedrock will be encountered be conducted using Love wave methods rather than Rayleigh wave methods.
- **Estimation of Soil Type and Stiffness using Resistivity and Shear Wave Velocity:** based on laboratory and field testing, the soil type (sand or clay) of the levee and foundation soil can be identified with confidence using resistivity alone when the water content of the soil is relatively high (i.e., wet with water content greater than 60%). When the soil is relatively dry (water content less than 60%), determination of soil type using resistivity alone is more difficult requiring additional information. With the addition of shear wave velocity information, knowledge of the water table location, or even sparse in-situ data, the soil type can be estimated based on reference shear wave velocity curves for each soil type and the resistivity values or by developing site specific correlations between the non-invasive results and the in-situ data available at the site. The estimation of the soil stiffness is based on shear wave velocity with results from the both field sites proving the ability to resolve changes in stiffness in the subsurface. The ability to estimate soil type and stiffness for levees is critical to determining the areas of concern in levees.
- **Detection of Utilities or other Elements Crossing the Levee:** based on work at the Wood River Levee a variety of utilities including draining pipes, gas lines, and sewer lines crossing levees can be detected by primarily using surface wave methods, but also to a more limited extent using resistivity. Resistivity was only effective at detecting metal or conductive utilities. This can have significant benefits if the location of abandoned utilities is not known as any elements which cross the levee can be primary locations for internal erosion to take place. These sections of levee can be repaired before internal erosion takes place.
- **Detection of Old River Meanders Crossing the Levee:** based on work at the Wood River Levee, the location of old river meanders can be detected using surface wave methods. These sections of levee where previous meanders of the river crossed under the

present day location of the levee are primary locations for piping through the foundation of the levee, which can lead to sand boils during large flooding events and potentially to failure of the levee. Being able to rapidly identify these areas along a levee provides a significant benefit to levee owners as only repair of discrete areas is need to significantly improve the resilience of the levee system.

6 Recommendation and Conclusions

Levees are a critical piece of civil infrastructure used to prevent billions of dollars each year in flood damage throughout the United States. However, many of these levees are rated in poor condition by the 2016 ASCE report card. These levees need to be evaluated in a cost effective manner to determine problematic areas using rapid methods which provide a continuous understanding of the subsurface or internal condition of the levee. This study has detailed a number of laboratory and field experiments to evaluate the effectiveness of geophysical methods at resolving the subsurface layering and detecting potential problems areas which could lead to failure of the levee during high water events.

Several conclusions can be drawn from the laboratory portion of the project. There is a clear correlation between resistivity and the degree of saturation and bulk density of a soil. An increase in either parameter is associated with a decrease in electrical resistivity. The resistivity values were found to be highly dependent on the degree of saturation up to approximately 60%, at which point increasing saturation does not result in significantly different resistivity values. When the soil is close to saturation, the effect of density or water quality on resistivity diminishes which makes the task of identifying soil type easier. Among the parameters investigated, it was observed that an estimate of the degree of saturation in conjunction with electrical resistivity offers the best estimate of soil type.

Although degree of saturation cannot be easily determined from typical in-situ tests, it is very well correlated with the location of the water table, which is typically either known or can be determined in the field. Knowing the location of the water table, it can be assumed soils below or very near the water table depth have a saturation greater than 60%. Therefore, soils below the water table can easily be distinguished based on their resistivity alone (i.e., due to the large separation in resistivity between soils with a degree of saturation greater than 60%). However, uncertainty in interpretation increases above the water table as the soils can have a broader range of electrical resistivity depending on water content and density and this uncertainty increases as the depth to the water table increases. When interpreting the resistivity results above the water table, additional information is necessary to accurately identify the soil type from resistivity data.

The first field investigation of Kinion Lake Dam was a high resolution survey to resolve potential subsurface anomalies using a number of surface wave and resistivity methods. The results indicate that bedrock can be mapped effectively using both surface wave (Vs) and resistivity measurements with surface wave measurements providing a more reliable solution. For mapping bedrock, Love wave surface wave methods were shown to perform much better for shallow bedrock locations than Rayleigh wave methods, which performed better for deeper bedrock locations. Finally, seasonal measurements of resistivity were shown to be effective at detecting potential internal erosion better than singular resistivity measurements. This behavior is caused by areas which contain large quantities of free water (cavities with less soil material) having very low resistivity values while the same locations have high resistivity values during dry conditions due to the rapid loss of the free water from the area. Unaffected areas surrounding

the area of internal erosion tend to lose pore water more slowly and are less effected by seasonal variations in water content.

The second field investigation involved resistivity measurements from CCR and Vs measurements from surface wave methods for a more coarse evaluation (larger distance between testing locations) of the Mel-Price reach of the Wood River Levee. From the results, the general subsurface layering can be resolved with confidence. The geophysical methods were able to resolve both the surface clay layer and the inner sand core of the levee. Surface wave testing was even able to resolve a lower clay layer in the subsurface which is discontinuous at location where old river meanders cross under the levee. These old river meanders have eroded portions of the clay layer, which could affect seepage rates through the foundation materials. These results provide confidence that the geophysical methods can be used to detect old river meanders and weak spots in other levees. These weak spots especially old river meanders can be prime locations for piping through the foundation, which could lead to failure. Detecting these areas and remediating them can significantly improve the resilience of the levee system.

Beyond simply detecting changes in the subsurface layering of the levee, the methods were able to detect the location of major underground utilities crossing the levee at number of locations. Resistivity measurements were most effective at detecting metal or conductive utility lines, but had a more difficult time resolving non-conductive utilities. Vs measurements were able to detect utilities which increased the overall stiffness of the subsurface either due to the pipe itself or an increase in the Vs of the material surrounding the pipe.

Overall, the combined use of resistivity and Vs from CCR and surface wave methods provides a rapid and near continuous means to evaluate levees and earthen dams. The methods were shown to be capable of detecting many common defects in levees and earthen dams including the location of soft layers, old river meanders, inclusions or utilities, and internal erosion, any of which could lead to failure of the levee during a high water event.

7 References

AASHTO, 2012. Standard T 288-12. Standard method of test for determining minimum laboratory soil resistivity. Washington, DC: American Association of State Highway and Transportation Officials.

Allaud, L., & Martin, M., 1977. Schlumberger: The history of a technique. Wiley.

Archie, G. E., 1942. The electrical resistivity log as an aid in determining some reservoir characteristics, 146-154.

ASCE, 2007. The New Orleans hurricane protection system: What went wrong and why. Reston: American Society of Civil Engineers.

ASCE, 2013. Minimum Design Loads for Buildings and Other Structures. ASCE/SEI 7-10 ed. Reston: American Society of Civil Engineers.

ASCE, 2017. Dams | ASCE's 2017 Infrastructure Report Card. [Online] Available at: http://www.infrastructurereportcard.org/wp-content/uploads/2017/01/Dams-Final.pdf

ASCE, 2017. Levees | ASCE's 2017 Infrastructure Report Card. [Online] Available at: http://www.infrastructurereportcard.org/wp-content/uploads/2017/01/Levees-Final.pdf

Asch, T., Deszcz-Pan, M., Burton, B. & Ball, L., 2008. Geophysical characterization of American river levees, Sacramento, California, using electromagnetics, capacitively coupled resistivity and dc resistivity. Reston: U.S. Geological Survey.

ASTM D2487-11, 2011. Standard practice for classification of soils for engineering purposes (unified soil classification system). ASTM International.

ASTM G57-06, 2012. Standard test method for field measurement of soil resistivity using the Wenner four-electrode method. ASTM International.

Baines, D. et al., 2002. Electrical resistivity ground imaging (ERGI): a new tool for mapping the lithology and geometry of channel-belts and valley-fills. Sedimentology, June, 49(3), pp. 441-449.

Ben-Menahem, A. & Singh, S. J., 1981. Seismic Waves and Sources. New York City: Springer-Verlag.

Besson, A., Cousin, I., Samouëlian, A., Boizard, H., & Richard, G., 2004. Structural heterogeneity of the soil tilled layer as characterized by 2D electrical resistivity surveying. Soil and Tillage Research, 79(2), 239-249.

Briaud, J. L., Chen, H., Govindasamy, A. V., & Storesund, R., 2008. Levee erosion by overtopping in New Orleans during the Katrina hurricane. Journal of Geotechnical and Geoenvironmental Engineering, 134(5), 618-632.

Briaud J.-L., Ting F., Chen H.C., Cao Y., Han S.-W., Kwak K., 2001. Erosion Function Apparatus for Scour Rate Predictions, Journal of Geotechnical and Geoenvironmental Engineering, 127(2), 105-113.

Bolt, B., 1993. Earthquakes. New York City: W.H. Freeman.

Cardarelli, E., Cercato, M. & De Donno, G., 2014. Characterization of an earth-filled dam through the combined use of electrical resistivity tomography, P- and SH-wave seismic tomography and surface wave data. Journal of Applied Geophysics, April. pp. 87-95.

Chlaib, H., 2014. Geophysical applications for levee assessment. Scholars' Press.

Cox, B. R., & Teague, D. P. (2016). “Layering ratios: a systematic approach to the inversion of surface wave data in the absence of a priori information.” Geophysical Journal International, 207(1), 422-438.

Cox, B. & Wood, C., 2011. Surface Wave Benchmarking Exercise: Methodologies, Results and Uncertainties. Georisk 2011, Atlanta, ASCE, pp. 845-852.
Dahlin, T., 1996. 2D resistivity surveying for environmental and engineering applications. First Break, July, 14(7), pp. 275-283.
Dahlin, T., 2001. The development of DC resistivity imaging techniques. Computers & Geosciences, 27(9), 1019-1029.
Davis, J. L., & Annan, A. P., 1989. Ground-penetrating radar for high-resolution mapping of soil and rock stratigraphy. Geophysical Prospecting, 37(5), 531-551.
Dunbar, J., et al., 2003. An integrated approach for assessment of levees in the lower Rio Grande valley. Symposium on the application of geophysics to engineering and environmental problems 2003 (pp. 350-362) Environment and Engineering Geophysical Society.
Ellis, H., Groves, C., & Fischer, G., 2008. Rapid levee assessment for reliability and risk analysis. Geo-Congress: The Challenge of Sustainability in the Geoenvironment, New Orleans, LA. pp. 170-177.
Everett, M. E., 2013. Near-surface applied geophysics. Cambridge University Press.
Florides, G., & Kalogirou, S., 2005. Annual ground temperature measurements at various depths. 8th REHVA World Congress, Clima, Lausanne.
Foster, M., Fell, R. & Spannagle, M., 2000. The statistics of embankment dam failures and accidents. Canadian Geotechnical Journal, 37(5), pp. 1000-1024.
Foti, S., Lai, C. G. R. G. J. & Strobbia, C., 2015. Surface Wave Methods for Near-Surface Site Characterization. Boca Raton: CRC Press.
Fredlund, D. G., Rahardjo, H., & Fredlund, M. D., 2012. Unsaturated soil mechanics in engineering practice. Wiley.
Garman, K. & Purcell, S., 2004. Applications for Capacitively Coupled Resistivity Surveys in Florida. The Leading Edge, 23(7), pp. 697-698.
Hayashi, K. & Konishi, C., 2010. Joint Use of a Surface-wave Method and a Resistivity Method for Safety Assessment of Levee Systems. GeoFlorida 2010, Atlanta, ASCE, pp. 1340-1349.
Hayashi, K., Inazaki, T., Kitao, K., & Kita, T. Statistical soil type estimation using cross-plots of S-wave velocity and resistivity in Japanese levees.
Heisey, J. & Stokoe II, K. M. A., 1982. Moduli of Pavement Systems from Spectral Analysis of Surface Waves. Transportation Research Board, pp. 22-31.
Inazaki, T. & Hayashi, K., 2011. Utilization of Integrated Geophysical Surveying for the Safety Assessment of Levee Systems. SAGEEP 2001, Charleston, SEG.
Inazaki, T. & Sakamoto, T., 2005. Geotechnical Characterization of Levee by Integrated Geophysical Surveying. Proceedings of the International Symposium on Dam Safety and Detection of Hidden Troubles of Dams and Dikes 2005, Xi'an, China, CHINCOLD.
Herman, R., 2001. An introduction to electrical resistivity in geophysics. American Journal of Physics, 69(9), 943-952.
Jean-Louis Briaud., 2008. Case histories in soil and rock erosion: Woodrow Wilson bridge, Brazos river meander, Normandy cliffs, and New Orleans levees. Journal of Geotechnical and Geoenvironmental Engineering, 134(10), 1425-1447.
Johansson, S. & Dahlin, T., 1996. Seepage monitoring in an earth embankment dam by repeated resistivity. European Journal of Engineering and Environmental Geophysics, 1(3), pp. 229-247.
Kaufman, A. & Hoekstra, P., 2001. Electromagnetic Soundings. Oxford: Elsevier Science & Technology.

Keller, G. V., & Frischknecht, F. C., 1966. Electrical methods in geophysical prospecting. Pergamon Press.

Kita, T., Inazaki, T., & Hayashi, K., 2013. 2-dimensional linear array microtremor survey techniques for earthen levee investigations. Proceedings of the 11th SEGJ international symposium, Yokohama, Japan, 18-21 November 2013 (pp. 214-217) Society of Exploration Geophysicists of Japan.

Kusuda, T., & Achenbach, P. R., 1965. Earth temperature and thermal diffusivity at selected stations in the United States (No. NBS-8972). National Bureau of Standards Gaithersburg MD: DTIC.

Lane, J., Ivanov, J., Day-Lewis, F., Clemens, D., Patev, R., & Miller, R., 2008. Levee evaluation using MASW: Preliminary findings from the citrus lakefront levee, New Orleans, Louisiana. Symposium on the application of geophysics to engineering and environmental problems 2008 (pp. 703-712) Environment and Engineering Geophysical Society.

Llopis, J., & Simms, J., 2007. Geophysical surveys for assessing levee foundation conditions, feather river levees, Marysville, CA. Symposium on the application of geophysics to engineering and environmental problems 2007 (pp. 82-89) Environment and Engineering Geophysical Society.

Loke, M., 1999. Electrical Imaging Surveys for Environmental and Engineering Studies: A Practical Guide to 2-D and 3-D Surveys. San Jose: http://www.geometrics.com.

Loke, M. & Barker, R., 1996. Rapid least-squares inversion of apparent resistivity pseudosections by a quasi-Newton method Normal access. Geophysical Prospecting, January.pp. 131-152.

Love, A., 1911. Some Problems of Geodynamics. London: Cambridge University Press.

Love, A., 1927. A Treatise on the Mathematical Theory of Elasticity. Cambridge: Cambridge University Press.

McKenna, J., Dunbar, J., Wakeley, L., & Smullen, S., 2006. Near surface geophysical methods to assess levee integrity and potential failure. Symposium on the application of geophysics to engineering and environmental problems 2006 (pp. 320-326) Environment and Engineering Geophysical Society.

McNeill, J., 1980. Electromagnetic Terrain Conductivity Measurement at Low Induction Numbers, Ontario: Geonics Limited.

Mihalakakou, G., Santamouris, M., Lewis, J., & Asimakopoulos, D., 1997. On the application of the energy balance equation to predict ground temperature profiles. Solar Energy, 60(3-4), 181-190.

Miller, R., & Ivanov, J., 2005. Seismic tests on IBWC levees: Weslaco, Texas (Open-file Report No. 2005-56). Lawrence, Kansas: Kansas Geological Survey.

Min, D.-J. & Kim, H.-S., 2006. Feasibility of the surface-wave method for the assessment of physical properties of a dam using numerical analysis. Journal of Applied Geophysics, July, 59(3), pp. 236-243.

Mofarraj, B., 2017. Laboratory Resistivity Measurements for Soil Characterization, Fayetteville, AR: University of Arkansas.

Mohamed, A. M., Abu El Ata, A., Azim, F. A. & Taha, M., 2013. Site-specific shear wave velocity investigation for geotechnical engineering applications using seismic refraction and 2D multi-channel analysis of surface waves. NRIAG Journal of Astronomy and Geophysics, Volume 2, pp. 88-101.

Nazarian, S. & Stokoe II, K. H., 1983. Evaluation of Moduli and Thicknesses of Pavement Systems by Spectral-Analysis-of-Surface-Waves Method, Washington: Transportation Research Board.

NOAA., 2017. What is LIDAR?, 2017, from http://oceanservice.noaa.gov/facts/lidar.html

NRCS, 2011. Geophysical Study Muddy Fork Site 1 near Prairie Grove, AR, Little Rock: Natural Resources Conservation Service.

NRCS, 2016. ERI Report, Muddy Fork Site 1 (Kinion Lake Dam), Washington County, Arkansas, Little Rock, AR: NRCS.

Oldenborger, G., Pugin, A.-M. & Pullan, S., 2013. Airborne time-domain electromagnetics, electrical resistivity and seismic reflection for regional three-dimensional mapping and characterization of the Spiritwood Valley Aquifer, Manitoba, Canada. Near Surface Geophysics, pp. 63-74.

Palacky, G., 1987. Clay Mapping Using Electromagnetic Methods. First Break, 5(8), pp. 295-306.

Palacky, G., 1988. Resistivity characteristics of geologic targets. Electromagnetic methods in applied geophysics (pp. 52-129) Society of Exploration Geophysicists.

Palaseanu-Lovejoy, Monica, Cindy A. Thatcher, and John A. Barras. Levee Crest Elevation Profiles Derived from Airborne Lidar-Based High Resolution Digital Elevation Models in South Louisiana. ISPRS Journal of Photogrammetry and Remote Sensing 91 (2014): 114-26.

Panthulu, T., Krishnaiah, C. & Shirke, J., 2001. Detection of seepage paths in earth dams using self-potential and electrical resistivity methods. Engineering Geology, November, Volume 59, pp. 281-295.

Park, C. B., Miller, R. D. & Xia, J., 1999. Multichannel Analysis of Surface Waves. Geophysics, May-June, 64(3), pp. 800-808.

Pellerin, L., Groom, D. & Johnston, J., 2003. Multi-receiver OhmMapper survey over a former fuel tank site. 9th EAGE/EEGS Meeting, Houten, 2003, EAGE.

Piegari, E., & Maio, R. D., 2013. Estimating soil suction from electrical resistivity. Natural Hazards and Earth System Sciences, 13(9), 2369-2379.

Rein, A., Hoffman, R. & Dietrich, P., 2004. Influence of natural time-dependent variations of electrical conductivity on DC resistivity measurements. Journal of Hydrology, 15 January, 285(1-4), pp. 215-232.

Rix, G. J., Stokoe II, K. H. & Roesset, J. M., 1991. Experimental Study of Factors Affecting the Spectral-Analysis-of-Surface-Waves Method, Washington: Transportation Research Board.

Rutherford, C., et al., 2016. Preliminary observations of levee performance and damage following the 2015-16 Midwest floods in Missouri and Illinois, USA (No. GEER-045) Geotechnical Extreme Events Reconnaissance (GEER).

Samyn, K. et al., 2014. Integrated geophysical approach in assessing karst presence and sinkhole susceptibility along flood-protection dykes of the Loire River, Orléans, France. Engineering Geology, Volume 183, pp. 170-184.

Sapia, V. et al., 2017. Multidisciplinary geophysical approach to map a disposal site: The Ponza island case study. Journal of Applied Geophysics, pp. 264-274.

Sasaki, Y., Tamura, K., Yamamoto, M., & Ohbayashi, J., 1995. Soil improvement work for river embankment damage by 1993 Kushiro Oki earthquake. The First International Conference on Earthquake Geotechnical Engineering, Tokyo, Japan. , 1. pp. 43-48.

SCS, 1970. Investigation of Structure Deficiency: Foundation Drilling and Grouting Muddy Fork of Illinois River Watershed - Site No. 1, Little Rock: NRCS.

Seaton, W. J. & Burbey, T. J., 2002. Evaluation of two-dimensional resistivity methods in a fractured crystalline-rock terrane. Journal of Applied Geophysics, August, 51(1), pp. 21-41.
Seladji, S., Cosenza, P., Tabbagh, A., Ranger, J., & Richard, G., 2010. The effect of compaction on soil electrical resistivity: A laboratory investigation. European Journal of Soil Science, 61(6), 1043-1055.
Sharma, P. V., 1997. Environmental and engineering geophysics. Cambridge University Press.
Sjödahl, P., Dahlin, T. & Johansson, S., 2005. Using resistivity measurements for dam safety evaluation at Enemossen tailings dam in Southern Sweden. Environmental Geology, December, 49(2), pp. 267-273.
Sjödahl, P., Dahlin, T., Johansson, S. & Loke, M., 2008. Resistivity monitoring for leakage and internal erosion detection at Hällby. Journal of Applied Geophysics, Volume 65, pp. 155-164.
Stokoe, K. H., Roesset, J., Bierschwale, J., & Aouad, M., 1988. Liquefaction potential of sands from shear wave velocity. Proceedings, 9nd World Conference on Earthquake, , 13. pp. 213-218.
Strutt, J. W., 1885. On Waves Propagated along the Plane Surface of an Elastic Solid. Proceedings of the London Mathematical Society, November, 1-17(1), pp. 4-11.
The Federal Emergency Management Agency (FEMA), Department of Homeland Security., 2006. Emergency Management and Assistance, Title 44, V. 1.
Thomson, W. T., 1950. Transmission of Elastic Waves through a Stratified Soil Medium. Journal of Applied Physics, 21(89), pp. 89-93.
Timofeev, V., Rogozinski, A., Hunter, J. & Douma, M., 1994. A New Ground Resistivity Method for Engineering and Environmental Geophysics. Symposium on the Application of Geophysics to Engineering and Environmental Problems 1994, pp. 701-715.
Tran K.T. and Luke B., 2017. Full Waveform Tomography to Resolve Desert Alluvium. Soil Dynamics and Earthquake Engineering, Vol. 9, pp. 1-8, DOI: 10.1016/j.soildyn.2017.04.018.
Tran K.T., McVay. M., Faraone M., and Horhota D., 2013. Sinkhole detection using 2-D full seismic waveform tomography. Geophysics; 78 (5): R175–R183.
Tran K. T. and McVay M., 2012. Site characterization using Gauss-Newton inversion of 2-D full seismic waveform in time domain. Soil Dynamics and Earthquake Engineering; 43: 16-24.
U.S. Army Corps of Engineers, 2000. Design and Construction of Levees, Washington: USACE.
U.S. Army Corps of Engineers, 2004. General Design and Construction Considerations for Earth and Rock-Fill Dams, Washington: USACE.
U.S. Army Corps of Engineers, 2016. NID National Inventory of Dams. [Online] Available at: http://nid.usace.army.mil/cm_apex/f?p=838:5:0::NO
Van Genuchten, M. T., 1980. A closed-form equation for predicting the hydraulic conductivity of unsaturated soils. Soil Science Society of America Journal, 44(5), 892-898.
Vireux J. and Operto S. 2009. An overview of full-waveform inversion in exploration geophysics: Geophysics; 74(6): WCC1-WCC26.
Vrjiling, J. K., 2003. Probabilistic design and maintenance of water defense systems. Risk-Based Maintenance of Civil Structures, 8th Series Workshop, Delft, Netherlands.
Wang, G. et al., 2016. Layered internal structure and breaching risk assessment of the Higashi-Takezawa landslide dam in Niigata, Japan. Geomorphology, 15 August, Volume 267, pp. 48-58.
Wathelet, M., 2008. An improved neighborhood algorithm: Parameter conditions and dynamic scaling. Geophysical Research Letters, May. 35(9).

Wood, C., Ellis, T. & Teague, D. C. B., 2014. Comprehensive Analysis of the UTexas1 Surface Wave Dataset. Geo-Congress 2014, Atlanta, ASCE, pp. 820-829.

Zywicki, D. J. & Rix, G. J., 1999. Frequency-Wavenumber Analysis of Passive Surface Waves. SAGEEP 1999, Tulsa, SEG, pp. 75-84.

Zywicki, D. J. & Rix, G. J., 2005. Mitigation of Near-Field Effects for Seismic Surface Wave Velocity Estimation with Cylindical Beamformers. Journal of Geotechnical and Geoenvironmental Engineering, August, 131(8), pp. 970-977.